Chapter 1
Introduction

Carbon nanotubes (CNTs) have become one of the most exciting and extensively studied materials of the last two decades. They have captured the interest as nanoscale materials due to their nanometric structure and their impressive list of superlative and outstanding properties. All these ingredients have encouraged their exploitation for promising applications. One of the most interesting ones is related with the use of CNTs as electrochemical platforms for biosensing purposes, the topic in which the present thesis is framed. Accordingly, the main aim of this introductory chapter is to explain the fundamental concepts of the building blocks that constitute this thesis. Therefore, Sect. 1.1 introduces the transducer element: carbon nanotubes (CNT). In this section, the properties of CNTs, their synthesis and purification are explained. Section 1.2 describes the different carbon nanotube platforms developed for biosensor purposes and their fundamentals. Section 1.3 describes the biological recognition elements used for sensing events on the different CNT platforms. Finally, Sect. 1.4 provides an overview of the fundamentals of the main techniques that have allowed characterizing the biosensor devices and following the sensing events.

1.1 Novel Sensing Materials

Nanoscience and Nanotechnology address the study, control, manipulation, and assembly of nanometre(nm) scale components into materials, systems and devices for human interest and needs [1]. The rapid progress of nanotechnology and advanced nanomaterial production offer significant opportunities for designing powerful sensing devices with enhanced performances. Such nanomaterials can exhibit properties and functions different from the ones corresponding to bulk or macroscopic version of them. Additionally, such nanostructures can become suitable materials that favour the integration with biomaterials or biological systems. Under this context, carbon nanotubes have been exploited as a novel material with huge potential in bioanalytical and biosensing applications.

M. Pacios Pujadó, *Carbon Nanotubes as Platforms for Biosensors with Electrochemical and Electronic Transduction*, Springer Theses, DOI: 10.1007/978-3-642-31421-6_1,

1.1.1 Carbon Nanotubes: Structure and Properties of Carbon Nanotubes

This section will be addressed to the discovery, structure and properties of carbon nanotubes. Specifically, special attention will be given to the electronic, mechanical, chemical, electrochemical and optical properties which lead to immediate applications of the CNTs.

1.1.1.1 Discovery, Structure and Electronic Properties

The ability to form very long chains interconnecting C–C covalent bonds allows carbon to form an almost infinite number of compounds. Being one of the most versatile elements, carbon is the chemical basis of all known living systems on Earth; it is the fundamental element of many important biological compounds including sugars, DNA and proteins.

Until few decades ago, it was thought that there were only three structurally different forms or allotropes of carbon since they were abundant in nature: the hardest substance, diamond; one of the softest known substances, the layered graphite and the non-crystalline form, amorphous carbon. However, in the last time we have been witnesses of the discovery of two other carbon allotropes, the fullerene and the carbon nanotubes.

The true identity of the discoverers of carbon nanotubes is a subject of some controversy. For years, scientists assumed that Sumio Iijima, a Japanese physicist, had discovered CNTs in 1991. He published a paper describing his discovery which initiated a flurry of excitement and could be credited by inspiring the many scientists now studying applications of carbon nanotubes. Though Iijima has been given much of the credit for discovering carbon nanotubes, it turns out that the timeline of CNTs goes back much further than 1991.

In 1952, two Russian scientists gave the world its first clear look at carbon nanotubes. LV Radushkevich and VM Lukyanovich published clear images showing multi-walled carbon nanotubes (MWNTs) with a 50 nm diameter (the first known, transmission electron microscope images of carbon nanotubes). Unfortunately, their findings were not given much publicity: their paper was in Russian, published in a Russian journal (Journal of Physical Chemistry of Russia), and was the period of the Cold War.

Before they came to be known as carbon nanotubes, in 1976, Endo, Koyama and Oberlin, observed hollow tubes of rolled up graphite sheets synthesised by a chemical vapour-growth technique [2]. The first specimens observed would later come to be known as single-walled carbon nanotubes (SWNTs). The three scientists were also the first ones to show images of a nanotube with a solitary graphene wall.

In 1981, Russian scientists published more findings. The carbon multi-layer tubular crystals (as they were known then) were made by rolling graphene layers

into cylindrical shapes. In 1987, Howard Tennet was given a patent for his cylindrical discrete carbon fibrils.

In 1985 the three Nobel Price Winners, Robert F. Curl, Sir Harold W. Kroto and Richard E. Smalley performed experiments that aimed at understanding the mechanisms by which long chained carbon molecules are formed in interstellar space and circumstellar shells. Graphite was vaporized by laser irradiation, producing a remarkably stable cluster consisting of 60 carbon atoms: the first buckminsterfullerene C_{60} [3].

The research gained new impetus when it was shown in 1990 that C_{60} could be produced in a simple arc-evaporation apparatus readily available in all laboratories. It was just by analysing samples from such evaporator that the Japanese scientist Sumio Iijima of the NEC Corporation discovered fullerene-related carbon nanotubes in 1991 [4]. These were elongated fullerenes with diameters as small as 0.7 nm and lengths of up to several microns which were termed carbon nanotubes.

The graphene layers have become the starting point to explain the structure of carbon nanotubes. A single-walled carbon nanotube is a rolled-up tubular shell of graphene sheet which is made up of benzene-type hexagonal rings of carbon atoms. The structure is conveniently expressed in terms of a one-dimensional unit cell. Indeed, the appearance of a closed cage in CNTs can be easily rationalized by considering the presence of high energy dangling bonds at the boundaries of a finite graphene layer. The total energy of carbon atoms in a layer can be reduced by promoting the formation of a closed structure which eliminates the dangling bonds, even at the expense of increasing the strain energy.

The way the graphene sheet is wrapped up can be described by a pair of indices (n, m) that define the chiral vector, $\vec{C} = n\vec{a}_1 + m\vec{a}_2$, *in* which $\vec{a}_1$ and $\vec{a}_2$ are the basis vectors of the hexagonal graphene lattice [5–10] as shown in Fig. 1.1. Three different types of nanotube structures can be generated by rolling up the graphene layer: zigzag ($m = 0$), armchair ($n = m$) and chiral nanotubes (the rest of vectors).

Although CNTs are closely related to 2D graphene, the tube curvature and the quantum confinement[1] in the circumferential direction of the nanotube bring about the unique properties that make CNTs different from graphene. One of these unusual properties is the electronic conductivity which strongly depends on the chirality and CNT diameter. CNTs can exhibit singular electronic band structures and can show metallic and semiconducting behaviour. As a general rule, (n, m) tubes with $n - m$ being an integer multiple of 3 are metallic while the remaining tubes are semiconducting. The band gap of semiconducting tubes can be approximated by the relation $E_g = 0.8\,\mathrm{eV}/d$, with d being the diameter of the nanotube [11, 12]. Therefore, the bigger the diameter, the more metallic behaviour is found.

The verification of the electronic properties of carbon nanotubes was of great interest in light of the theoretical predictions. It turned out to be very challenging to measure them due to the small diameter of the tubes. At the beginning, many of

[1] The electron wavelength around the circumference of a nanotube is quantized due to periodic boundary conditions. Along the tube the electrons are not confined.

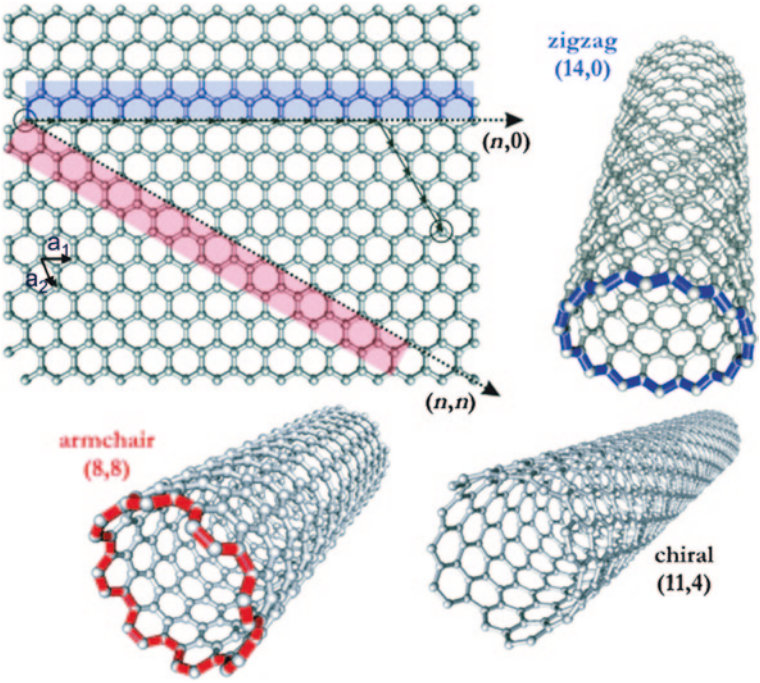

Fig. 1.1 Roll-up of a graphene sheet leading to three different types of SWNTs. Reprinted with permission from Ref. [10]

the studies on the electrons properties were on bulk CNT material by performing, for instance, electron spin resonance. Then, a more sophisticated methodology was employed based on scanning tunnelling microscopy (STM) which allowed addressing individual carbon nanotubes. The tip of the STM was used as a spectroscopic probe to collect the tunnelling conductance of each tube, providing a direct measure of the local electronic density of states (DOS)[2] of the nanotube. Since the STM has the additional power to obtain atomically resolved images of the tube's hexagon lattice, the electronic structure could be correlated with the chiral structure of the tube and with the carbon nanotube semiconducting or metallic properties.

Figure 1.2 shows the density of electronic states for a metallic and a semiconducting carbon nanotube. The DOS is not a continuous function of energy as in the case of bulk 3D materials (e.g. graphite) but they present discontinuous spikes which are typically present in one-dimensional materials (Van Hove singularities).

[2] Density of states (DOS) of a system describes the number of electron states per unit volume and per unit energy that are available to be occupied.

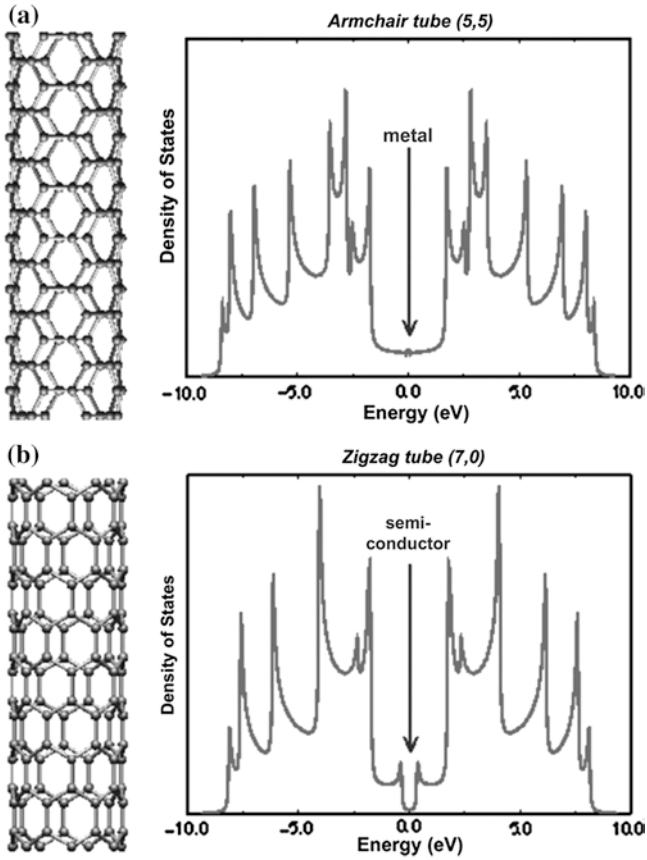

Fig. 1.2 Density of states (DOS) for a metallic (**a**) and semiconducting (**b**) carbon nanotube with the sharp Van Hove singularities. The density of states at the Fermi energy (E = 0) (Fermi energy is the energy of the highest occupied state at the absolute zero temperature.) for the metallic tube is finite but zero for the semiconducting one, providing a band-gap in the latter case. The DOS at the right of the Fermi energy are part of the conduction band (unoccupied states) whereas the one at the left corresponds to the valence band (occupied states)

Another way to verify the electronic properties of carbon nanotubes is by performing electron transport studies by contacting them in a field-effect transistor (FET) configuration. In this configuration, three electrodes are employed. Two of them (source and drain electrodes) are used to contact the nanotube and allow the flow of current through the tube when a voltage is applied between them. The third electrode (gate) is separated from the nanotube by a dielectric, and when a voltage is applied through such electrode, a modulation of the tube current is produced. The charge carriers of the carbon nanotube are modulated in a big extent if the contacted nanotube is a semiconducting but the nanotube conductance remains almost constant if the nanotube is metallic. Therefore, by sweeping the

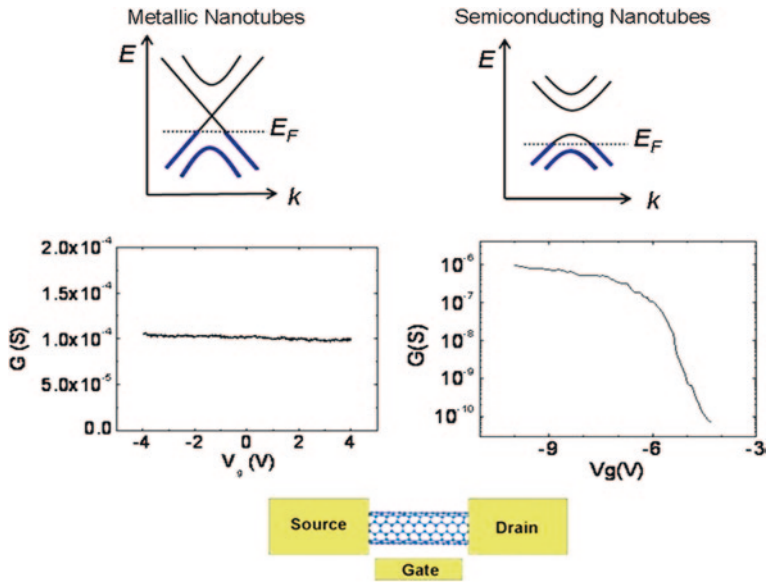

Fig. 1.3 Energy bands for a metallic and a semiconducting carbon nanotube. Note that in the case of the metallic tube, the conductance (G) as a function of the gate voltage (V_G) remains almost constant but in the case of the semiconducting one, the conductance is highly modulated by the gate voltage due to the presence of the band-gap

gate voltage of a CNT-FET and collecting the conductance profile one can discriminate between a metallic and a semiconducting behaviour. Sweeping the gate voltage shifts the Fermi level which allows probing the band energy of the tubes. In the case of the metallic CNTs (Fig. 1.3), there are always electronic states for the conduction which makes the conductance profile to keep unchangeable as the gate voltage is varied. However, in the case of the semiconducting tubes, the presence of the band gap makes the current change several orders of magnitude from a certain value (state "on") up to zero when the gate voltage is probing the region of the gap (state "off").

Moreover, carbon nanotubes can exhibit other distinct electronic characteristics such as a ballistic flow of electrons with long electron mean-free paths and the capability of supporting very large current densities [13–15]. For instance, carbon nanotubes have been shown to withstand current densities up to 10^9 A cm^{-2}, a density which is about 2–3 orders of magnitude larger than in metals such as Al or Cu.

The bonding in CNT is basically sp^2; however, the circular curvature, apart from yielding quantum confinement and quantized conductance, also causes σ–π rehybridization, an effect that is stronger as the CNT diameter decreases [16–18]. In such case, three σ bonds are slightly out of plane and for compensation the π orbitals are more delocalized outside the tube. That is a big difference with respect to graphite in which the sp^2 hybrid orbital form three in-plane σ bonds with an out-of-plane π orbital. The electron cloud distortion induced by the curvature,

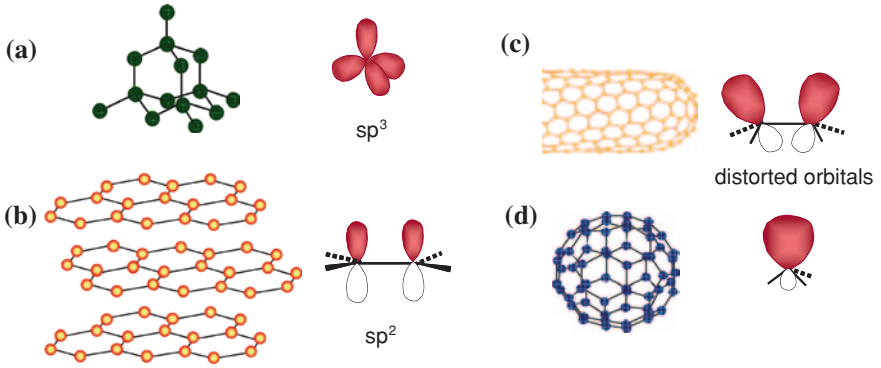

Fig. 1.4 Bonding structures for different carbon materials: **a** diamond, **b** graphite, **c** carbon nanotubes and **d** fullerenes

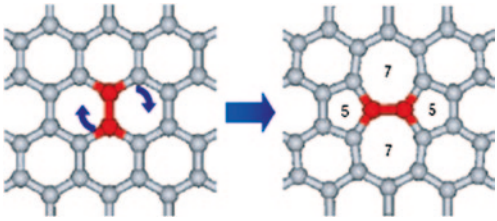

Fig. 1.5 Atomic arrangement of the Stone–Wales (SW) model. SW transformation leading to the 5–7–7–5 defect generated by rotating a C–C bond in a hexagonal network. Reprinted with permission from Ref. [25]

which yields a rich π-electron conjugation outside the tube, can make CNT more electrochemically active and electrically and thermally more conductive (Fig. 1.4).

The latter fact together with the combination of size (small diameter), structure and topology confer nanotubes remarkable mechanical properties such as high stability, strength and stiffness together with low density and elastic deformability.

However, the mentioned mechanical properties can be affected by imperfections in their structure. That is, carbon nanotubes (CNTs) can have a lot of defects such as vacancies, metastable atoms, pentagons, heptagons, Stone–Wales (SW or a pair of 5–7 rings) defects [19], discontinuities of walls, and heterogeneous atoms [20]. Therefore, being SW defects stable and commonly present in CNTs, they are believed to play key roles not only in the mechanical [21] properties of CNTs, but also in electronic [22], and chemical [23] properties. Figure 1.5 shows the pairs of 5–7 (pentagon–heptagon) defects. They are created at high strains in the nanotube lattice. This leads a step-wise diameter reduction (localized necking) of the nanotube [24].

Thus, the σ–π rehybridization, the high surface area and the presence of potential topological defects constitute key points for chemical, electrochemical and

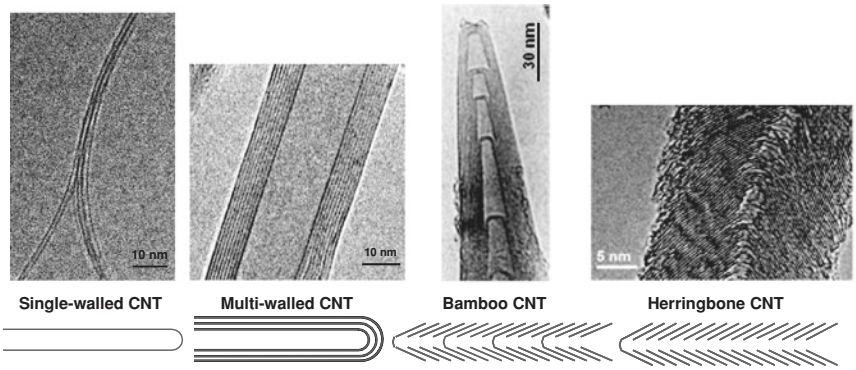

Fig. 1.6 Different structures of Carbon Nanotubes. From *left* to *right*, Single-walled CNT, Multi-walled CNT, Bamboo CNT and Herringbone CNT. Reprinted with permission from Ref. [33]

biochemical reactivity. As a result, molecular adsorption, doping and charge transfer can be more facilitated if compared with its analogue graphite.

So far we have considered CNTs formed by a single graphene wall (SWNT) with diameters ranging generally from 0.4 up to 1.5 nm and with an important diversity in electronic conductivity, from semiconducting to metallic behaviour. However, CNTs can also be made by multiple graphene layers disposed in different arrangements. Such structures, known as multi-walled carbon nanotubes (MWNTs), have typically diameters in the range of 2–100 nm and metallic behaviour.

MWNTs can be described as an assembly of concentric single-walled carbon nanotubes with different diameters and chiralities (hollow MWNTs) or with the graphene planes forming an angle with respect to the axis of the tube (herringbone or bamboo MWNTs), see schemes in Fig. 1.6. The bamboo-like tubes differ from the herringbone ones in that some of the graphene layers are periodically closed along the length of the tube forming compartments. The main difference between the hollow morphology and the herringbone and bamboo ones lies on the high density of terminating edge planes that contain the last two morphological variations of MWNTs.

1.1.1.2 Mechanical Properties

As stated before, the sp^2 bond between the individual carbon atoms makes carbon nanotubes extremely stiff and resistant to physical forces. The Young's modulus[3] of perfect CNTs has been theoretically calculated using different models [26–28].

[3] Young's modulus is a measure of the stiffness of an elastic material and is a quantity used to characterize materials.

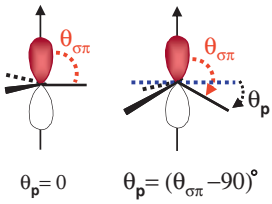

Fig. 1.7 Scheme of the pyramidalization angle in distorted sp^2 bonding in comparison with a trigonal structure

Commercially available SWNTs can achieve Young's modulus as high as 1,000 GPa. The precise value depends on the diameter (chirality) and the amount of disorder in the nanotube walls.

The maximum tensile strength[4] of SWNTs has been reported to be 30 GPa [29]. The same authors found a tensile strength of 63 GPa for MWNTs [30], while Demczyk et al. estimated the tensile strength of MWNTs to be 150 GPa [31]. Due to the nonlinearity of the radial compression, moduli from 9.7 to 80.0 GPa where found when com pressing a 10 nm tube from 26 to 46 % [32].

1.1.1.3 Chemical Properties

The high specific surface of CNTs together with the σ–π rehybridization and the presence of structural defects, facilitate different chemical processes such as (bio) chemical derivatization, intercalation, molecular adsorption, doping, charge transfer, etc. [15–17, 26–28, 33]. These characteristics are being considerably exploited for different applications such as biochemical and chemical sensing, energy storage or separation techniques.

Although graphite, fullerene and carbon nanotubes are built from the same basic element, C, the chemical reactivity is substantially different among them. The chemical reactivity is higher for a CNT than for a graphene layer but lower if compared with fullerene [16–18, 34]. Such behaviour can be closely related to the surface curvature of the carbon structure [15–17, 26, 27, 33]. The reactivity of fullerenes is mainly due to the high strain generated by the spherical geometry which affects the pyramidalization angle θp among carbon bonds which is defined as the difference between the σ–π orbital angle and 90° [34]. θp is a quantitative measure of the curvature at a tri-coordinated carbon atom. As illustrated in Fig. 1.7, this angle quantifies the deviation of a carbon atom from the plane passing through the three adjacent carbon atoms. The higher the θp, the more reactive the specie is. In a pure sp^2 hybridization (trigonal, graphene), $\theta p = 0$. Fullerenes have a θp of 11.6° due to 2D curved structure which results in sp^2–sp^3 or σ–π mixing, as discussed above with CNT (Fig. 1.4). In this case, reactions that lead to a strain relief are enhanced such as the ones related to the addition chemistry [16–18, 34–36].

[4] The tensile strength of a material is the maximum amount of tension that it can take before failure, for example breaking.

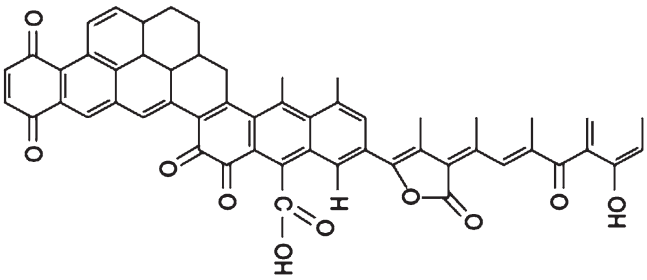

Fig. 1.8 Different oxygenated functionalities that can appear at CNT edges

In the case of CNTs, the strain appears as a consequence not only of the curvature-induced pyramidalization but also from π orbital misalignment between adjacent pairs of conjugated carbon atoms which favours the chemically reactivity of the CNT walls as compared to that of flat graphene layers [34]. Furthermore, since pyramidalization angles and π-orbital misalignment angles of CNT scale inversely with the diameter of the tubes, a differentiation is expected between the reactivity of carbon nanotubes of different diameters. A higher surface reactivity with decreasing diameter is thus expected [35].

The reactivity of different graphitic carbon allotropes is also characterized by having chemical anisotropy. Taking as a reference, for instance, the layered structure of Highly Ordered Pyrolytic Graphite (HOPG), it is known that its basal plane is more inert than the highly reactive edges which contain unsatisfied valences or dangling bonds prone to reaction with oxygen or water [37]. Such anisotropy is also observed in adsorption processes. The same anisotropy in the chemical reactivity can be considered on CNT, since the walls behave differently than the ends which can be either capped or just finishing in terminal edges [9, 26, 30, 31]. The chemical reactivity is increased at the capped ends (due to the presence, for instance, of pentagons) or at the edges of an open nanotube, which become the more reactive sites of the CNT irrespective of its diameter. Such anisotropy in the chemical reactivity will also have strong implications from the point of view of electrochemistry and will be approached in the next sections.

Although the CNT ends exhibit a higher chemical reactivity than the walls, the presence of local defects on the walls constitutes also efficient reactive sites. For instance, when CNTs are subjected to oxidative acid treatment, the local generation of carboxylic, ketones, alcohols and ester groups leads to active sites that can be profited for (bio)molecular anchoring [26, 30–32, 34]. Such acid treatments also open the CNT capped ends, bringing about an increase of oxygen rich terminal groups.

Figure 1.8 depicts a general overview of the different oxygen functionalities that can appear at the edges of CNTs [17, 37]. Such defects together with the reactivity associated with the generated strain from the curvature and π misalignment are very important for the attachment of a wide diversity of molecules. In this context, it is expected that the chemical reactivity is increased in MWNT with higher density of reactive edges, being the favoured structures the bamboo or herringbone CNTs.

1.1.1.4 Electrochemical Properties

In general, the electrochemical performance of carbon materials is basically determined by the electronic properties, and given its interfacial character, by the surface structure and surface chemistry (e.g. surface terminal functional groups or adsorption processes) [37, 38]. Such features will affect the electrode kinetics, potential limits, background currents and the interaction with molecules in solution [37]. From the point of view of electroanalysis, the remarkable benefits of CNT-modified electrodes have been widely praised, including low detection limits, increased sensitivity and decreased overpotentials [39–42]. Thus, the enhancement of the CNT electrode kinetics to different redox species, in terms of increased faradaic current and minimization of the redox overpotential, has made the nanotubes to be considered as electrocatalytical materials, a topic that will be discussed later on.

The electronic properties of CNTs, and specially their band structure, in terms of density of electronic states (DOS), are very important for the interfacial electron transfer between a redox system in solution and the carbon electrode. There should be a correlation between the density of electronic states and electron transfer reactivity. As expected, the electron transfer kinetics is faster when there is a high density of electronic states with energy values in the range of donor and acceptor levels in the redox system [37]. Conventional metals (Pt, Au, etc.) have a large DOS in the electrochemical potential window, whereas carbon electrodes have a considerable lower DOS (especially in the case of HOPG) that can be incremented by the introduction of disorder. For instance, the low DOS of HOPG can be reflected in a remarkable low double layer capacitance when the basal plane is considered [37, 38]. Interestingly, SWNTs have additionally a non-trivial variety of diameter-dependent DOS distribution and as a consequence, a very rich electrochemical behaviour is expected. SWNTs of different diameters will yield different rate constants due to the structure-dependent variations in the DOS which could be tracked by electrochemistry [43].

As mentioned, the chemical anisotropy characteristic of graphitic materials is also present in their electronic properties. For instance, it is well known that in the layered structure of HOPG, the electronic conductivity measured in the direction perpendicular to the basal plane, is about four orders of magnitude lower than that measured in the edge plane [38]. Such anisotropy also influences the electrochemical behaviour inducing an electrochemical anisotropy as well. It has been demonstrated that in graphite, the basal plane exhibits slow electron transfer kinetics whereas the reactive edge sites increase the electron transfer rate. For instance, the electron transfer rate constant, k^o, for a $Fe(CN)_6^{3-/4-}$ redox system is smaller than 10^{-6} cm s^{-1} in the case of basal HOPG and around 0.06–0.10 cm s^{-1} in the case of edge HOPG [38]. The same electrochemical anisotropy has been attributed to CNTs. The open ends of carbon nanotubes have been likened to the edge planes of HOPG whereas the tube walls are suggested to have similar electrochemical properties to those of basal HOPG [44–48].

Figure 1.9b shows the typical electrochemical response that was found when comparing CNT modified electrodes, edge plane and basal plane pyrolytic

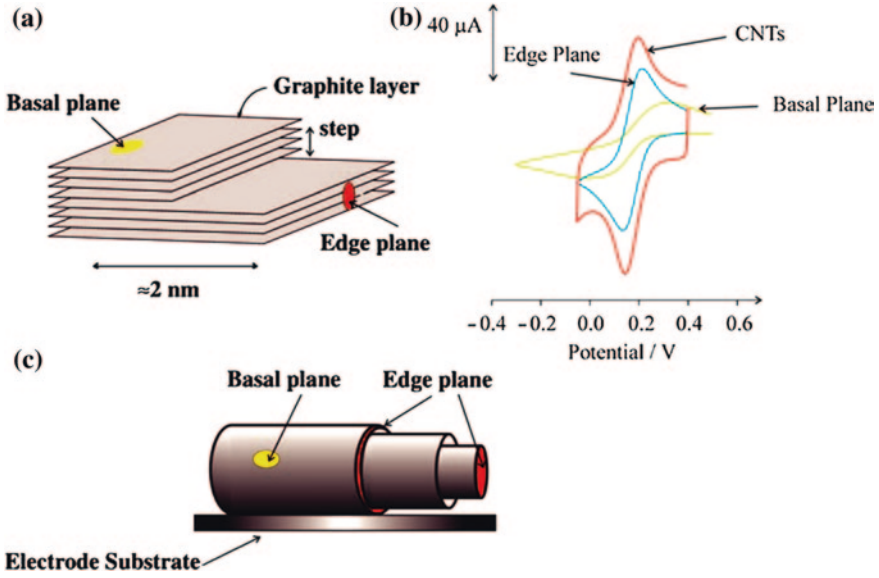

Fig. 1.9 **a** Schematic representation of the layered structure of HOPG with the indication of the different edge and basal planes; **b** voltammetric response of $Fe(CN)_6^{3-/4-}$ using basal plane, edge plane pyrolytic graphite and CNT electrodes; **c** scheme of a MWNT on an electrode surface showing the edge plane and basal plane like sites. Reprinted with permission from Ref. [50]

graphite electrodes. Basal pyrolytic graphite exhibits higher peak separations (which depends on the surface edge defect density) and consequently lower electron transfer rates [47]. However, edge plane pyrolytic graphite electrodes and carbon nanotube modified substrates show smaller and similar peak separation corresponding to fast electron transfer kinetics. Such finding only demystified the claim that CNTs provide novel electrochemical attributes such as those electrocatalytical effects [46–49]. Indeed, CNT can exhibit electrocatalytic effects but in the same way as can be found on edge pyrolytic graphite systems. That only reinforces the idea that the edge-plane like sites (like the ones at the open ends of nanotubes) are the ones responsible for such electrocatalytic behaviour. However, the electrochemical anisotropy on CNT should not also lead us to completely disregard the intrinsic electrochemical properties of the CNT walls.

One distinct advantage of the CNTs comes from the nanometre size which can also be manipulated to design novel electrode architectures [49, 51] or for signal amplification purposes [36, 37, 48]. Related with the latter issue, CNTs-systems exhibit a high effective surface area which is beneficial not only for enhancing electrochemical currents of diffusing electroactive species but also for allowing the load of high density electrochemical active (bio)molecules which can improve electrochemical signals [52, 53].

It is important to point out that not all redox systems will exhibit electrocatalytic activity when probed on high density edge CNT electrodes or edge pyrolytic

graphite. Such phenomenon depends on the particular mechanism of the redox system [37]. It is important to mention that among the redox species, there are some of them whose electrochemical behaviour only depend on the carbon DOS but are insensitive to the surface structure/morphology or chemistry [37, 38]. That is the case of many outer-sphere[5] redox species like $Ru(NH_3)_6^{2+/3+}$, ferrocene and anthracene. However, electrocatalytic effects are relevant on redox systems which involve specific chemical interactions with the electrodes and therefore are very dependent on the surface structure and surface oxygen functionalities [37, 38]. In general, an electrocatalytical behaviour is observed, correlated with redox species that are very sensitive to the surface characteristics such as the inner-sphere[5] redox species NADH, O_2, catecholamines and $Fe(CN)_6^{3-/4-}$ [54, 55]. Moreover, at this point it is important to recall the relevance of surface oxygen functionalities on electrocatalysis processes. Edge defect sites or unsatisfied valence are prone to react with oxygen and water. Such moieties can play an important role in electrocatalytical processes by enhancing the electron transfer kinetics.

Another relevant factor affecting the electrochemical performance of carbon nanotubes is adsorption. CNTs exhibit high specific surface area which can develop high polarizability and additionally oxygen functionalities which can contribute with permanent dipoles [37]. Both effects can induce dipole interactions with adsorbates and favour the adsorption, which can be assisted by other interactions such as hydrophobic ones. Adsorbates can strongly alter the electron transfer rates and the electrocatalytical activity. Positive effects can be found with the adsorption of some metalloproteins on CNTs which facilitates the electron exchange between the redox core and the carbon electrode and allows electrocatalytic activity to be monitored. Negative aspects are found when impurities are adsorbed on CNT substrates decreasing dramatically the electrochemical performance of the electrodes. In that case, activation procedures have been developed for removing such impurities. Precisely, surface preparation, as briefly discussed later on, is very important for the electrochemical performance on CNT electrodes.

To summarize, one can say that the electrochemical performance of CNT electrodes is correlated to the DOS of the CNT electrode with energies close to the redox formal potential of the solution species. The electron transfer and adsorption reactivity of CNT electrodes are remarkably dependent on the density of edge sites/defects which are the more reactive sites for that processes, increasing considerably the electron transfer rate. However, it is also worth mentioning that an exaggerated increase of edge sites/defects can also become detrimental for the CNT electrochemical properties due to the disruption of their electronic

[5] Outer-sphere or non-bonded electron transfer refers to an electron transfer (ET) event that occurs between chemical moieties that remain separate species before, during, and after the ET even, with electron tunnelling from one to the other, probably across the salvation layer. This is opposed to inner sphere electron transfer in which the electroactive species interact strongly with the surface. The ET undergoes by a chemical bridge being the reactants, intermediates or products strongly adsorbed on the electrode surface.

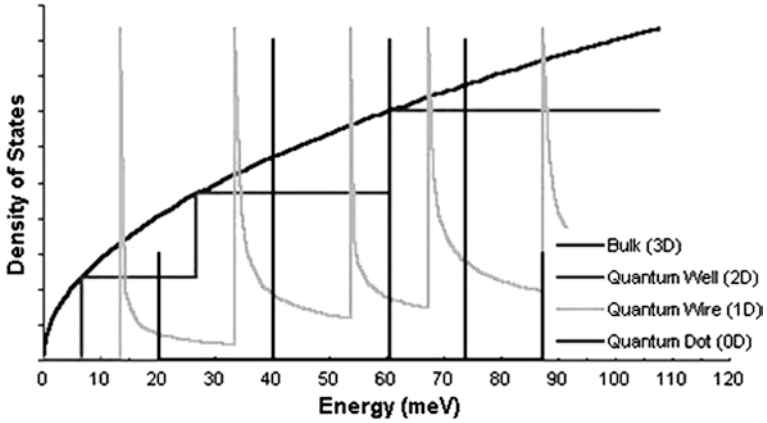

Fig. 1.10 A bulk 3D material has continuous DOS, but a 1D wire has Van Hove singularities

conductive properties. Additionally, surface oxygen functionalities can exert a big influence on the electrode kinetics. However, not all redox systems respond in the same way to the surface characteristics or can have electrocatalytical activity. That is very dependent on their redox mechanism. Moreover, the nanometre size and the high surface area are the key factors in the electrochemical performance of the carbon nanotubes.

1.1.1.5 Optical Properties

Whereas mechanical, chemical and electrochemical properties of the carbon nanotubes are well established and have immediate applications, the practical use of their optical properties is yet unclear. In particular, CNTs seem to be promising candidates for nanoscale light-emitting diodes (LEDs) [56, 57], photo-detectors [58] based on a single nanotube, bolometer [59] and optoelectronic memory [60] devices.

The remarkable CNT capabilities for light detection applications are closely related to their quasi one dimensional structure. As mentioned, the typical feature of one-dimensional crystals is that their DOS is not a continuous function of energy, but it descends gradually and then increases in a discontinuous spike. In contrast, three-dimensional materials have continuous DOS. The sharp peaks found in one-dimensional materials are the discussed before Van Hove singularities and are shown in Fig. 1.10.

Van Hove singularities lead to optical transitions which are sensitive to the chirality of the tubes. Optical transitions occur between the v_1–c_1, v_2–c_2 and can be labelled as E11, E22, etc. (Fig. 1.11). Crossover transitions c_1–v_2, c_2–v_1, etc., are dipole-forbidden and thus are extremely weak, but they can be possibly observed using cross-polarized optical geometry [61]. As the energies between the Van

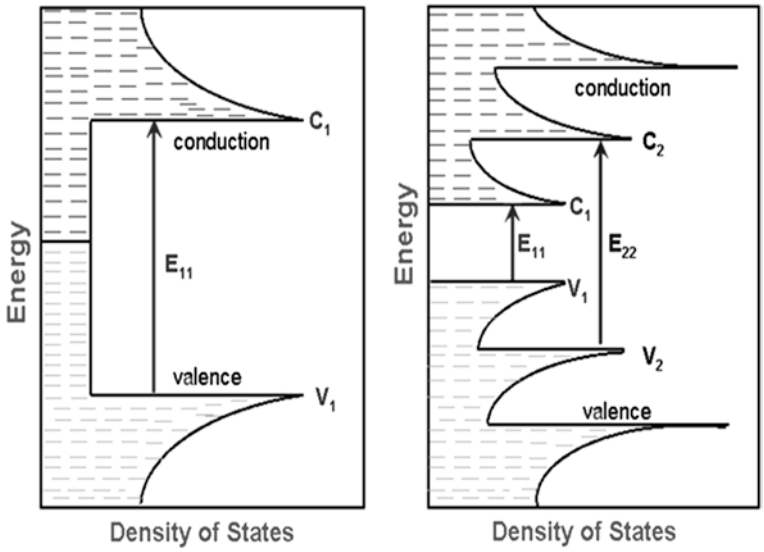

Fig. 1.11 Typical densities of states as a function of energy for metallic (*left*) and semiconducting (*right*) single-wall carbon nanotubes. $v_1 \rightarrow c_1$ corresponds to the 'first Van Hove' optical transition. $v_2 \rightarrow c_2$ corresponds to the 'second Van Hove' optical transition

Hove singularities depend on the nanotube structure, by varying this structure, one can tune the optoelectronic properties of carbon nanotube. Such fine tuning has been experimentally demonstrated using UV illumination of polymer-dispersed CNTs [62].

Optical transitions are rather sharp and strong. Consequently, it is relatively easy to selectively excite nanotubes having certain (n, m) indices, as well as to detect optical signals from individual nanotubes.

Experimentally, optical properties of CNTs are studied by optical ellipsometry, electron energy loss spectroscopy, reflectivity measurements, absorption experiments, photoluminescence, Raman spectroscopy, etc.

Among these techniques, photoluminescence (PL) is widely used to deduce (n, m) indices. In PL an electron in a nanotube absorbs excitation light via E_{22} transition, creating an electron–hole pair (exciton). Both electron and hole rapidly relax (via phonon-assisted processes) from c_2 to c_1 and from v_2 to v_1 states, respectively. Then they recombine through a c_1–v_1 transition resulting in light emission. As no excitonic luminescence can be produced in metallic tubes, this permits to identify semiconducting nanotubes.

Besides, carbon nanotubes have quite interesting Raman spectra due to resonance effects and electron–phonon interactions [63–66]. There is very strong excitation wavelength dependence of the spectra resulting from the CNT electronic band structure. Features in the Raman spectra, which will be discussed in detail later on, are diagnostic of the CNT structural quality.

1.1.2 Synthesis of CNTs

Carbon nanotubes can have different individual structures, morphologies and properties, as well as different collective arrangements and emerging properties, all of which are determined by the method of preparation and further processing [67]. Hence, a wide variety of synthetic methods have been developed to produce the desired materials and properties for specific scientific studies or technological applications.

Typical methods for carbon nanotubes synthesis are electric arc discharge [68], laser ablation [69] and chemical vapour deposition (CVD) [70]. A scheme of the three methods is depicted in Fig. 1.12.

The early processes used for CNT production were arc discharge and laser ablation approach; they allowed synthesis of SWNTs in relatively large (gram) amounts [71]. Arc-discharge and laser ablation rely on the condensation of carbon atoms generated from evaporation of solid carbon sources. The arc method creates CNTs through arc-vaporization of two carbon (graphite) electrodes placed end to end, separated by approximately 1 mm, in an enclosure that is usually filled with inert gas at low pressure. A direct current of 50–100 A, driven by a potential difference of approximately 20 V, creates a high temperature discharge between the two electrodes which vaporizes the surface of one of the carbon electrodes and forms a small rod-shaped deposit on the other electrode. MWNTs produced by arc discharge are long and straight tubes closed at both ends with graphitic walls running parallel to the tube axis. For the growth of single-walled tubes, a metal catalyst (such as cobalt, iron or nickel) mixed with graphite powder is needed. Growth temperature in the arc discharge is considerably higher than other CNT production methods (typically in the range of 2,000–3,500 °C). Consequently, crystallinity and structural perfection of arc-produced CNTs are higher (due to mechanisms of annealing of defects at high temperatures) and a significantly higher yield per unit time is obtained in comparison to other methods. In the laser ablation method, the synthesis is carried out in a horizontal flow tube under a flow of inert gas at controlled pressure. In this set-up, the flow tube is heated to ~1,200 °C by a tube furnace. Laser pulses enter the tube and strike a target consisting of a mixture of graphite and a metal catalyst such as Co or Ni. SWNTs condense from the laser vaporization plume and are deposited on a collector outside the furnace zone.

Both methods provide high quality CNTs with very little defects. Nevertheless, the equipment requirements and the large amount of energy consumed make them less favourable for nanotube production. Moreover, they produce highly entangled CNT bundles which are difficult to manipulate and assemble for building addressable structures.

The third method, based on CVD, has been widely used to grow CNTs in recent years and performed in our laboratory to understand different issues of this thesis work. In this case, the formation of tubes occurs as a result of thermal decomposition of a liquid or gas phase carbon source such as CO or hydrocarbon (C_2H_2 CH_4, etc.), catalyzed by metallic particles (typically Fe for SWNT, Co or Ni

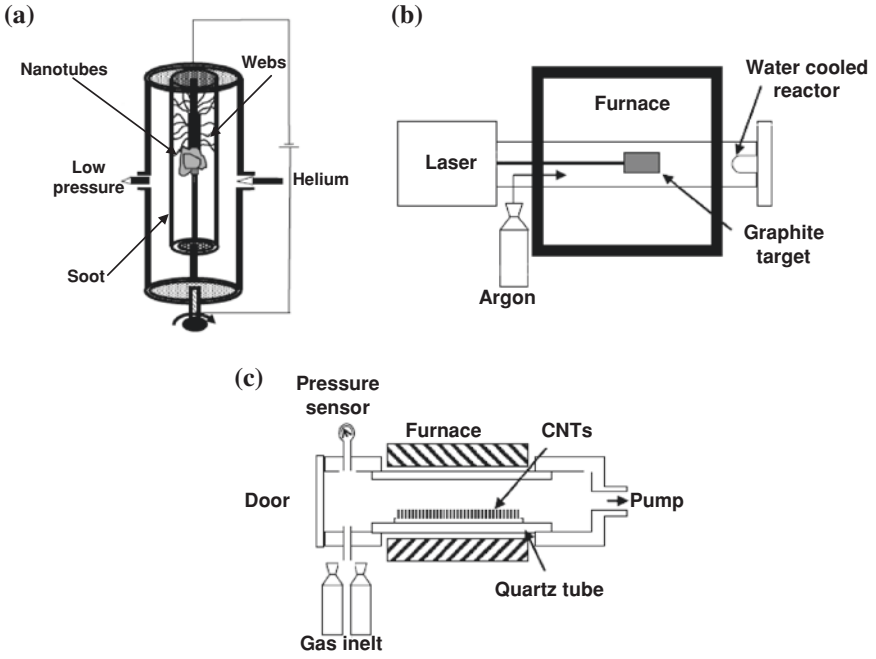

Fig. 1.12 Schematics of the three established CNT production techniques: **a** electric arc discharge, **b** laser ablation and **c** chemical vapour deposition (CVD)

nanoparticles for MWNT), which also serve as nucleation sites for the initiation of carbon-nanotube growth. It operates at considerable lower temperatures (typically between 600–1,200 °C; the lower temperatures for MWNT) with the handicap of bringing about more defective CNTs than in the case of the other methodologies. The process is sensitive to the catalyst structuring, as well as to the reaction conditions. The growing interest in the CVD process lies on the greater possibilities of this method for successful synthesis of well-separated individual SWNTs and also aligned SWNTs or MWNTs with more controllable diameter and length. It has also the advantage of being the only technique that allows synthesis of CNTs directly on a substrate or wafer, thus facilitating device integration (these nanotubes can be directly used to fabricate nanoscale electronics).

The entire CVD process mainly consists of two steps, namely catalyst preparation and CNT growth.

The catalyst is generally prepared by dispersing a solution of a metal cation on a substrate. For instance, different concentrations of iron ($Fe(NO_3)_3$) in isopropanol or of a catalyst mixture ($Fe(NO_3)_3/MoO_2(AcAc)_2$/alumina) nanoparticles in methanol, are deposited over portions of silicon wafers with silicon oxide thermally grown via spin-coating. In the next phase, the sample is introduced in the quartz tube of the CVD reactor with a flow of argon (the catalyst has to be in an oxygen-free atmosphere); then, the carbon source enters to produce the growth of the nanotubes.

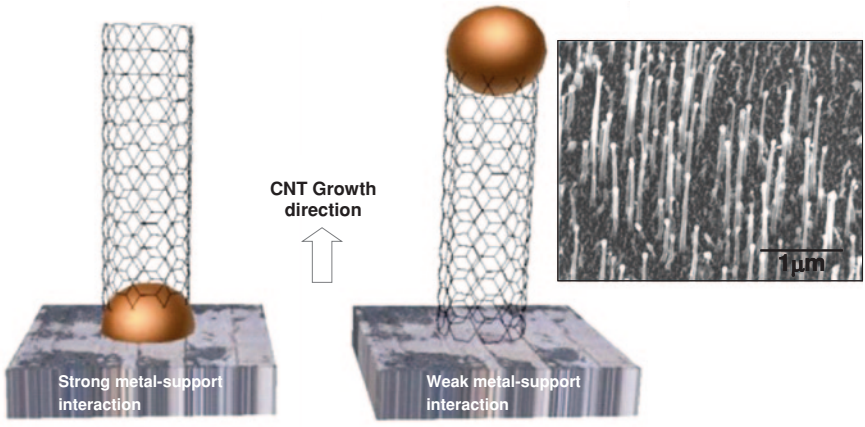

Fig. 1.13 Carbon nantube mechanistic models: base-growth mechanism (*left*) and tip-growth (*right*) with a SEM image showing Ni catalyst particle at the top of the CNT

One model that can explain the mechanism of CVD growth is the "yarmulke" one [72]: the carbon atoms released by decomposition of hydrocarbons will form graphitic sheets covering the catalytic metal surface and in the nano-sized particle, an hemispherical cap covering the exposed portion of particle will be generated. Under the right conditions, this carbon cap will peel off from the metal nano-particles as long as carbon atoms are added to the edges of the lid. Consequently, the structure takes the form of a tube whose edge is in contact with the nanoparticle and where carbon atoms continue being added. In this mechanism, the diameter of the nanotube is correlated with the catalyst particle diameter. To lift-off the lid and begin the growth of CNTs, the metal particle must have sufficient curvature (for example, must be small enough) so that graphite layers of the cover could be sufficiently tight and the lid could be lifted and the addition of carbon in tubular form could be energetically favourable. In other words, the nucleation and growth will happen only if the metal catalyst particle does not exceed a certain size. If the particle is too large and the graphite layer is not sufficiently tight and does not lift off, the particle simply is covered with carbon.

Taking as an example methane as precursor gas, the catalytic effect of the metal breaks down the methane into carbon (graphitic and amorphous carbon competing) and hydrogen; this reaction is enhanced in high temperature conditions: $CH_4 \leftrightarrows C\ (C_{graphite} + C_{amorphous}) + 2H_2$. The catalyst in the form of nanoparticles also serves as growth centre to form the basis of nanotubes [73]. Therefore, the diameters of nanotubes are correlated with the diameters of the particles, thus leading to control its diameter at its creation [74].

During the CVD growth processes, the catalyst nanoparticle can exhibit two different behaviours depending on the interaction substrate/particle. When the catalyst remains anchored to the substrate (strong interaction), the synthesis mode is

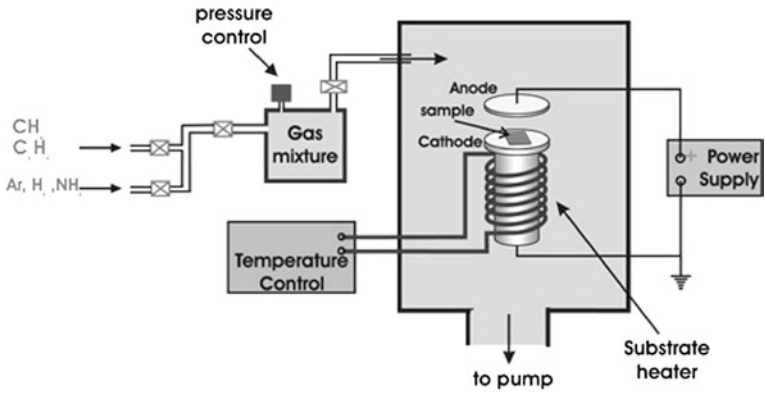

Fig. 1.14 Plasma-enhanced CVD reactor

called "base-growth". On the contrary, the growth follows a "tip-growth" mechanism when the particle lifts off the substrate (weak interaction) and is observed at the top of the CNTs (Fig. 1.13) [75, 76].

Carbon nanotubes can self-assemble during CVD growth into vertically aligned films or patterns perpendicular to the substrate surface. High density of catalyst particles is needed and then high density of vertically aligned carbon nanotubes is obtained. During CVD growth, nanotubes interact with their neighbours via Van der Waals forces to gain rigidity, which allows the nanotubes to self-orient and grow perpendicular to the substrate [71]. However, in plasma-enhanced chemical vapour deposition (PECVD), the growth direction of nanotubes can be controlled by applying electric fields [70].

PECVD first emerged in microelectronics because certain processes cannot tolerate the high temperatures of the thermal CVD operation. The low temperature operation is possible because the precursor dissociation (necessary for the deposition of all common semiconductor, metal and insulator films) is enabled by the high energy electrons in otherwise cold plasma [77].

The samples are placed onto a heating plate in the centre of the PECVD reactor (Fig. 1.14), which is then pumped down to a low base pressure (~1 mTorr) to evacuate atmospheric gasses. Then the substrate is heated (at 450–700 °C depending on process and chemistry) and the carbon-containing and reacting gases are introduced into the chamber. A high voltage applied to the electrode above the sample causes an ionization of the gases, resulting in plasma formation. The energy from heating the substrate and from the high-voltage plasma causes decomposition of the gas into its components. CNTs grow aligned perpendicular to a substrate surface due to the generated electrical field created by the plasma environment.

Even though a big body of applications has been undertaken with CNTs, there is still a long list of unsolved fundamental issues in the carbon nanotube growth mechanism which make the CNT production with defined characteristics and properties (selective synthesis) rather challenging. For instance, one unfulfilled

aspiration is the control over nanotube chirality to obtain pure metallic or semiconducting materials needed for electronics applications (such as interconnects or transistors) or to control diameter and lengths of the CNTs. Such lack of control added to the difficulties in CNT purification, sorting and processing are responsible for the high dispersion of results and performance of CNT devices.

1.1.3 CNT Purification Methods

Purification has been an important effortful task since the discovery of carbon nanotubes; it is a process that separates nanotubes from non-nanotube impurities produced as a result of CNT synthesis. These impurities generally include catalyst metal nanoparticles (iron, cobalt, nickel) together with amorphous carbon and fullerenes that are unavoidably present in the CNT soot.

The lack of a good purification protocol can also constitute an important issue that hampers the applications. Therefore, an exhaustive pretreatment or purification process is required. Generally, the purification methods can be separated into dry methods and wet methods, but usually purification consists of multi-step purification procedures: dry method followed by wet method.

Dry methods of purification refer to methods that can selectively remove, through gas-phase oxidation, amorphous carbon species due to their higher reactivity compared to that of carbon nanotubes. The simplest method is air oxidation at temperatures below the CNT decomposition [78].

Wet methods treat nanotubes in solution for purification purposes. The use of nitric acid (HNO_3) is the most common wet method used as it is straightforward, inexpensive and effective. After repeated filtration steps and maybe also centrifugation steps, purified nanotubes can be obtained [79, 80].

Other procedures rely on the use of either concentrated HNO_3 reflux with H_2SO_4 or HCl, or hydrogen peroxide reflux [81, 82]. Such treatments can eliminate a big amount of residual metal particles and other impurities. As mentioned, most dry methods of purification are also followed by a step of acid treatment to dissolve metal catalyst and/or metal oxides formed during the gas-phase oxidation step [83]. However, and even after prolonged washing treatments, metal catalyst can be still detected on CNT samples [84, 85]. The difficulties in removing the catalyst have been ascribed to the fact that in some cases, the particles are sheathed and protected by graphene sheets. Some groups have claimed that such metal impurities in CNT can cause electrocatalysis on certain electroactive species [50, 86]. In the case of graphene sheathed metal impurities, the redox processes are not taken place in close contact to the metal catalyst, so it is not fully clear how the metal electrocatalysis is taken place when exhaustive purification is performed. One plausible explanation may be related with the possibility that the metal impurity might induce changes in the electronic band structure of the CNT by adding additional energy states which might enhance the electron transfer kinetics.

Table 1.1 Material and electrochemical properties of an ideal electrode

High electrical conductivity
Hard and durable
Homogeneous microstructure throughout the bulk
Reproducible physical, chemical, and electronic properties
Good chemical inertness
Low and stable background current
Morphological and microstructural stability over a wide potential range
Rapid electron-transfer kinetics for a wide range of redox systems
Easily fabricated, shaped, and inexpensive in cost

One of the challenges in achieving high-quality electroanalytical measurements is the reproducible control of the physical and chemical properties of the electrode in order to get low background current and a rapid rate of electron transfer for the target analyte.

1.2 Carbon Nanotubes as Platforms for Electrochemical and Electronic Biosensors

Among all platforms with interest for biosensors, carbon nanotubes can be presented as a groundbreaking material that offers novel possibilities over other systems for the development of novel sensing approaches. In the following section, we will pay special attention to carbon nanotubes and their integration as solid electrodes.

1.2.1 Solid Electrodes

Solid electrodes have been a mainstay in electroanalytical chemistry for nearly five decades now [87]. For a solid material to function as an electrochemical electrode it must possess several characteristics; Table 1.1 lists some desirable electrode properties for electroanalytical purposes.

The most common solid electrode materials used as electrodes for studying electron transfer kinetics and mechanisms for determining thermodynamic parameters are: carbonaceous materials such glassy carbon [88, 89], carbon fibres [90], carbon paste or carbon composite (which consists of graphite particles in contact, incorporated in an inert matrix) [91, 92], carbon black [93], various forms of graphite (powdered graphite, pyrolytic graphite, highly ordered pyrolytic graphite) [94–97] and carbon nanotubes [98, 99]; metals such as gold [100, 101], mercury [102, 103], silver [104] or platinum [105] and semiconductors for example metal oxides [106, 107] and conducting organic salts [108].

The choice of an electrode material depends to a great extent on the useful potential range of the electrode in the particular solvent employed and the qualities and purity of the material [109].

A general advantage of metal electrodes is that their high conductivity results in low (usually negligible) background currents. It is usually fairly easy to increase

sensitivity and reproducibility at solid electrodes by forced convection. Their surfaces can be modified by electrodeposition or chemical modification; although the latter is more common with carbon electrodes. Another advantage of the use of metal electrodes is the ease of construction of the electrode assembly, and the ease of polishing.

Of all the solid electrodes utilized in electroanalytical chemistry, carbon materials are probably the most challenging and this is due to the changing surface chemistry depending on the microstructure of the carbon. As a consequence, the electrochemical properties can vary from material to material, but this can also become an advantage.

Carbon [110] exists in various conducting forms. An important issue related to surface reactivity is the available potential range of carbon electrode materials over which background reactions contribute negligibly to the observed current. Such reactions depend strongly on the nature of the carbon electrode material as well as the preparation of the surface [38]. The kinetics of surface oxidation and hydrogen evolution are significantly slower on carbon than on most commonly used metal electrodes, and the resulting wide potential window is one reason for the widespread use of carbon materials for electrodes [37].

Moreover, carbon materials have significantly more complex chemistry than metals. Carbon has a high surface activity, which explains its susceptibility to being poisoned by organic compounds. Bonds with hydrogen, hydroxyl and carboxyl groups, and sometimes quinones, can be formed at the carbon surface. The presence of these groups signifies that the behaviour of these electrodes can be very pH-sensitive, but this has also been purposely used to modify the electrode surface. That is, these groups provide sites for covalent linking to biorecognition elements (or other materials) or for their integration onto polymer surface structures, key points for the development of biosensors.

Thus, the advantages of carbon electrodes include low cost, wide potential window, relatively inert electrochemistry, richness in surface chemistry and electrocatalytic activity for a variety of redox reactions.

Among all carbon conducting forms, CNTs exhibit the mentioned remarkable electrical, chemical, mechanical and structural properties that make them a versatile material for the design of unusual electrode configurations.

1.2.2 CNT Platforms

In order to guarantee an efficient performance of the CNT based electrochemical devices, attention has to be paid not only to CNT synthesis and purification but also to the way that the CNT electrode is built up. In this section, the different carbon nanotube deposition techniques and carbon nanotube arrangements on different electrode surfaces will be described: on one side, randomly dispersed CNT in a polymer matrix or the spaghetti-like CNT dispersed on conductive surfaces; and on the other side, CNT arrays grown in situ on substrates with large scale control

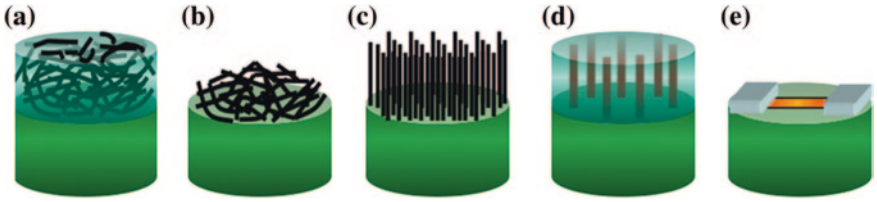

Fig. 1.15 Illustration of different CNT electrode configurations: from *left* to *right*, **a** randomly dispersed CNT composites, **b** randomly dispersed CNTs on a surface, **c** vertically aligned CNTs (VACNTs), **d** oriented CNTs embedded in a polymer matrix, **e** individual CNT electrode (CNT-field-effect transistor)

of location and orientation, embedded or not in a polymer matrix. Finally, individual CNT electrodes will be briefly discussed. Figure 1.15 illustrates these different CNT electrode arrangements.

1.2.2.1 Rigid Carbon Nanotube Composite

Composites result from the combination of two or more dissimilar materials. Each individual component keeps its original nature while giving the composite distinctive chemical, mechanical and physical qualities, different from those shown by the individual components [111]. From this definition, due to the conducting or insulating character and to the nature and arrangement of each component, composites comprise a wide scope ranging from metal/ceramic composites, polymer-based composites to natural or biomimetic biocomposites. Among the broad world of composites, the conducting ones attract special attention because of their special applications in electronics and electrochemistry. Composites for electrode applications are formed by at least one conducting and one insulating phase. In this context, carbon-based materials arise as ideal conducting phase in composites used for electrochemical sensors. One of the more practical uses of carbon based electrodes is in a form of a resin composite. In general, carbon composite materials present improvements in the electrochemical response of the conventional solid carbon electrodes. They can exhibit the interesting advantages of high mechanical stability, easy surface renewal without extensive polishing, lower background current and in some cases, microelectrode array behaviour. The later aspect, brings about even more remarkable high signal/noise ratio, fast electrode response, low detection limits and low cost. The last point makes them ideal for mass produced sensors, especially when one compares them with other materials such as gold and platinum [112].

The electrical properties of the composite will therefore depend on the nature of each of the components, their distribution, and also on their relative quantities. The electrical resistance is determined by the connectivity of the conducting particles inside the polymeric matrix. This means that the relative quantity of each composite component has to be studied in terms of percolation curves [113] to determine the optimal composition. Different composite material based on graphite powder embedded in diverse kinds of polymeric matrices have been developed in the

last few decades, obtaining interesting electrochemical applications such as in the enzymatic, DNA-detection, immunosensing field, etc. [114–117]. Nowadays, high interest is focused on composites based on carbon nanotubes (CNTs).

Many soft and rigid composites of carbon nanotubes have been reported [42]. They are formed by randomly dispersion of CNTs with insulating polymeric matrices such as granular Teflon [118], chistosan [119], polystyrene [120], polysulfone [121] and epoxy [122, 123] or by their incorporation into a silicate gel matrix [124, 125]; or with conductive polymers such as polypyrrole [126] and polyaniline [127] which can be fabricated by chemical or electrochemical polymerization [42, 124, 128, 129]. Irrespective of the nature and the way in which the composite is built up, these matrices are important for providing robustness to the CNT platform and at the same time for facilitating the analyte trapping which can result quite advantageous for some applications in the (bio)chemical sensing field. They also exhibit the valuable advantage of generating a fresh surface by only polishing every time that is needed for successive experiments.

Note that the use of insulating polymers can be more advantageous than the conductive polymers when employed in electrochemistry (e.g. cyclic voltammetry). This is because the former electrodes exhibit a more discernible response for the redox species from the background current [124].

Motivated by these attractive properties, part of this work focuses on the transduction capabilities of rigid carbon nanotube-epoxy composites to give more highlights to a previous and brief study of such CNT-epoxy systems as platforms for electrochemical sensing [123]. These rigid carbon nanotube composites constitute a simple and cheap electrode material where the insulating polymer (epoxy resin) can help to reduce the background signal thus enhancing the signal noise ratio.

Some drawbacks in CNT composites reside in the CNT itself, such as in the lack of homogeneity of the different commercial CNTs lots due to different amount of impurities in the nanotubes, as well as dispersion in their diameter/length and state of aggregation (isolated, ropes, bundles). These variations are difficult to quantify and can affect the final properties of the CNT-composites.

1.2.2.2 CNT/Glassy Carbon

Both SWNTs and MWNTs can be deposited directly from CNT dispersions as a random network or thin film on conventional electrodes. From the point of view of their construction, such electrodes are very easy to prepare but they may suffer from mechanical instability, thus limiting their application. A typical electrode substrate for building up non-oriented CNT films is glassy carbon.

Glassy carbon (GC), also referred to as vitreous carbon, is widely used as a solid carbon electrode for electroanalysis [109]. Unlike HOPG and other graphites, GC is hard and microstructurally isotropic; the interwoven sp^2 carbon ribbon gives rise to its mechanical hardness, so the material is polishable and impermeable to gases and liquids. The density of the GC is less than the HOPG one, indicating that the material contains some void space (nanoporosity) [130]. Moreover,

glassy carbon is often used as a support material because of its electrochemical inertness in a wide potential window, its amorphous structure with a random distribution of active sites for nucleation [131], its mentioned easy regeneration, robustness and low cost [132, 133].

The modification of glassy carbon is currently done by casting drops of purified CNTs dispersed either in organic or aqueous solvents and allowing the electrode to dry [134–136]. Glassy carbon provides a hydrophobic surface which considerably stabilizes the CNT films.

Another carbon substrate widely employed is the basal plane pyrolytic graphite [46, 47, 49]. In this case, carbon nanotubes are abrasively immobilized onto basal pyrolytic graphite electrodes by gentle rubbing the electrode surface with a fine quality filter paper containing CNTs.

However, in some cases and even more when the CNT layer is too thin, the underlying glassy carbon or basal pyrolytic graphite electrodes can provide some interferences in the electrochemical response. On the other side, very thick 3D CNT films can contribute with large capacitive background currents due to the large surface area which can hamper electroanalytical applications, as often occur when using the highly porous bucky paper [122, 137]. In such CNT papers, formed basically by filtration of purified SWNTs, a small faradaic signal can be lost in the high capacitive currents. However, such high CNT surface area systems result beneficial for energy storage or electrochemical actuator applications.

Gold or platinum electrodes have also been used as conducting supports for developing CNT modified electrodes. Although an enhanced electrochemical response can be evidenced, the CNT films (when casting from CNT dispersion) are not very stable on such hydrophilic surfaces and tend to be removed in contact with aqueous media, a problem that can be solved by covalent CNT attachment to the gold surface through thiol linkages.

1.2.2.3 Vertically Aligned Carbon Nanotube Electrodes (VACNT-Microelectrode/Macroelectrode)

For a thorough understanding of the fundamental CNT electrochemistry, many applications require well-organized and oriented carbon nanotube arrays. For instance, up-right CNT configurations (e.g. perpendicular to the substrate) can provide a high density of oriented electroreactive edges facilitating, on one side, the electron transfer process, and on the other side, the covalent linkage of molecules.

There are two major approaches for obtaining oriented CNTs: by self-assembly procedures (many groups have reported the assembly of shortened SWNTs in an orthogonal orientation on a gold electrode modified with thiol self-assembled monolayers with $–NH_2$ terminal groups which can attach the CNTs via carbodiimide chemistry) and by in situ growth of aligned CNTs with plasma-enhanced chemical vapour deposition (PECVD). However, by applying thermal CVD processes, high density of vertically aligned carbon nanotubes can be achieved if a dense enough distribution of the catalyst particles is deposited.

Some groups have exploited these methodologies and have developed, for instance, vertical 3D CNT ensembles with different CNT density embedded or not in an insulating matrix (SiO_2) [137–139]. These CNTs are grown directly onto an electrode surface (e.g. Si coated with a Cr film) by using plasma enhanced-CVD [137–140].

In our approach, we will use commercial macroelectrodes (or forest CNT macroelectrodes) of high-density multi-walled carbon nanotubes (about 0.2 g cm^{-3}) grown on a silica substrate by chemical vapour deposition and microelectrodes composed of patches of 300 μm × 300 μm with high density of vertically aligned carbon nanotubes (also grown by thermal CVD process) which have been developed in the National Microelectronics Centre (CNM, Barcelona) [141].

1.2.2.4 CNT-Ultramicroelectrode Arrays

Arrays of CNTs can provide more benefits from the electroanalytical point of view if their geometrical disposition is perfectly controlled in order to make them act as nanoelectrode arrays [138, 139]. That can be accomplished with the "opal inversion" technique which will be discussed in this section, for the development of CNT-ultramicroelectrode arrays (CNT-UMAs).

The discovery of the unusual properties of the ultramicroelectrodes in the eighties opened new electrochemical and analytic possibilities, and new schemes of detection that were not possible with conventional electrodes [142–145]. Ultramicroelectrode is a term used to describe microelectrodes where at least one of their dimensions is smaller than the thickness of the target analyte diffusion layer [146]. Basically, these types of electrodes exhibit a fast non lineal diffusion as the dominant way in the mass transport. When the electrode is miniaturized, the diffusion of the species on the surface of the electrode is predominantly radial, for which the species are driven also axially increasing significantly the mass transfer rate. Quickly a steady state current, independent of the convection, is reached which is directly proportional to the analyte concentration. That confers to the electrode a very fast response, very high signal/noise (faradaic current/non faradaic charging current) relation, and consequently very low limits of detection, all these properties highly desired in amperometric sensors.

Other benefits that present these ultramicroelectrodes are their low ohmic potential drop and their application in highly resistive media. However, the current of an individual ultramicroelectrode is very low and extremely sensitive instrumentation is required for its detection [142–145]. An alternative way to maintain the electroanalytical advantages of the individual ultramicroelectrodes but with a response of amplified current is by means of arrays of ultramicroelectrodes (UMAs). These arrays may consist of multiple identical microelectrodes connected in parallel with a well-controlled and uniform interdistance among each ultramicroelectrode or in a more random distribution. From the theoretical point of view, the signal from these devices is amplified as many times as the number or microelectrodes that defines the UMA [147]. The state and magnitude of the diffusion will depend mainly of the diameter of these microelectrodes and of the

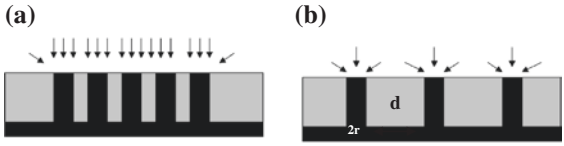

Fig. 1.16 Packaging density of microelectrodes: **a** *M* Macroelectrode behaviour, **b** *UMA* Ultramicroelectrode array

distance among them, by which the optimization of the most adequate geometry according to the requirements is indispensable.

It has been assessed that loosely packed arrays where the inter-electrode distance $d \gg 2r$ (r being the radius of a single microelectrode) yield the expected current signal (*m* times amplified) whereas closely packed arrays, where $d \approx 2r$, behave as a macroelectrode having a current that is proportional to the total geometric area of the microelectrodes in the array [148] (Fig. 1.16).

Therefore, one of the big challenges in this area is the preparation and production of these ultramicroelectrodes. The most utilized methodologies are based on the use of inert templates in which metallic microelectrodes can be dispersed [149, 150], serigraphic processes of thick layer ("screen printing") [151, 152] or lithographic techniques of thin layer employed in the fabrication of the microelectronic circuits. With these techniques individual miniaturized configurations in the shape of disks, bands, fine wires, rings, or forming a matrix or interdigitated structures could be obtained [142–145]. While the two first techniques are more versatile with extensive range of applications, cheap and open to a larger scientific community, the last one needs more expensive equipment but presents the advantage of a greater control in the miniaturization of the systems, high reproducibility and greater massive production. The microelectronic technique also allows integrating in a same chip the transducers with their complementary electrodes (reference and auxiliary electrodes) and the corresponding circuit lines for the signal processing. Apart from that, the microelectronic technology permits the production of microelectrodes of different nature in a same chip (Fig. 1.17), which can be individually addressed in an electrochemical experiment. This type of system results very appropriated for complex samples with more than one analyte since it allows working with different ranges of sensitivity and selectivity and, therefore, to enlarge the precision of the measurement. Additionally, if the assembly is constituted by microelectrodes of different material, a greater specificity of the multisensor may be devised.

An interesting alternative to the lithographic techniques of the microelectronics is the one proposed in this thesis work. This technique allows the development on CNT-UMAs based on the concept of self-assembly of an inert template and on the deposition of the catalyst material for CNT growth by different physicochemical processes. Once the template is removed, a nanostructured pattern of catalyst seeds is achieved. This allows, later on, controlling the geometric disposition of the transducer (CNTs). The technique, being cost effective, constitutes a relatively simple one and of great accessibility that takes advantage of the capacity of self-organization of some materials that form highly ordered structures on surfaces. As an example of these types of materials, we can mention the microspheres of polystyrene, which dispersed on a substrate, tend to form structures with hexagonal packaging [40]. These materials

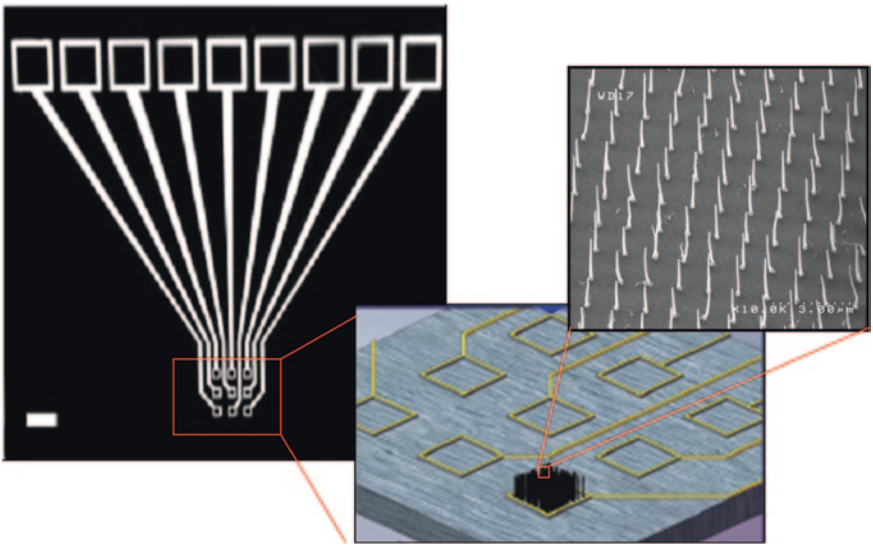

Fig. 1.17 Use of the microelectronic technology. From *left* to *right*, 3 × 3 individual nanoelectrode array with accompanying contact pads; CNTs grown using PECVD; SEM image of a zoom of the array showing CNTs growth. Adapted with permission from Ref. [153]

turn out to be very versatile as templates for the formation of porous patterns or highly periodic micro/nanostructures by means of the "opal inversion" technique.

Electrochemical Properties of High Density Versus Low Density of CNTs

To understand the electrochemical behaviour of such systems, it is worth showing an example where the response of ultramicroelectrodes developed by means of lithographic techniques is compared with the macroelectrode one [138]. The system UMAs requires the spacing among individual nanoelectrodes to be sufficiently larger than the diameter of the nanotubes to prevent the overlap of diffusion layers from the neighbouring electrodes. Figure 1.18 shows different density CNT arrays and their corresponding electrochemical response. At high density of CNTs, the electrochemical response is dominated by a planar diffusion transport evidenced by the common peak shape in the cyclic voltammetry; whereas at low density of CNTs, the electrochemical response is basically sigmoidal which is typical of radial diffusion mass transport. Thus, low density CNT nanoelectrode arrays displays the desired independent nanoelectrode behaviour showing diffusion-limited steady-state currents in cyclic voltammetry over a wide range of scan rates [138].

Therefore, the size and the spatial distribution of CNTs can be precisely controlled to ensure that each one behaves as an independent nanoelectrode. We accomplish this, as mentioned before, with "opal inversion" technique. So, this configuration can be very promising for developing ultrasensitive electrochemical sensors.

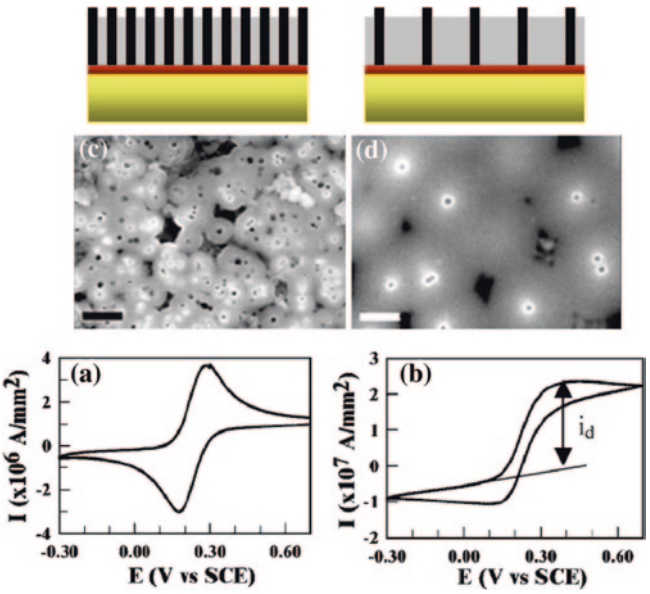

Fig. 1.18 **a**, **b** CV measurements in 1 mM of $Fe(CN)6^{3-/4-}$ and 1 M KCl with the high-density MWNT nanoelectrode array (2×10^9 electrodes cm^{-2}) and low density one (with ca. 7×10^7 electrodes cm^{-2}) respectively; **c, d** show the scanning electron images for the high and low density arrays. Readapted with permission from Ref. [138]

1.2.2.5 Carbon Nanotube Field-Effect Transistor

An electrochemical sensor response can be accomplished by using not only the common electrochemical configurations but also devices based on electronic detection in a field-effect transistor configuration (FET) [154]. We have already addressed this device when discussing the electronic properties of the CNTs. At that time, we pointed out that this kind of system allowed probing the electronic properties of the CNT and discriminating semiconducting nanotubes from metallic ones.

The first demonstrations that semiconducting single-walled carbon nanotubes could be used as conducting channels in FETs with switchable properties appeared in 1998 [155, 156]. As stated before and shown in Fig. 1.19, such configuration consists of a semiconducting single-walled carbon nanotube or a network of semiconducting SWNTs which are contacted by two electrodes, the source (S) and drain (D) electrodes. There is also an additional electrode which is separated from the CNT by an insulator film, gate electrode (G). A voltage applied between source and drain allows a current flow in the conducting carbon nanotube which can be modulated by applying a voltage on the gate electrode. Thus, the role of the gate voltage is to control the charge carriers in the current flow. The gate voltage can induce accumulation of holes (electrons) in the channel if it is polarized

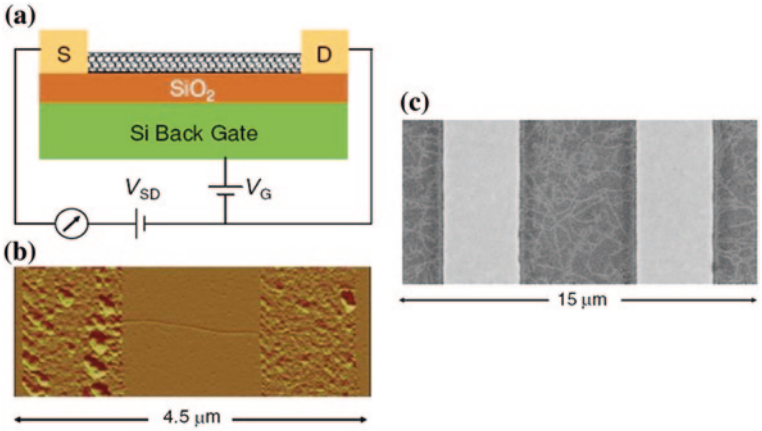

Fig. 1.19 **a** Typical scheme of a CNT-FET with the different electrodes in the so-called backgate configuration: source (*S*), drain (*D*) and the backgate electrode (*G*) (doped silicon), SiO_2 is the dielectric or insulator layer; **b** atomic force microscopy image of a typical CNT-FET device with individual SWNTs connecting the (*S*) and (*D*) electrodes; **c** scanning electron microscopy image of a FET device consisting of a random array of CNTs. Adapted with permission from Ref. [154]

negatively (positively) which makes the valence and conduction bands to move upwards (downwards) relative to the Fermi level.[6]

A simplistic picture for describing the flow current through the nanotube is by matching the valence or conduction band of the nanotube with the Fermi energy (E_f) (Fermi energy is the energy of the highest occupied state at the absolute zero temperature.) of the contact electrodes through the effect of the electric field provided by the gate voltage. However, the electric field generated by the gate voltage which controls the current flow through the CNT is dependent not only on the electronic characteristics of the nanotube itself (that is on their band-gap characteristics) but also on the interface between the SWNTs and the metal electrodes where Schottky barriers (SB)[7] can be formed (Fig. 1.20). Schottky barriers can be generally formed when a semiconductor is brought into direct contact with a metal due to the mismatch of the work functions[8] of the metal and the CNT. A charge

[6] It can also be seen as if the Fermi level were shifting upwards or downwards relative to the conduction and valence bands with electron or hole doping respectively.

[7] Schottky barrier is a potential barrier formed if a semiconductor is brought into direct contact with a metal. A charge transfer occurs until the Fermi levels of the metal and the semiconductor are aligned. The charge transfer creates a depletion zone in the semiconductor near the junction (electrical dipole). Such depletion causes a rectifying behaviour. Rectifying means that carrier transport is hindered in one of the two possible current directions. Not all metal–semiconductor junctions form Schottky barriers. A metal–semiconductor junction that does not rectify current is called an ohmic contact. Rectifying properties depend on the metal's work function, the band gap of the intrinsic semiconductor, the type and concentration of dopants in the semiconductor, and other factors.

[8] The work function is the minimum energy needed to remove an electron from a solid to a point immediately outside the solid surface (or energy needed to move an electron from the Fermi level into vacuum).

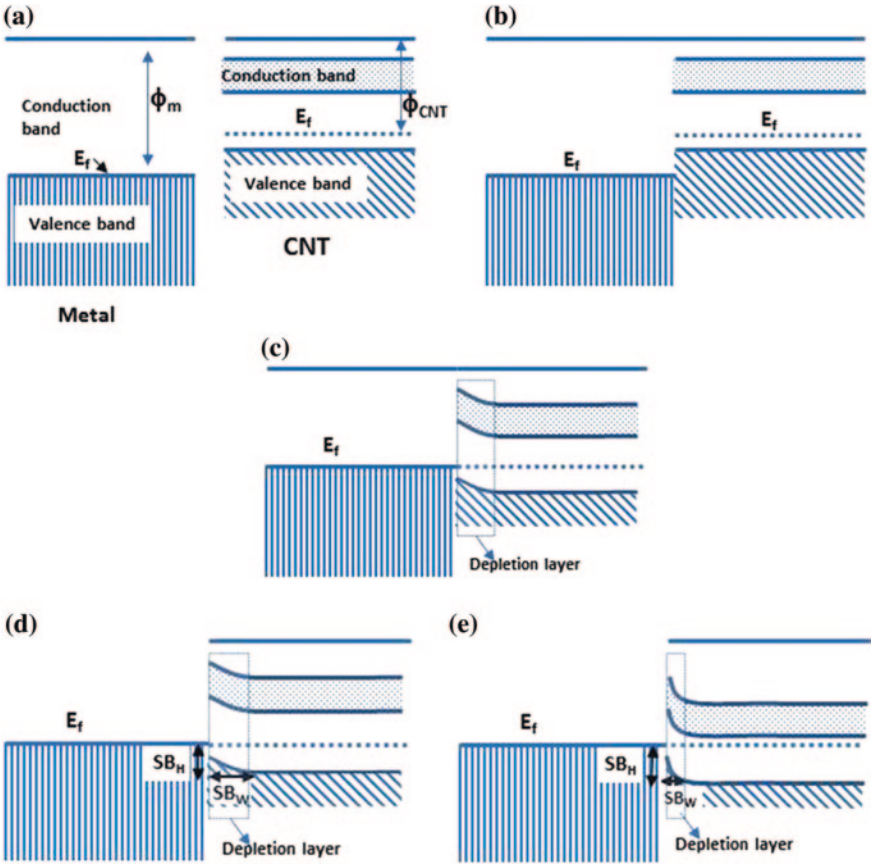

Fig. 1.20 Scheme illustrating the formation of Schottky barriers (*SB*). In (**a**) the band diagrams for the metal contact and for a semiconducting p-type nanotube are shown. The metal has a higher work function or barrier height (ϕ) than the CNT. The CNT has been schematized as a p-type since oxygen from the environment can dope the CNT with holes. In this case, the Fermi level of the CNT is close to the valence band. When the CNT and the metal contact are brought together (**b**), the Fermi level of both materials will try to equilibrate by flowing charge carriers between them (**c**). That results in a bending of the bands forming a depletion layer which gives place to the generation of Schottky barriers that inhibit the charge carrier transport. However, the height (SB_H) and thickness (SB_W) of the barrier can be changed with the gate voltage. In (**d**, **e**) the height and the thickness of the barrier height are indicated. It also shows how the thickness of the tunnelling barrier can be decreased with the gate voltage. Generally, in CNT-FETs the charge transport at the Schottky barriers is carried out by tunnelling processes and therefore for allowing the current flow the barrier thickness has to be decreased with the gate electrode voltage

transfer occurs at the interface which results in the bending of the conduction and valence bands. Such bending generates a charge depletion (potential barrier) that opposes further charge transfer. There are two of such barriers, one at the source electrode and the other at the drain one and can dominate the transport characteristics of the CNT. The thickness (SB_W) and height (SB_H) (Fig. 1.20d) of such

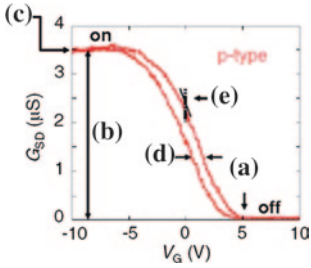

Fig. 1.21 p-type CNT-FET device characteristics: **a** threshold voltage, **b** conductance modulation, **c** maximum conductance, **d** hysteresis, **e** transconductance

barrier can be increased or decreased with the electric field provided by the gate electrode and thus modulating the current flow either of holes or electrons. In general in CNT-FETs the flow current is more dependent on the thickness than on the height of the barrier. Mechanisms based on tunnelling processes and hence on the thickness of the barrier are more important at the contact/CNT interface than the ones depending on temperature which are more dependent on the height of the barrier. Therefore, when the Schottky barrier becomes thinner, tunnelling of the charge carriers can be produced favouring the current flow in the CNT-FET.

So far we have stated that the charge transport in a CNT-FET is not only determined by the electronic characteristics of the semiconducting CNT itself but also by the interfacial Schottky barriers which can be modulated with the gate electrode. Next, we will illustrate the typical features that characterize the CNT-FET response.

In Fig. 1.21 the basic features of the so called "transfer characteristic" of a FET device are shown for a p-type CNT-FET. Applying a variable gate voltage (V_G) through the gate electrode, the source-drain current (I) or conductance (G) is measured at a fixed source-drain voltage (V_{SD}). In the plot (a) represents the threshold voltage which corresponds to the minimum voltage that is required to switch on the conductance of the tube, (b) represents the modulation (considered as the variation of the conductance from the threshold voltage), (c) represents the maximum conductance, (d) illustrates the device hysteresis and (e) indicates the transconductance[9] which is the relation between the current change as a function of the gate voltage change and provides information of the charge carrier mobility.

In this case, the CNT-FET is totally switched off for the positive voltages, a typical behaviour for a p-type system in which the holes are the dominant charge carriers. As said, most CNT-FETs exposed to air show p-type behaviour but become more ambipolar in vacuum. Such doping effect can take place during the synthesis and handling of nanotubes or by oxygen adsorption on the CNT-metal interface when exposed to air or by charge transfer from high work function contact electrodes. For instance, the oxygen changes the work function of the metal contact compared to its value in vacuum shifting the energy of the Fermi level of the metal with respect to the valence and conduction band edges in the CNT and thereby

[9] The transconductance, g_m, can be expressed as $g_m = C_t|V_G - V_{thr}|\mu/L$, where C_t is the total capacitance, V_G is the gate voltage, V_{thr} is the threshold gate voltage, μ is the charge carrier mobility and L is the length of the tube.

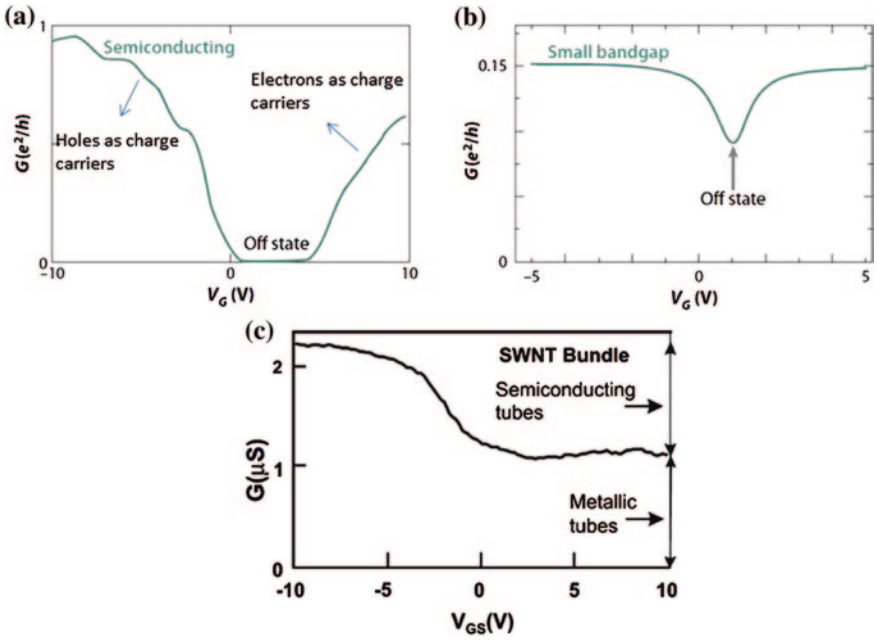

Fig. 1.22 CNT-FET response with **a** ambipolar characteristics, **b** when the CNT has also an ambipolar behaviour but with a small band-gap, **c** when CNT network contains metallic tubes

altering the hole and electron Schottky barrier heights. This mechanism has been demonstrated when removing oxygen from a CNT-FET by annealing in vacuum. The transfer characteristics of the device gradually changed from p-type to ambipolar as the oxygen was removed [157]. Thus, CNT-FETs can exhibit different features depending on their own characteristics and their environment and Fig. 1.22 collects some of them. The first example represents a CNT-FET with ambipolar characteristics. Ambipolar behaviour is observed when the Schottky barriers for holes and electrons are similar and the current flow can be done by holes or electrons. Therefore, high currents for both negative and positive gate voltages and different on/off current ratios are expected depending on the magnitude of the CNT band-gap. In principle, the CNTs are naturally ambipolar, they can transport holes and electrons. However, and as mentioned before, depending on the CNT processing, the metal contacts and their effects on the Schottky barriers, the CNT-FET can sometimes act as a unipolar device and preferentially transport only one type of carrier. The figure also shows the device characteristics when a CNT-FET has a small band-gap. In this case, a very poor on/off current ratio is also expected. Finally, the figure additionally shows the response of a CNT-FET device formed from a CNT network in which metallic tubes are present. In such case, the G–V_G signals cannot be totally switched off due to the fact that metallic tubes cannot be modulated with V_G.

Following, we will illustrate how the band diagrams of the metal contact/CNT are bent under full device operation, that is with a fixed S/D voltage and

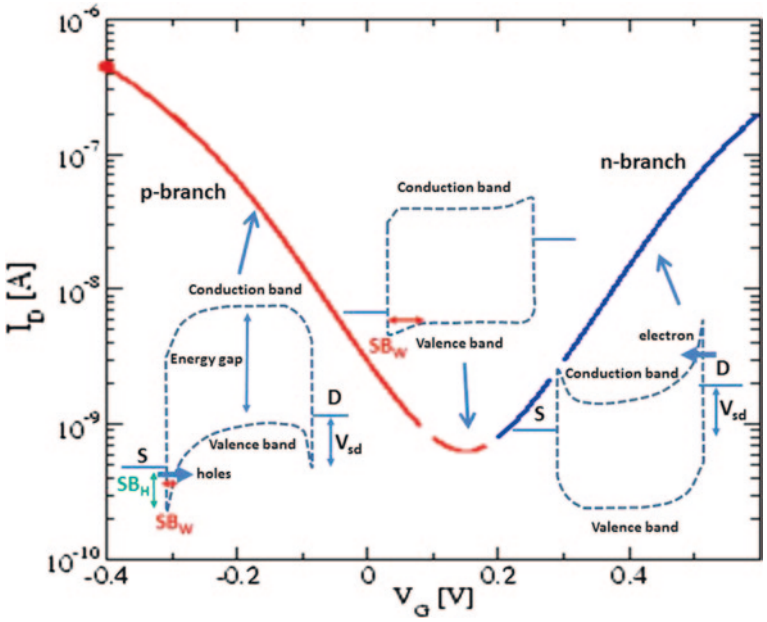

Fig. 1.23 A typical conductance versus gate voltage profile for an ambipolar CNT-FET. The *plot* shows the p-branch, at negative voltages where the hole charge carriers are dominant in the current flow and also the n-branch at positive gate voltages where the electrons are the dominant charge carriers. The figure also depicts how the band diagrams (valence and conduction bands are bent at the different gate electrodes producing Schottky barriers at the source (*S*)/CNT and drain (*D*)/CNT interfaces. The curve has been carried out by applying a fixed voltage between *S* and *D* (S_{SD}). The schematic band diagrams also show the main charge transport at the different branches: high tunnelling of holes from the source in the p-branch at which the Schottly barrier is thin; low charge transport due to thick Schottky barriers at intermediate gate voltages; high tunnelling of electrons from the drain at which the Schottky barriers become thin again. Note that current flow of electrons between the contacts takes place from higher energy to lower energy (e.g. the Fermi level of the drain is at higher energy than the one of the source), the current flow of holes takes place on the other sense from lower energy to the higher one. The scheme also indicates the Schottky barrier height (SB_H) and thickness (SB_W)

a variable gate voltage. In the Fig. 1.23, the conductance of an ambipolar CNT-FET device is shown together with their respective band diagrams for different gate voltages. As the gate electrode is negatively biased, positive charge carriers (holes) are attracted towards the CNT and accumulate in it. This additional charge causes the valence and conduction bands to move up relative to the Fermi level in the CNT. That makes the Schottky barrier for the holes at the source become thin enough to allow for a considerable amount for tunnelling. For intermediate gate voltages, the barrier is too thick for tunnelling and the conductance in the CNT device decreases. At high positive gate voltages, the bands bend down making the Schottky barrier for electrons at the drain contact thinner, giving rise to an electron tunnelling current.

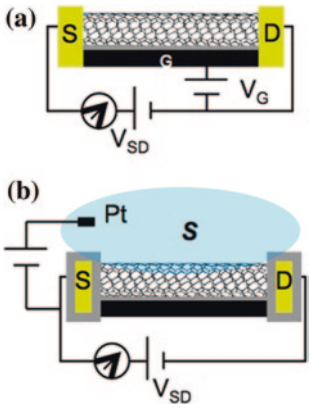

Fig. 1.24 Comparison schemes of **a** CNT-FET in the backgate configuration: source (*S*), drain (*D*) and the backgate electrode (*G*); **b** CNT-FET in liquid configuration: passivated source (*S*) and drain (*D*) electrodes, Pt wire (pseudo reference electrode), solution containing analyte (*S*)

A very important point to highlight with respect to the CNT-FET devices is that the CNT conducting channel exhibits some advantages with respect to conventional silicon based FETs and which makes attractive for sensing purposes. The nanotube is located on the surface open to the environment (contrary to the conventional silicon FETs in which the conducting channel is buried in the bulk material). Moreover, and due to the tubular structure of the tube, the current flow takes place at its surface in direct contact with the environment. They also conduct ballistically, which could lead to faster devices. All these features make CNT-FETs be very sensitive to tiny changes in the surrounding environment and can become promising candidates for the development of ultrasensitive (bio)chemical devices.

We have mentioned that in general, the gate electrode is a doped silicon substrate at the back of the device (backgate electrode). However, in other circumstances it is appropriate to perform electronic detection in aqueous environment, which is the more suitable environment for monitoring biomolecules or biological processes. Figure 1.24 schematizes the difference between both systems. Under aqueous environment, the electrolyte can induce gating effects in an alternative way to the conventional back gating configuration by using an electrode immersed in a solution [154]. In this configuration, a reference or pseudoreference electrode (usually Ag/AgCl wire or Pt wire respectively) is placed in contact with a solution containing the analyte which at the same time is in contact with the SWNTs. The electrostatic potential difference between the solution and the CNTs is controlled through the gate voltage and the potential at the metal–liquid interface. In such liquid environment, the bio-analyte reaches the CNT surface altering locally the electrostatic conditions or inducing charge transfer at the CNT-liquid interface. In this configuration, passivation of metal contacts is required for minimizing electrochemical side reactions; thus, limiting the sensing region only to the carbon nanotube [154]. It has been found that the CNT-FET configuration in liquids increases the device sensitivity; nevertheless, the main disadvantage is related to the stability and miniaturization of the liquid gating electrode and/or conditions of the electrolyte [158].

1.3 Electrochemical and Electronic Applications of CNT Electrodes

In this section, we will describe the applications of CNTs when used as electrode platforms for instance as electrochemical actuators, as electrochemical energy-harvesting devices and as biosensors (enzymatic and redox protein biosensors, CNT/DNA and genosensors, immunosensors, CNT aptasensors).

Special attention will be paid on biosensors and related issues: the immobilization methods of the biorecognition element onto the electrode surface and the biosensing events that take place on the different CNT platforms together with the mechanism of action of some biological recognition elements.

1.3.1 Electrochemical Actuators and Electrochemical Energy-Harvesting Devices

Many applications rely on the direct conversion of electrical energy to mechanical energy through a material response. The more common materials for electromechanical actuators are represented by electrostrictive[10] materials. However, applications are restricted by the maximum allowable operation temperature, the need for high voltages, and limitations on the work density per cycle [159]. CNTs appear as a new class of electromechanical actuators which generate higher stresses than natural muscle. Like natural muscles, the macroscopic actuators are assemblies of billions of individual nanoscale actuators. The first CNT actuator developed was a SWNT buckypaper which produced elongation/contraction because of the change in dimensions of the nanotube in the covalently bonded direction caused by charge injection with an applied electric potential (electrochemical doping) [159]. Other CNT actuators have been reported [160, 161], but there are still many challenges to overcome in order to develop tailored practical devices mainly because of the uncontrollable properties of nanotube buckypaper and polymer CNT nanocomposite actuators.

Moreover, carbon nanotubes can be employed either as electrode materials or conductive fillers for the active materials in various electrochemical energy-storage systems [5]. The design of 3D CNT ensembles with high surface area and mesoporous character (graphitized structure with internal channels) can yield large double layer capacitances, or provide suitable electrode frameworks for ion intercalation or catalyst entrapment/deposition, all being important for the development of electromechanical systems or electrochemical energy storage systems. Therefore, for energy generation and storage, nanotubes hold promise as supercapacitors, Li-ion batteries (LIBs), fuel cells and solar cells due to their high specific surface area and mesoporous character and their electronic and optical properties [5].

[10] Electrostriction is a property of all electrical non-conductors, or dielectrics, that causes them to change their shape under the application of an electric field.

1.3.2 Biosensors

One of the cornerstones of CNT applications in electrochemistry lies in the development of (bio)sensors. It has been pointed out the outstanding electrochemical properties of CNTs as a consequence of their electronic band structure and their richness in surface structure and chemistry. As mentioned before, CNTs have revealed in many cases electrocatalytical properties accompanied by enhanced electron transfer rates, increased signal currents and decreased overpotentials. Although these properties have been demonstrated to be not so different from the ones corresponding to edge HOPG, the main advantage in the use of electrochemical CNT devices comes from their nanometre size, their high surface area and their versatility to tailor the CNT surfaces in different geometrical arrangements in order to expose the more electroactive sites and facilitate the electron exchange. Another advantage comes from their chemical anisotropy and their interesting covalent/non-covalent chemical functionalization possibilities, many of them facilitated by their curved surface, which can be used for selective chemical modification in the development of electrochemical and electronic biosensors.

1.3.2.1 Immobilization Methods onto the Electrode Surface

In this part we will talk about the different immobilization methods of the biorecognition element onto the electrode surface. As we will see, the chemical and biochemical modification of CNTs possesses special interest because it opens the door to the achievement of novel hybrid systems for functional devices by combining the unique properties of CNT with the ones resulting from functionalization, for instance with complexing agents, fluorescent and electroactive groups, (bio)catalysts, or biomolecules (proteins, carbohydrates, nucleic acids, etc.).

Chemical and Biochemical Functionalization

Chemical modification turns out to be one of the key issues for the development of selective electrochemical (bio)sensors for (bio)recognition or catalyst materials to be used in energy-storage devices. Moreover, chemical modification also aids to overcome one of the drawbacks for CNT applications which is the difficulty of dispersing them in solvents, especially in aqueous media.

As produced CNTs are tightly bundled in ropes (through Van der Waals interactions) which make them insoluble in aqueous and organic solvents, thus compromising their processability. Additionally, and taking into account the lack of control over CNT size and chirality during synthesis, chemical modification is becoming a very useful tool for post-produced CNT sorting.

The chemical modification of CNT can be endohedral (inside the cavity of the tube) or exohedral [162]. There are some examples in literature which have

demonstrated the filling of CNT with fullerenes, biomolecules (proteins, DNA), metals and oxides which have been driven inside by capillary pressure [36, 162–169]. However, this thesis work has been focused on exohedral functionalization, taking place just at the external walls of the tubes. Both covalent (chemical bond formation) and non-covalent (physiadsorption) functionalizations can be carried out. For electrochemical devices, such functionalization schemes can be performed either before or after the CNTs are assembled on the electrodes.

Covalent Modification

As mentioned before, the CNT ends (either capped or as open edge ends) are chemically more reactive than the CNT walls. When the ends are open, the unsatisfied valence bonds become very reactive in presence of water or oxygen and normally they are found enriched in oxygenated functionalities. Additionally, the capped ends can be opened and enriched with oxygenated species by oxidizing treatments with chemical agents (e.g. HNO_3), oxygen plasma or electrochemical anodization. These treatments can also introduce oxidized points in the sidewalls [162]. Among the oxygenated functionalities, one of special interest is the carboxylic group. These –COOH residues constitute useful sites for further chemical functionalization through amide or ester bonds. The scheme in Fig. 1.25 shows the covalent bonding of primary amine molecules through amide bonds facilitated by the carbodiimide chemistry which is aided by activated reagents such as N-hydroxysuccinimide (NHS) and dicyclohexylcarbodiimide (DCC) for organic solvents or EDC (1-ethyl-3(3-dimethyl amino propyl)carbodiimide hydrochloride) and sulfo NHS (N-hydroxysulfo-succinimide) for aqueous coupling [10, 34, 170, 171]. Amines can also be coupled to carboxyl groups activated with $SOCl_2$. Ester linkages taken place by reacting the carboxyl-residues with alcohol functionalities are also shown in Fig. 1.25 [10, 170]. The amide formation is being widely used for the anchoring of proteins, amine terminated oligonucleotides, ion receptors, gold nanoparticles functionalized with aminethiols, polycationic electrolytes such as poly(ethyleneimine), etc.

On the other side and as discussed before, the chemical reactivity of CNT side walls increases with the tube curvature (e.g. decrease of the tube diameter), due to the increase of the pyramidalization angle and greater strain energy per atom [34, 35]. Such pyramidalization of the CNT atoms causes the exohedral lobes of the orbitals to be larger than their endohedral counterparts. The reactivity of the surface is thus enhanced by the pronounced exposure of the hybrid orbitals from the exterior which favours the orbital overlap with incoming reactants [35]. Accordingly, many reactions can be performed on the sidewalls of the CNTs, such as halogenation, hydrogenation, radical, electrophilic and nucleophilic additions, etc. [10, 34, 36, 162, 170, 172]. Exhaustive explored examples are the nitrene cycloaddition, the 1,3-dipolar cycloaddition reaction (with azomethinylides), radical additions using diazonium salts or radical addition of aromatic/phenyl primary amines. The aryl diazonium reduction can be performed

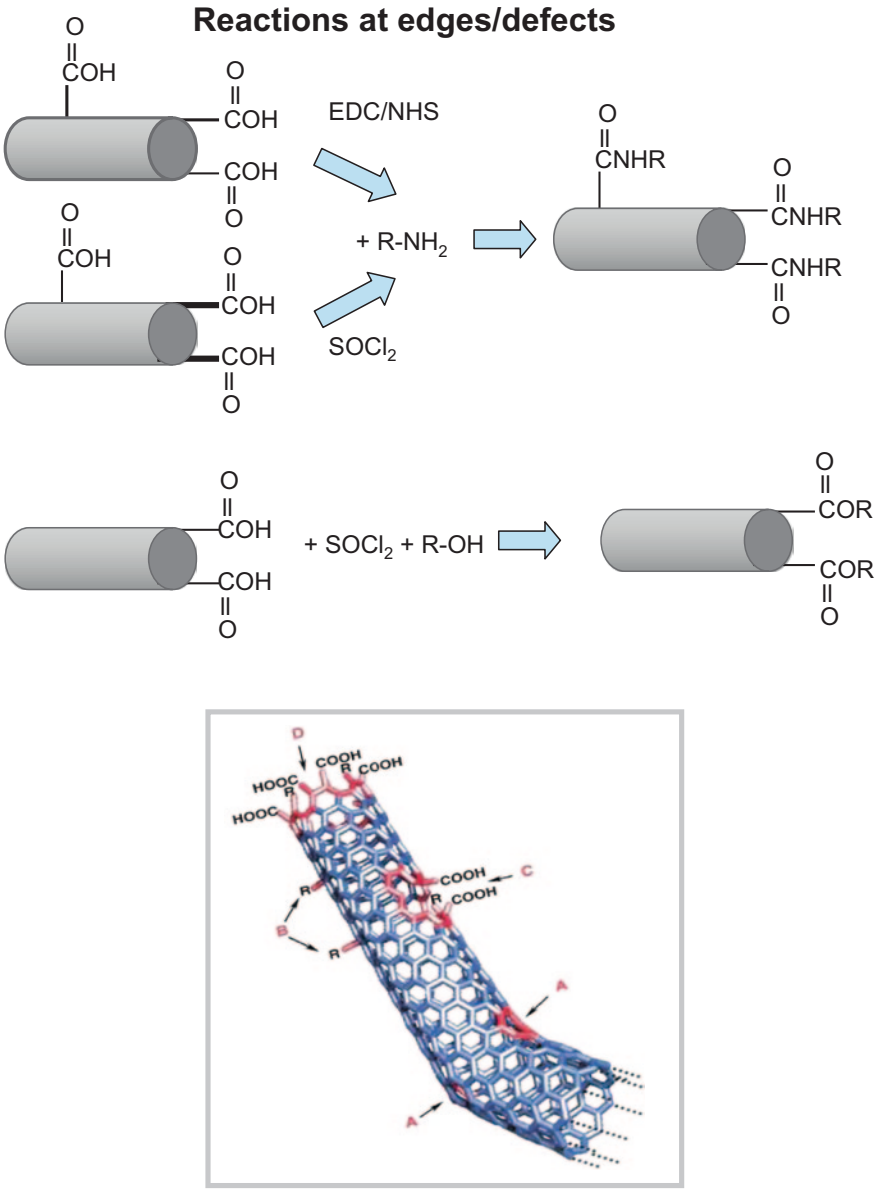

Fig. 1.25 Scheme showing common covalent reactions at the CNT edge/defects and at the CNT side walls: carbodiimide chemistry. The figure also shows the typical defects in a SWNT: **a** five- or seven-membered rings in the C network, instead of the normal six-membered ring, leads to a bend in the tube; **b** sp3-hybridized defects (R = H and OH); **c** carbon network damaged by oxidative conditions, which leaves a hole lined with –COOH groups; and **d** open end of the SWNT, terminated with oxygenated species such as –COOH groups. The last part figure has been reprinted with permission from Ref. [162]

by electrochemical means by forming a phenyl radical (by the extrusion of N_2) which couples to a double bond [170]. Similarly, electrochemical oxidation of aromatic or aliphatic primary amines yields an amine radical which can be added to the double bond on the carbon surface. The direct covalent attachment of functional moieties to the sidewalls strongly enhances the solubility of the nanotubes in solvents and also tailors the CNT surface for the different applications (for instance, in medical chemistry, solar energy conversion, selective recognition of chemical species, etc.) [170].

Non-covalent Modification

Covalent modification yields a very stable and effective derivatization. However, some drawbacks can emerge when pursuing applications especially with SWNTs. A high density of reactive sites or covalently functionalized points can lead to a loss of the CNT conjugation network with the consequent degradation of the CNT mechanical and electronic properties.

The large aromatic and hydrophobic character of CNTs make them ideal surfaces for non-covalent interaction with molecules via Van der Waals, π–π stacking or hydrophobic forces [36, 170]. There are many examples in literature of the non-covalent binding of amphiphilic agents on CNTs which have promoted CNT disentanglement and made them water soluble and biocompatible. Examples of such agents are some organic ionic surfactants such as sodium dodecyl sulfate or dodecylbenzene sulfonate. Other examples include polyaromatic compounds such as pyrenes with hydrophilic functional groups, proteins or polymers (polyethyleneglycol, tween 20, Triton X-100, polyvinylpyrrolidine, polystyrene sulfonate, DNA, RNA, polysaccharides, etc.) which coat or wrap the nanotube in such a way that the more hydrophobic part interacts with the CNT surface whereas the hydrophilic region faces the aqueous medium. An illustration is depicted in Fig. 1.26. Some of these polymers have also been used as blocking agents of non-specific binding of proteins in the development of biosensors (PEG, tween 20, Triton X-100).

A variety of these physisorbed molecules were used as anchor points for covalent immobilization in a so called hybrid approach [171]. That is the case of bifunctional pyrenes (e.g. 1-pyrenebutanoic acid succinimidyl ester, pyrene maleimide) or polymers with terminal amine/carboxylic groups which have been used for covalently immobilization of proteins, functionalized oligonucleotides, etc. (Fig. 1.26) [170, 172].

1.3.2.2 The Biosensing Event

As stated, in this section we will describe the biosensing events that can take place on the different CNT platforms together with the mechanism of action of the biological recognition elements. Specifically, we will discuss about Enzymatic and redox protein biosensors, CNT/DNA and genosensors, Immunosensors and CNT-Aptasensors.

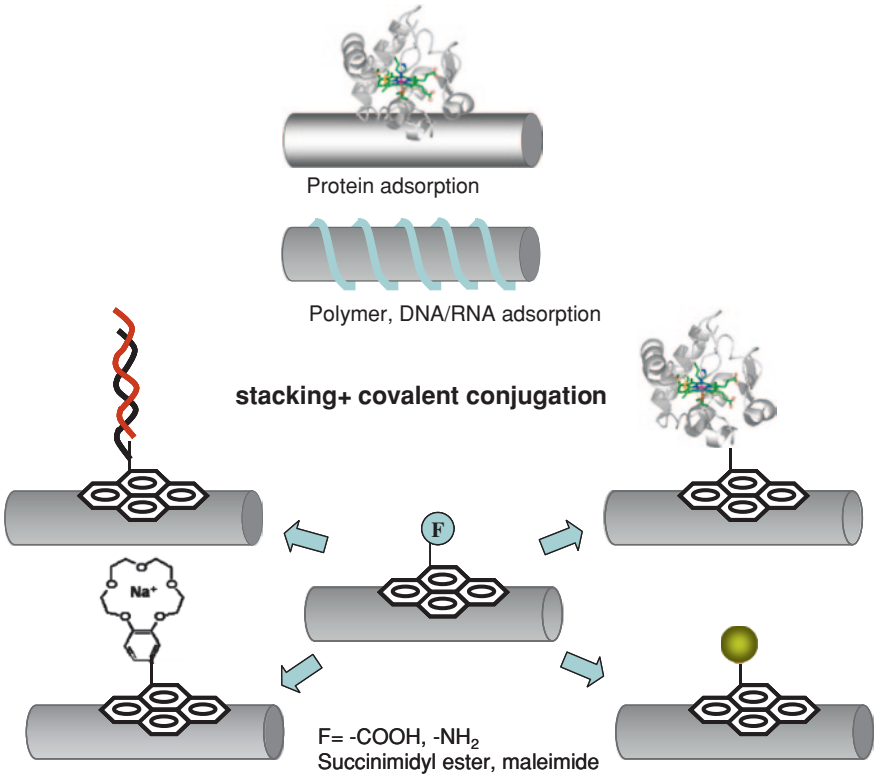

Fig. 1.26 Schematic representation of the typical non-covalent CNT functionalization and the hybrid approach by using pyrene linkers

Enzymatic and Redox Protein Biosensors

Electron transfer in biological systems is a very interesting topic not only because fundamental studies of such processes can help to unravel basic mechanisms in nature machinery, but also because such processes can be mimicked and exploited to develop sensors, bioreactors or novel fuel cells. In the electroanalytical field, there is an important interest in studying electron transfer between a redox biomolecule and an electrode for amperometric (bio)sensors. Such sensors are based on the ability of an enzyme to transduce the turnover with its corresponding substrate into a detectable, reliable and quantifiable current. One of the main goals in electroanalysis and mainly in enzymatic sensors is to achieve direct electron transfer between the protein redox centre and the transducer, keeping at the same time its bioactivity [40, 42, 51, 124, 172–174]. Thus, the electrode itself can replace physiological partners or natural electron acceptors, providing the driving force to energize the reaction and a sensor to measure the response. For instance, in the case of glucose oxidase (GOx), which catalyses the reaction:

glucose + O_2 → glucolactone + H_2O_2, with oxygen acting as its natural electron acceptor to regenerate the enzyme, the electrode can take the role of its natural partner oxygen.

A direct electron transfer warrants an efficient transduction of the enzymatic recognition of a target analyte and avoids the use of mediators or low-molecular weight relays [172]. However, such goal is rather difficult to achieve since proteins, when adsorbed on electrode surfaces, undergo denaturation with the consequent loss of their electrochemical activity and bioactivity. Moreover, some enzymes contain the redox active centre buried deep inside the protein. That makes generally difficult to obtain direct electron exchange between the protein and electrode surfaces so that mediators are needed to obtain an electrochemical response. Therefore, electrode materials with suitable physicochemical properties and enzyme immobilization methods are important for obtaining the direct electron transfer and preserving their bioactivities. CNTs seem to be an ideal material to immobilize proteins and promote direct electron transfer without the need of mediators and without losing the bioactivity of the biomolecules [40, 42, 124, 172, 173]. Moreover, CNTs have been shown to promote a dramatic decrease in the overpotential of some important species (H_2O_2, NADH) involved in electrocatalytic enzymatic reactions such as oxidases or dehydrogenases [40].

The use of aligned CNTs seems to be quite advantageous since the more electroactive ends of the nanotubes are readily accessible to species in solution. Moreover, the rigidity of the tubes allows them to be plugged into the biomolecules which enables direct electrical connection to the active centre of the enzyme and fast kinetics.

Direct electron transfer has also been achieved with many metalloproteins such as cytochrome C, horseradish peroxidase, microperoxidase (MP-11), myoglobin, hemoglobin, catalase, azurin, etc. immobilized on different CNT modified electrodes [44, 53, 134, 175–183]. The electrochemical performance of typical metalloproteins on different CNT electrodes will be discussed in this thesis work taking as an example the small water soluble myoglobin (Mb) and catalase (Cat).

Myoglobin and Catalase: Iron Based Proteins

Myoglobin is a small oxygen-binding protein of muscle cells, which stores oxygen and facilitates oxygen diffusion in rapidly contracting muscle tissue. It has a molecular weight of 16,700 Da and is comprised of a single polypeptide chain of 153 aminoacid residues of known sequence and a single iron protoporphyrin IX as the prosthetic group allocated in a hydrophobic pocket [184, 185]. At the centre of protoporphyrin, the iron atom is bonded to nitrogen atoms from four pyrrole rings. The protein contains a proximal histidine group attached directly to the iron centre, and a distal histidine group on the opposite face, not bonded to the iron. The distal side of the heme is either vacant or occupied by a water molecule which is easily exchanged by other ligand such as oxygen or hydrogen peroxide [173], Fig. 1.27. The distal histidine stabilizes a water-ligand to ferric iron and in the ferrous state this conformation stabilizes bound oxygen as the sixth ligand and

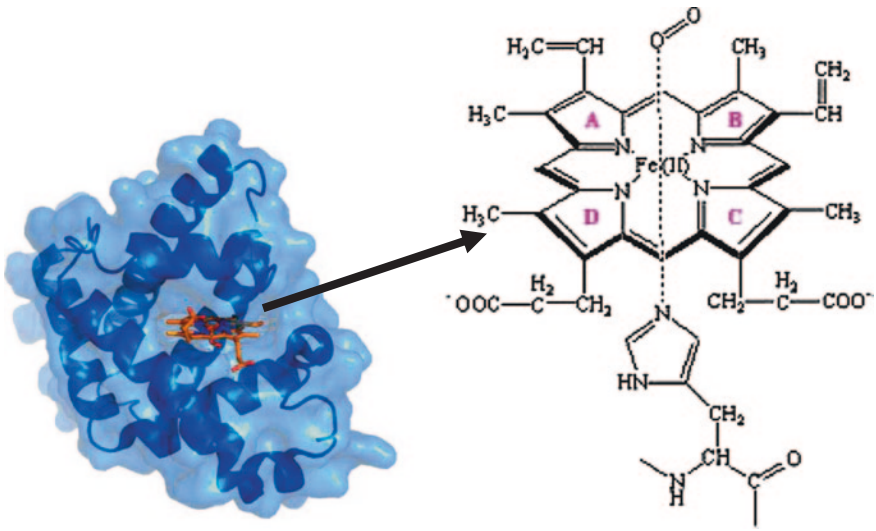

Fig. 1.27 Myoglobin molecule contains one heme prosthetic group inserted into a hydrophobic cleft in the protein. Representation of heme prosthetic group (biologically active group in Mb), its interaction with the polar proximal histidine and the oxygen ligand at the 6th axial site

suppresses the irreversible autooxidation of the heme group [173]. Thus, the distal histidine acts as a gate by controlling the access of ligand molecules to the distal pocket. The outside of the protein has both polar and apolar residues with an isoelectric point[11] of 6.8. Besides its important biological task, Mb attracts attention due to its hemin core capable of redox activity, which is unusual for a protein not naturally involved in electron transfer.

On the other hand, catalase is a large common antioxidative enzyme present in the peroxisomes of nearly all aerobic cells, serves to protect the cell from the toxic effects of hydrogen peroxide (H_2O_2) by catalyzing its decomposition into molecular oxygen and water without the production of free radicals [186–190]. All catalases are tetrameric, each subunit (molecular weight ~ 60,000 Da) consists of 506 aminoacid polypeptide chain with hemin as a prosthetic group which is embedded in the middle of each monomer. Catalase is one of the most efficient enzymes known, resulting in reaction rates approaching the diffusion-controlled limit. The optimum pH for human catalase is approximately 7.

As mentioned above, both proteins have the active redox centre embedded deep in the protein which makes difficult the direct electron transfer in conventional electrodes.

However, the transfer can be enhanced with a proper immobilization of the protein on adequate substrates. Additionally, the redox iron centre of both proteins is extremely sensitive to oxygen and peroxide and electrocatalytical activity can be

[11] Isoelectric point is the pH at which the number of positive charges and the number of negative charges of a compound (e.g. protein) are equal.

observed in presence of such analytes by monitoring the electron transfer between the electrode and the protein iron group. The possibility of enhancing the electrochemical response of this metalloproteins together with its high sensitivity to oxygen and H_2O_2 gives rise to a strong interest, specially, in the area of the electroanalysis, for the development of efficient electrochemical recognition (bio)sensors for clinical diagnosis or for environmental assays.

CNT/DNA and Genosensors

The modification of CNT with nucleic acids constitutes a very promising area for the development of devices for DNA-detection, gene therapy, drug discovery and delivery, etc. A genosensor consists in a substrate modified with specific oligonucleotides (probe DNA) that can detect targeted complementary DNA sequences (target DNA). The application of CNTs in electrochemical DNA biosensors is quite promising for many reasons: CNTs constitute novel platforms for DNA immobilization with important electrochemical transducing properties and high specific surface area which can increase not only the attached DNA amount but also concentrate a great number of enzymes or electroactive nanoparticles to amplify DNA hybridization [40, 173].

In order to prepare electroanalytical devices based on hybridization recognition, the first critical issue to face is related with the immobilization procedures on the surface of the transducer. It is important to guarantee a good orientation of the bases of the DNA probe on the CNT interface in order to get efficiency in the hybridization with the target DNA. The more basic approaches for DNA immobilization on CNTs are the physisorbed (multisite attachment) or the covalent anchoring (single point linkage). In the latter case, typical schemes are provided by the conjugation of DNA terminal functional groups with functional groups in the CNT surface via the carbodiimide chemistry, streptavidin/biotin interactions, etc.

In general, DNA is physisorbed on CNTs by wrapping the tube, with the bases (apolar region of the molecule) in close contact with the hydrophobic walls of CNT whereas the phosphate backbone faces the solution [170, 191]. Such orientation of the adsorbed DNA and the consequent reduced flexibility can decrease the efficiency of the hybridization event, indicating that for a more appropriate biofunctionalization, hydrophobic interactions need to be minimized. Therefore, when genosensors based on physical adsorption of oligonucleotides are considered, chemical treatment of the CNT surface (by promoting hydrophilic interactions) should be performed to increase the efficiency of the hybridization detection. On the other hand, single-point attachment of the DNA turns out to be a more flexible configuration which enhances hybridization kinetics.

Many of the electrochemical DNA-detection strategies that can be collected in the literature range from the use of labelling target DNA to label-free approach. Among the later, the direct electrochemical detection of DNA methodologies such as the oxidation of the DNA bases (mainly guanine) or the use of highly positively charged o-negative redox reporters as indicators of the hybridization process are of

considerable interest, though the indirect detection methods of DNA hybridization by using labels (i.e. covalently linked fluorescent tag DNA target) are very popular and in some cases mandatory [192].

Label-free electrical detection protocols based on DNA oxidation are attractive since they greatly simplify DNA hybridization assays as they offer an instantaneous detection of the duplex. However, such kind of detection schemes can suffer from some drawbacks [193]. DNA bases exhibit high oxidation potential and consequently higher background currents which can mask the electrochemical signal [194, 195]. In some cases, it is also necessary to manipulate the DNA probe by replacing guanine by inosine in order to avoid interferences of the guanine oxidation from the probe when monitoring the DNA target [192]. Other additional issues that can perturb the performance of the biorecognition event can arise from the functionalization process. For direct oxidation, a DNA multisite attachment provided by physisorption is required to guarantee close proximity between the CNT and the DNA for electron exchange. As mentioned, such configuration reduces flexibility of DNA for the hybridization process. A covalent single point attachment could overcome such difficulties but then base oxidation mediators (such as ruthenium complexes) should be used for achieving a quantifiable signal since the bases can not remain in close contact with the electrode surface.

Labelled DNA detection schemes rely on the chemical labelling of target DNA sequences with redox active molecules, enzymes, nanoparticles, etc. [117, 192, 196–199]. In the case of enzymatic labels bound to the DNA target, the enzyme triggers the catalysis of a redox active reaction under hybridization. For instance, by using a horseradish peroxidase-labelled DNA target, H_2O_2 peroxide is produced which can be detected amperometrically, so the redox reaction of H_2O_2 is an indication of the hybridization process. A variation on such approach involves a three-component "sandwich" assay, in which the redox label is attached to a synthetic sequence specifically designed to bind an overhang portion of the probe and target DNA. All these approaches need an extra chemical labelling step either in the target DNA or in the synthetic oligonucleotide which makes the process more expensive and effortful [193]. One practical alternative to DNA base oxidation detection or chemical labelling schemes is to use redox active reporter molecules that intrinsically associate with the double helix in a non-covalent manner. These reporter molecules can interact with the DNA either by electrostatic interactions or by intercalation in the double strand DNA. A simple example of the former molecules is the highly positively charged $Ru(NH_3)_6^{3+}$ which can strongly interact with the negatively phosphate backbone. Such approach with non-covalent and reversible redox reporters is very sensitive, simple and does not damage the sample which allows further use.

Immunosensors

An immunosensor is a device comprising an antigen or antibody species coupled to a signal transducer, which detects the binding of the complementary species. An extensive range of analytes can be detected and measured by immunosensors, e.g.

medical diagnostic markers such as hormones (steroids and pituitary hormones), drugs (therapeutic and abused), bacteria and environmental pollutants such as pesticides.

An indirect immunosensor uses a separate labelled species that are detected after binding by, e.g. fluorescence or luminescence (e.g. a heterogeneous immunoassay). A direct device detects the binding by a change in potential difference, current, resistance, mass, heat, or optical properties (e.g. a homogeneous immunoassay). Although indirect sensors may encounter fewer problems due to non-specific binding effects, the direct sensors are capable of real-time monitoring of the antigen–antibody reaction. A wide range of molecules can be detected with detection limits ranging between 10^{-9} and 10^{-13} mol L^{-1}.

Although it has not been dealt in this thesis work, CNTs have also promising applications in the immunosensing field and many examples of such sensor devices can be found in literature. For example, immunosensors with an electrochemiluminescence read-out signal have been designed using CNTs as support of the immunorecognition systems [200].

As an alternative to immunosensors, we have developed CNT-aptasensors which confer some advantages when we use specific detection schemes, as for instance, based on field-effect transistors, but this will be discussed in the following section.

CNT-Aptasensors

Advances in nucleic acid research led to the identification of specific oligonucleic acid sequences, which bind to wide array of non-nucleic acid target molecules like proteins, with high affinity and specificity. Such nucleic acid sequences are termed as aptamers [201]. The word aptamer derives from aptus that means 'to fit' [202]. These are RNA or DNA molecules (ca. 30–100 nucleotides) that recognize specific ligands and that are obtained in vitro by 'selection evolution of ligands with exponential enrichment', SELEX process [203].

The SELEX process (Fig. 1.28) starts by generating a large library of randomized RNA or DNA sequences. Usually, this library contains 10^{14}–10^{15} different RNA/DNA species that fold into different structures depending on their particular sequence. The library is incubated with the target protein of interest, and those RNAs/DNAs present in the library that bind the protein are separated from those that do not. The retained RNAs/DNAs are then amplified by RT-PCR and transcribed in vitro to generate a pool of RNAs/DNAs that have been enriched for those that bind the target of interest. This selection and amplification process is repeated (usually 8–12 rounds) until the RNA/DNA ligands with the highest affinity for the target protein are isolated. The winning aptamers are then cloned and sequenced.

Aptamer/protein binding results in a highly specific interaction, which has the ability to discriminate between related proteins that share common sets of structural domains [204–207].

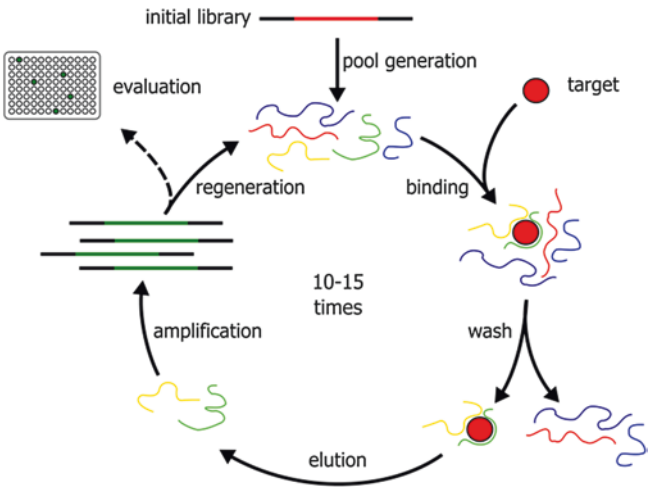

Fig. 1.28 Scheme of systematic evolution of ligands by exponential enrichment (SELEX). A library of DNA or RNA molecules is incubated with the protein target, and those that bind to it are separated from the rest. The sequences with affinity for the target are subsequently amplified to generate a pool of molecules that bind to the protein of interest

Aptamers are often called 'synthetic antibodies' because they can mimic antibodies in a number of applications and bind their targets with affinities and specificities that can be comparable to those of antibodies: the equilibrium dissociation constants of aptamers to targets are usually in the range of picomolar (pM) to micromolar (μM), similar to those of antibodies for antigens [208, 209]. However, aptamers present some advantages. Table 1.2 summarizes them [210]. Aptamers can be used not only for the molecular recognition in immunoassay-like tests, but also as sensing elements in biosensors. Biosensors based on aptamers as biorecognition elements have been coined 'aptasensors' [211]. The grey-coloured rows detail special advantages of aptamers over antibodies as recognition elements.

In the past few years, integration of functional aptamers into nanomaterials has become a new interdisciplinary field that aims at providing new hybrid sensing systems (sensors) for specific and sensitive molecular recognition [212, 213]. This novel integration has yielded various types of sensors for selective and sensitive detection of a wide range of analytes such as adenosine, cocaine, mercuric ion, thrombin, etc.

In this thesis work, the preparation, characterization and applications of CNTs that are conjugated with aptamers will be discussed, as well as the suitability of using different configurations of CNT (randomly dispersed on GC, VACNT, FET, etc.). It is worth highlighting that in terms of FET technology, aptamers provide a preferable choice over antibodies that will be discussed in detail later on. The study will be focused on aptamer nanosensors for the biosensing of proteins like thrombin and lysozyme.

Table 1.2 Advantages of aptamers over antibodies

	Aptamers	Antibodies
Binding affinity	nM-pM	nM-pM
Specificity	High	High
Production	Chemical process carried out in vitro and can therefore target any protein	Requires in vivo biological system
Target range	Wide: ions, small organic molecules, proteins, whole cells, etc.	Narrow: only immunogenic compounds
Batch to batch variation	Uniform activity regardless of batch synthesis	Activity of antibodies vary from batch to batch
Chemical modification	Easy and straightforward	Limited, can cause loss in affinity
Target site	Investigator determines target site of protein	Immune system determines target site of protein
Thermal denaturation	Return to original conformation after temperature treatment	Temperature sensitive and undergo irreversible denaturation
Shelf-life	Stable to long term storage and can be transported at ambient temperature	Limited
Cross-reactive compounds isolation	Can be isolated utilizing toggle strategy to facilitate pre-clinical studies	No method

Antibody generation, particularly for use in biosensors, has several drawbacks that are addressed by aptamers

Thrombin and Lysozyme

Thrombin

Thrombin is a serine protease that plays many roles in the coagulation cascade, it converts soluble fibrinogen into insoluble strands of fibrin, as well as catalyzes many other coagulation-related reactions [214]. Thrombin is a two chain enzyme composed of an NH_2-terminal "A" chain composed of 36 residues (Mr = 6,000 Da) and is non-essential for proteolytic activities and a COOH-terminal "B" chain composed of 256 amino acids (Mr = 31,000 Da) which remain covalently associated through a single disulfide bond. Human thrombin is 13 amino acids shorter than the bovine thrombin due to a thrombin cleavage site on the human protein that is not present in the bovine protein. Its isoelectric point is 7.0–7.6 [215]. Thrombin is usually considered as an important target when searching for anti-coagulants and antithrombotics to interfere in the blood coagulation [216]. Moreover, thrombin is considered as an useful tumour marker in the diagnosis of pulmonary metastasis [217]. Disorders in blood clotting are tightly linked to many serious health issues, including heart attacks and strokes [218]. Therefore, thrombin is typically the target in anticoagulation therapy for these diseases [219].

Lysozyme

Lysozyme, also called muramidase or peptidoglycan N-acetylmuramoyl-hydrolase, is an ubiquitous enzyme widely distributed in diverse organisms such as bacteria, bacteriophages, fungi, plants and animals [220]. It catalyzes in vivo the hydrolysis of the β(1–4) glycosidic linkage between N-acetylmuramic acid and N-acetylglucosamine alternating sugar residues in the bacterial peptidoglycan and causes bacterial cell lysis. Its primary sequence contains 129 amino acid residues. The molecular weight is 14,351 Da and its isoelectric point is 11.0 [221, 222]. Lysozyme's relatively small size and simplicity makes it an excellent model analyte for novel methods in protein detection. This enzyme works as a natural inner body antibiotic often termed "body's own antibiotic" because it possesses lytic activity against the polysaccharide wall of bacteria. Moreover, it has been discovered recently that antibodies against variants of lysozyme are present in patients with rheumatoid arthritis [223] which highlights the potential of lysozyme as a clinical index of these diseases.

1.3.2.3 Special Issues for the Biorecognition Process

Selectivity is especially important in real-world samples where the target concentration can be much less than the concentration of non-target biomolecules. Thus there are some issues that need to be taken into consideration for an efficient biorecognition event.

Blocking Agents

A trade-off exists between selectivity requirements and sample preparation complexity for most real-world applications. Most authors opine that obtaining adequate selectivity in complex real-world samples is the most daunting challenge to the field of biosensors in general [224]. A closely related concept is non-specific binding (NSB), in which non target biomolecules stick to the probe layer, preventing target binding or causing a false positive signal. To alleviate this problem, one should pre-expose the sensor modified with probe molecules to a solution containing specific blocking agents: molecules that cover the sensor gaps, for instance in our case the CNT walls left unprotected by the probe, thus preventing the non-specific adsorption of interferents when exposing to the specific target analytes.

However, there is no previous study which deals systematically in depth the problem of blocking the non-specific adsorption on the CNTs. Experimental applications are limited to blocking agents widely used to prevent protein adsorption on other surfaces, such as bovine serum albumin (BSA) or other antifouling agents such as polyethylene glycol (PEG) [225, 226], polyethylene glycol methacrylate [227–229] and surfactants like Tween 20 [226, 230, 231] that can also be deposited on areas surrounding the sensor to prevent target depletion via non-specific

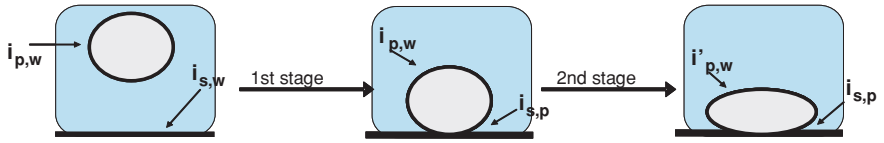

Fig. 1.29 Illustration of the proteins adsorption mechanism in two stages, where: *p* protein, *i* interface, *s* surface, *w* water. After the second stage, conformational changes can modify the interface with water resulting in i'_{pw}

binding [232, 233]. These agents have been widely used for biomedical applications and biosensors.

Taking as an example the non-specific adsorption of proteins on CNT, the major problem comes from the CNT hydrophobic surface and the fact that proteins are capable of conformational changes that increase their interactions (hydrophobic interactions) with surfaces [234].

Specifically, there are enthalpic and entropic contributions in the protein adsorption processes on surfaces. Enthalpic contributions include Van der Waals, hydrophobic and electrostatic (between the surface and the oppositely charged protein) interactions. Entropic contributions are based on mechanisms involving the release of counterions and/or water molecules that form the hydration shell, as well as conformational changes [234].

The protein adsorption mechanism considers two stages, being the first one more decisive (Fig. 1.29). It is based on two interfaces, one between the surface and the water and the other between protein and water. The first step consists in the formation of a new interface between the surface and the protein, with the consequent displacement of water. The second stage considers the reorganization of the protein on the surface.

It is possible to develop a strategy to block non-specific adsorption on CNT hydrophobic surface if the first stage is made difficult. One way to accomplish that is by modifying the CNTs surface with blocking agents that may confer a stable hydrophilic interface that hinders the displacement of water molecules from the CNT-protein interface.

From studies of self-assembled monolayers with terminal functional groups ethylene glycol (EG), it was demonstrated the capacity of these groups to stabilize water molecules by hydrogen bonds, and consequently, the generation of a solvation layer at the interface which energetically suppress adsorption of proteins on the EG modified surface [235]. Although the molecular mechanisms underlying protein resistance of ethylene glycol moieties have not yet been fully identified, it is believed that apart from the stabilization of hydration shells there is also a brush-induced "steric" repulsion that is thought to prevent direct contact between proteins and the underlying surface.

Apparently, studies that have tested different blocking agents with EG groups (PEG, Triton X-100, Tween 20, etc.) conclude that the blocking agent that has less number of EG units is the one which confers less resistance to protein adsorption.

However, this view is far from giving a complete explanation of the process; layout and density of the blocking agents on CNT should be taken into account and therefore, one should use more specific techniques that give information for instance on coating degrees, orientation and thickness of the agents chains such as surface plasmon resonance, grazing incidence X-ray diffraction, theoretical studies based on molecular dynamics simulations, etc.

The use of blocking agents has not been systematically studied, but several approaches have been found to work in specific situations. For instance, washing the sensor surface before readout can sometimes improve selectivity by washing away non-specifically adsorbed molecules while leaving the target intact, but this in an endpoint measurement and not real-time approach.

1.4 Characterizing the Biosensor Devices

In this part we will provide an overview of the fundamentals of the main techniques that have allowed characterizing the biosensor devices and following the sensing events. Specifically, we will describe the different electrochemical and electronic methods of detection used and surface characterization techniques.

1.4.1 Methods of Detection: Electrochemical and Electronic Biorecognition Processes

Although optical detection techniques are perhaps the most prevalent in biology and life sciences, electrochemical or electronic detection techniques have also been used in biosensors/biochips due to their great sensitivity, high specificity, and low cost. These techniques can be amenable to portability and miniaturization, when compared to optical detection techniques.

In the next lines, the electrochemical and electronic techniques used to characterize the biosensor devices of this thesis work will be described. These techniques include voltammetric techniques (cyclic voltammetry and differential pulse voltammetry), chronocoulometry, electrochemical impedance spectroscopy and electronic detection based on electric field.

1.4.1.1 Voltammetric and Chronocoulometric Measurements

Voltammetric techniques involve the application of a potential (E) to an electrode and the monitoring of the resulting current (i) flowing through the electrochemical cell. In many cases, the applied potential is varied over a period of time (t) while monitoring the current. Among all the common forms of voltammetry, we have focused in cyclic voltammetry and differential pulse voltammetry.

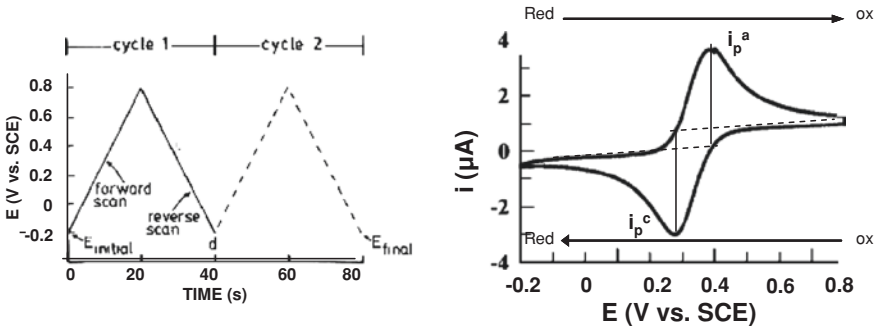

Fig. 1.30 **a** Typical excitation signal for cyclic voltammetry, triangular potential waveform with switching potentials at −0.2 and 0.8 V versus SCE; **b** cyclic voltammogram scheme

Cyclic voltammetry (CV) is perhaps the most versatile electroanalytical technique for the study of electroactive species [236]; it can provide qualitative information about the number of oxidation states and their stability, about mechanisms of electrochemical reactions, as well as their rate of heterogeneous electron transfer. It can also be used in combination with simulation software to calculate rates of homogeneous and heterogeneous reactions.

Cyclic voltammetry is often the first experiment performed in an electrochemical study of a compound, a biological material, or an electrode surface. For instance, CV allows following biorecognition events with electron transfer exchange. The effectiveness of CV results from its capability for rapidly observing the redox behaviour over a wide potential range. The resulting voltammogram is analogous to a conventional spectrum in that it conveys information as a function of an energy scan.

Specifically, CV consists of cycling the potential of an electrode, which is immersed in an unstirred solution, and measuring the resulting current. The potential of this working electrode is controlled versus a reference electrode such as a saturated calomel electrode (SCE) or a silver/silver chloride electrode (Ag/AgCl). The controlling potential which is applied across these two electrodes can be considered an excitation signal (for CV is a linear potential scan with a triangular waveform) as shown in Fig. 1.30.

The important parameters in a cyclic voltammogram are the peak potentials ($E_p{}^c$, $E_p{}^a$) and peak currents ($i_p{}^c$, $i_p{}^a$) of the cathodic and anodic peaks, respectively. If the electron transfer process is fast compared with other processes (such as diffusion), the reaction is said to be electrochemically reversible, and the peak separation is

$$\Delta E_p = E_{pa} - E_{pc} = 2.303 \cdot RT/nF.$$

Thus, for a reversible redox reaction at 25 °C with n electrons ΔE_p should be $0.0592/n$ V.

The formal reduction potential (E^o) for a reversible couple is given by:

$$E^o = \frac{E_{pc} + E_{pa}}{2}$$

For a reversible reaction, the concentration is related to peak current by the Randles–Sevcik expression (at 25 °C):

$$i_p = 2.686 \times 10^5 n^{\frac{3}{2}} A c_0 D^{\frac{1}{2}} v^{\frac{1}{2}}$$

where i_p is the peak current in amps, A is the electrode area (cm^2), D is the diffusion coefficient ($cm^2\ s^{-1}$), c_0 is the concentration in mol cm^{-3}, n the number of electrons and v is the scan rate in V s^{-1}.

Accordingly, the current is directly proportional to concentration and increases with the square root of the scan rate. A typical cyclic voltammogram is shown in Fig. 1.30b.

For the cases that the electron transfer processes are "slow" (relative to the voltage scan rate) the reactions are referred to as quasi-reversible or irreversible electron transfer reactions. In this situation the voltage applied will not result in the generation of the concentrations at the electrode surface predicted by the Nernst equation. This happens because the kinetics of the reactions is 'slow' and the equilibrium is not established rapidly (in comparison to the voltage scan rate). In this situation, the overall form of the voltammogram recorded is similar to that above, but unlike the reversible reaction, now the position of the current maximum shifts depending upon the reduction rate constant (and also the voltage scan rate). This occurs because the current takes more time to respond to the applied voltage than in the reversible case.

In the irreversible processes, the individual peaks are widely separated and the peak current is given by:

$$i_p = 2.99 \times 10^5 (\alpha n_a)^{\frac{1}{2}} n A C_0 D^{\frac{1}{2}} v^{\frac{1}{2}}$$

with α being the transfer coefficient and n_a is the number of electrons involved in the charge transfer step. The current is still proportional to the bulk concentrations but will be lower in height depending on the value of α. As before, the peak current increases linearly with $v^{1/2}$.

For quasi-reversible systems, the shape of the peak and the peak parameters are functions of α and a parameter Λ, the latter one defined as:

$$\Lambda = \frac{k}{(DvnF/RT)^{\frac{1}{2}}}$$

where k is the heterogeneous electron transfer rate constant.

As Λ increases, the process approaches the reversible case. For small values of Λ, the system exhibits a more irreversible behaviour. Then, the peak current is given by:

$$i_p = i_p(rev) K(\alpha, \Lambda)$$

where i_p(rev) is the reversible value of i_p and K is a function of Λ and α. In this case i_p is not proportional to $v^{1/2}$.

Differential pulse voltammetry (DPV) is an important electroanalytical tool which provides increased sensitivity and more efficient differentiation and resolution of different species compared to CV.

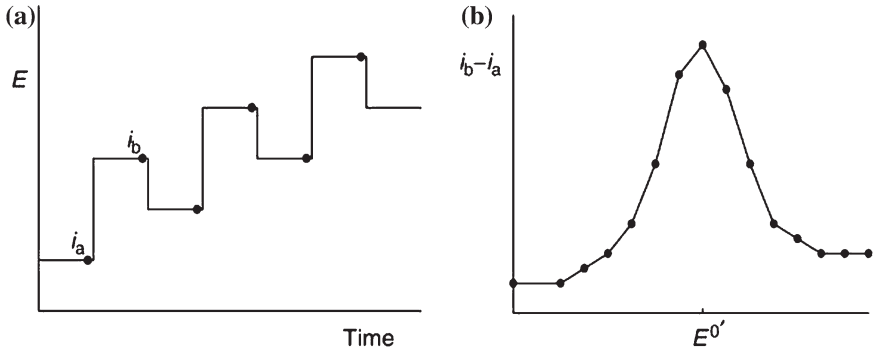

Fig. 1.31 **a** Diagram of the potential waveform used in DPV; **b** differential pulse voltammogram

This technique uses a series of fixed potential pulses of small amplitude (10–100 mV) which are superimposed on a slowly changing base potential as shown in Fig. 1.31.

The current is sampled immediately before each potential pulse is applied (i_a) and immediately before each pulse ends (i_b), and it is the difference between these current responses ($i_b - i_a$), that is used to produce the voltammogram. By sampling the current just before the potential is changed, the effect of the charging current can be decreased.

Chronocoulometry (CC) is one of the classical electrochemical techniques frequently used in electroanalytical chemistry. As its name implies, CC is the measurement of charge (coulombs) as a function of time (chrono). Applications of this technique include measurement of electrode surface area, diffusion coefficients, concentration, kinetics of both heterogeneous electron transfer reactions and chemical reactions coupled to electron transfer, adsorption, and the effective time window of an electrochemical cell. In our particular case, chronocoulometry measurements can help to estimate the accumulated cationic redox marker at the oligonucleotide CNT modified surface as indicative of the hybridization process [237].

In this method a pulse of potential is applied and the response in current is monitored as a function of the time. From the integration of the current profiles versus time, one can obtain the charge (Q_{TOT}). The charge contains information of the double layer charging (at very short times), the charge of the species adsorbed and the charge of the species diffusing at the electrode (longer times) according to the following relation :

$$Q_{TOT} = Q_{dl} + Q_{ads} + Q_{diff} = Q_{dl} + nFA\Gamma_o + \frac{2nFAD_o^{1/2}C_o}{\pi^{1/2}}t^{1/2}$$

The total charge (Q_{TOT}) measured in response to the potential step thus, comes from three sources:

(a) Charge of the double layer (Q_{dl});
(b) Charge of the adsorbed species (Q_{ads});
(c) Charge of the species diffusing at the electrode (Q_{diff}).

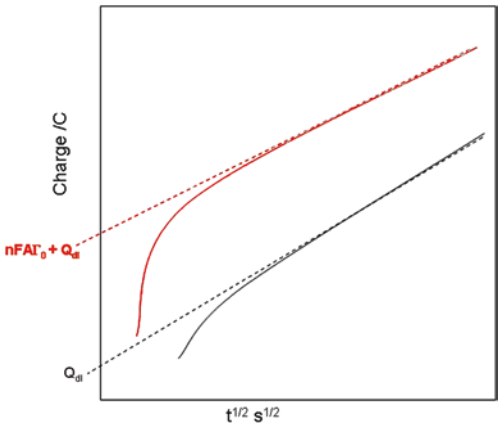

Fig. 1.32 Illustration of the procedure in order to get the amount of electroactive species adsorbed on an electrode, Γo_o The *red curve* represents the chronocoulometric measurements for an electrode immersed in an electrolyte that contains low concentration of electroactive species that can be adsorbed on the electrode surface. The *black curv*e is the chrono measurement in presence of the background electrolyte but in absence of the electroactive species (Color figure online)

F is the Faraday constant (96,500 C), A is the electrode area, n the number of electrons and C_o is the concentration of the redox species at the bulk electrolyte, D is the diffusion coefficient of the species and Γ_o is the amount of adsorbed species at the interface of the electrode.

One of the important applications of CC is the estimation the amount of electroactive species adsorbed on the surface, for which one has first to subtract the double layer charging [237]. To estimate it, chronocoulometric measurements in the background electrolyte (without the presence of the electroactive species that can undergo adsorption on the electrode) are performed. By extrapolation from the linear region of the curve of charge as a function of $t^{1/2}$, one can obtain the ordinate at the origin which corresponds to the double layer charge (Q_{dl}). Then the chrono measurements are performed in presence of the redox markers that can adsorb on the surface. Again, the ordinate of the origin is estimated which comprises the charging of the double layer plus the charge of the adsorbed amount (Γ_o). Therefore, from both measurements one can get the adsorbed amount by Q_{dl} subtraction as shown in Fig. 1.32.

1.4.1.2 Electrochemical Impedance Spectroscopy

Electrochemical Impedance spectroscopy (EIS) is a very versatile tool widely used in different fields (corrosion [238, 239], semiconductor electrodes [240, 241], polymers and coatings [242, 243], batteries and fuel cells [244–246], electrode kinetics and mechanisms [247, 248], biomedical and biological systems [224, 249], solid-state systems [250], etc.). Since EIS turns out to be very sensitive to probe the interfacial properties of a modified electrode, it has become an attractive tool to monitor biorecognition events at the electrode surface [251–253].

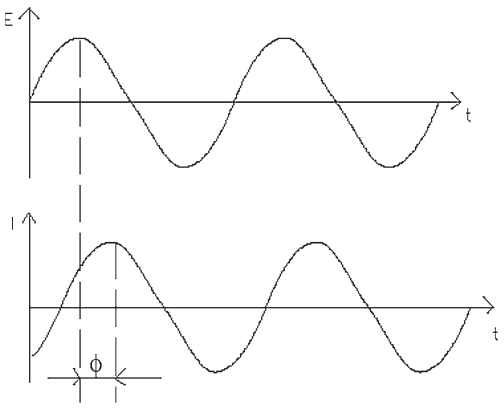

Fig. 1.33 AC excitation signal applied and sinusoidal current response in the system under study

Specifically, EIS allows characterizing the double layer interface at the electrode, the physicochemical processes of a widely differing time constants, sampling electron transfer at high frequencies and mass transfer at low frequencies. The processes occurring in the electrochemical cell can be modelled by using combination of resistors and capacitors (equivalent circuits) [254]. The experimental spectra can be fitted with the use of equivalent circuits and obtain the values of electrical parameters such as resistances, capacitances, etc., which characterize the electrochemical interface.

Voltammetry or amperometry involve measuring the direct current (DC) current at an electrode as a function of applied electrode-solution voltage. In contrast, electrochemical impedance (Z) is based on the collection of an alternating current (AC) resulting from applying a sinusoidal potential (E_t) of small amplitude (typically 10 mV).

Suppose that we apply a sinusoidal potential excitation E_t:

$$E_t = E_0 \cdot \sin(\omega \cdot t)$$

where E_t is the potential at time t, E_0 is the amplitude of the signal, and $\omega = 2\pi f$ is the radial frequency; f is the frequency expressed in Hertz (Hz).

The response to this potential is an AC current signal with a current intensity I_t also depending on t, with the same frequency but with an amplitude I_0 and a phase angle ϕ depending on the impedance of the system (as represented in Fig. 1.33).

$$I_t = I_0 \cdot \sin(\omega \cdot t + \phi)$$

An expression analogous to Ohm's law allows us to calculate the impedance of the system, expressed in terms of a magnitude Z_0, and a phase shift ϕ

$$Z = \frac{E_t}{I_t} = \frac{E_0 \cdot \sin(\omega \cdot t)}{I_0 \cdot \sin(\omega \cdot t + \phi)} = Z_0 \cdot \frac{\sin(\omega \cdot t)}{\sin(\omega \cdot t + \phi)}$$

According to Euler's expression:

$$\exp(j\phi) = \cos\phi + j \sin\phi$$

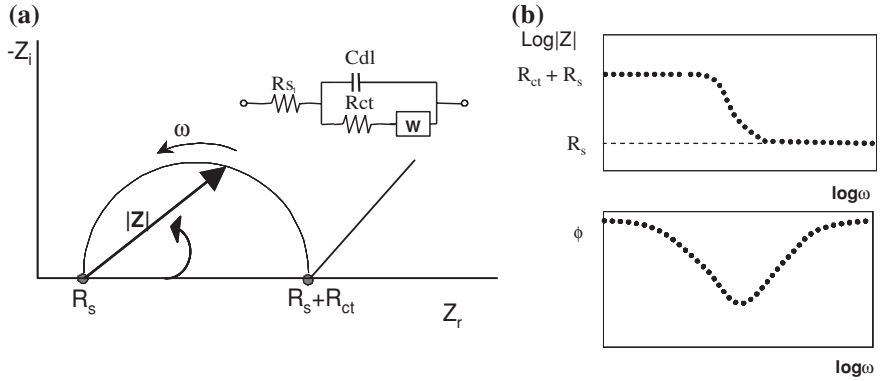

Fig. 1.34 Different representations of the impedance data. **a** Nyquist plot representing the impedance vector in the complex plane; **b** bode diagrams and the typical equivalent circuit at the electrochemical interface (Randles circuit)

A common way to represent the impedance vector model is to use complex notation:

$$E(t) = E_0 \cdot \exp(j\omega \cdot t)$$

$$I(t) = I_0 \cdot \exp(j\omega \cdot t - j\phi)$$

Impedance then is represented as:

$$Z = \frac{E}{I} = Z_0 \exp(j\phi) = Z_0 (\cos\phi + j \sin\phi) = Z_r + jZ_i$$

where Z_r is the real part of the impedance and Z_i the imaginary part.

There are many ways to plot impedance data. One of the more common impedance representations is the 'Nyquist plot' in which the imaginary part or the impedance is plotted versus the real part. It provides visual insight into the system dynamics at the electrochemical interface. As shown in Fig. 1.34, such plot exhibits a kind of semicircle profile plus a linear region. The points at which the impedance data cut the real impedance axe, represent resistance values. In the typical plot of the figure R_{ct} is the charge-transfer resistance, which is inversely proportional to the rate of electron transfer and consequently provides us information about the easiness for electron transfer at the electrode interface (a rough estimation of R_{ct} is related with the width of the semicircle); C_{dl} is the double-layer capacitance and can be obtained from the maximum value of the imaginary part of impedance at the semicircle; R_s is the electrolyte resistance and can be extracted from impedance data at the higher frequencies; W is the Warburg impedance and is identified with the linear portion of the impedance spectra that appears at the lower frequencies. The Warburg impedance arises from mass-transfer limitations between the solution and electrode surface and can be used to measure effective diffusion coefficients. It can be modelled as a

frequency dependent reactance with equivalent real and imaginary components $W = \sigma \cdot (\omega)^{\frac{1}{2}} \cdot (1 - j)$ where ω = radial frequency and σ = Warburg coefficient (constant for a defined system).

Another way to represent the impedance results is by using the 'Bode diagram' where the modulus of the impedance (Log|Z|) and the phase angle (ϕ) between the AC potential and the AC current as a function of the frequency (log ω) are plotted (Fig. 1.34). In this diagram, the impedance data which are frequency independent represent the behaviour of the resistive processes (phase angles close to 0) whereas the ones that are dependent on the frequency are more related to capacitive or diffusive processes (phase angles between −90° or −45° respectively). Thus the impedance spectra can give us a broad overview of the different processes taking place at the electrochemical interface (capacitive, resistive, diffusion effects) and which one is dominating more at a specific range of frequencies.

It has long been recognized that the impedance of solid electrodes usually deviates from purely capacitive behaviour; this is empirically modelled as a constant phase element (CPE) [255, 256]. The complex impedance of a CPE is given by:

$$\frac{1}{Z_{CPE}} = (j\omega)^n C$$

where ω is the radial frequency (expressed in rad s^{-1}), C condenser capacitance and $0.5 < n < 1$ ($n = 1$ corresponds to the ideal capacitor and $n = 0.5$ corresponds to a Warburg element).

The use of CPE elements is widely extended in the experimentalists since capacitors often do not behave ideally and can be explained mathematically by dispersion in local capacitance values. Microscopic roughness can cause this effect [257], but microscopic chemical inhomogeneities and ion adsorption play an even larger role [258–260]. Solid electrodes can be expected to have a certain amount of CPE behaviour, and thus modelling the electrode-solution interface as purely capacitive is often simplistic and can reduce the quality of data fitting.

1.4.1.3 Electric Field Detection

Electronic detection based on electric field is quite promising for the bio-world since most biological processes involve electrostatic interactions and charge transfer which can be sensitively captured by FET devices, enhancing at the same time the merging of biology and electronics. Under this context, we have mentioned before that the CNT-FET configuration specifically holds promise for the development of (bio)chemical sensors since the semiconducting CNTs behave as conducting channels in the transistor approach, in direct contact with the environment and with all the current flowing at the surface of the tubes. All these features make the conductance of these devices be extremely sensitive to very small changes in the environment and to the interaction with chemical and biological species.

Many papers can be found in literature in which the capabilities of CNT-FETs have been explored. The devices have been found to be sensitive to different gases

such as NH_2 or NO_2 [261] and due to size compatibility of the nanoscale devices, they have also shown to be very appropriate for single (bio)molecule detection [262].

As also pointed out before, one can get two different device architectures, one based on an individual CNT or on a random CNT network. On the former type of device, some irreproducibilities can be obtained from device to device due to the geometry-dependent variation in the electronic characteristics of individual nanotubes or in variations of the Schottky barriers. In the latter configuration, current flows along several conducting channels that determine the overall device conductance. In this architecture the device operation depends upon the density of nanotubes and also on the extent of metallic nanotubes which do not exert conductance modulation. However, the advantage of such device, though less sensitive than single nanotube devices, resides in the fact that they offer more reproducibility and manufacturability.

The presence of an immobilized biomolecule or the reaction between biomolecules (ligand-receptor) can be monitored in real-time by examining the conductance change in the device. The technique can become sensitive enough to follow conformational changes of biomolecules or to capture electronic data that may produce electronic signatures specific to a biological process. This technique can be termed as a label-free methodology with detection limits that can be down to the picomolar range. Indeed, one can consider that the CNT in the FET can act a "channel modulation label" to sense changes in their immediate environment.

Although a big amount of biosensing studies has been carried out by using carbon nanotube transistors, the physical mechanism behind the sensing process is still not so clear and the lack of a good understanding of the sensing mechanism can hamper the further exploitation of these promising nanosensors. Following, it will be shown how one can use the $I–V_G$ curves as a tool to illustrate the changes in the CNT conductance profile from the interaction of (bio)chemical species with the CNT-FET. The evaluation of the I/V_G profiles can give insights of the different mechanisms that could take place when using CNT-FETs. In Fig. 1.35a we can see the change of the current as a function of V_G in the case of electrostatic gating by adsorbed species on the CNT. Such species can induce a partial charge transfer or doping in the CNT and thus shifting the I/V_G curve. For instance, the adsorption of positively charged species induces additional negative charge in the SWNT, thus producing n-doping in the SWNT and shifting the I/V_G curve towards more negative voltages. The opposite holds for negatively charged adsorbents.

Figure 1.35b shows that during the interaction with (bio)chemical species changes in the Schottky barrier at the metal/CNT contacts can be produced. Adsorbed species at the contacts can modulate the local work function of the contacts and thus the band alignment or bending.

Figure 1.35c shows the effect of a reduced gate efficiency which may occur when the gate capacitance is reduced due to low permittivity ε of adsorbed biomolecules relative to the electrolyte. However, this effect can become only important in case of near-full coverage of the CNT by the species and under the disputable assumption that ions cannot permeate through the adsorbed biomolecular layer.

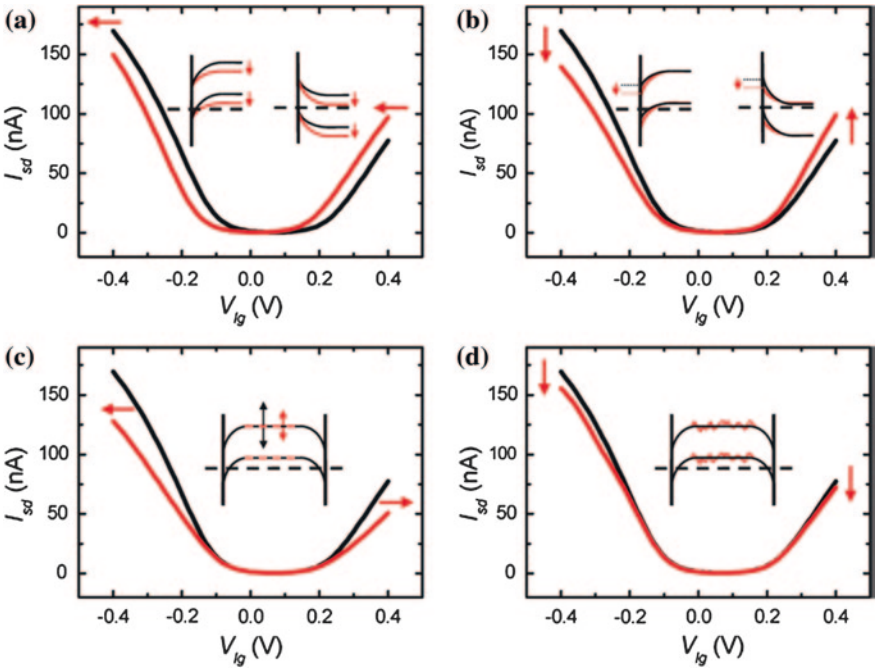

Fig. 1.35 Calculated I–V_G curves before (*black*) and after (*red*) protein adsorption for four different sensing mechanisms. The bias voltage is 10 mV. **a** Electrostatic gating effect corresponding to a shift of the semiconducting bands downward; **b** Schottky barrier effect that corresponds to a change of the difference between metal and CNT work function; **c** capacitance mechanism for 90 % coverage of CNT with protein; **d** mobility mechanism that corresponds to a mobility reduction of charge carriers to a mere 2 % of the initial value. Reprinted wit permission from Ref. [263]. Copyright (2008) American Chemical Society

Finally, Fig. 1.35d shows the effect of reduced carrier mobility by adsorption of species which produce scattering centres. That effect induces conductance suppressing in both p and n-branches [154, 263].

So far we have presented different processes that can induce changes in the characteristics of the CNT-FET device. However, the experimental identification of the sensing mechanisms according to these features is not trivial and a certain ambipolar character of the FET is important to distinguish unequivocally the sensing mechanism, a feature that sometimes is not easy to get.

Another important issue for design and applications of CNT sensors is related with the region of the device where (bio)molecule adsorption causes significant conductance changes. There have been some reports which suggest that the work function modulation is the dominant sensing mechanism. That implies that the sensitive region is limited to the nanoscale contact regions. However, there have also been some papers that also clearly indicated that in addition, strong electrostatic gating reliably occurs along the bulk of CNT channel. This latter issue has been confirmed by passivating the contacts with some insulating layer made from polymethylmethacrylate (PMMA).

Some authors claim that the most common mechanisms can be explained by a combination of electrostatic gating and Schottky barrier effects.

As mentioned in previous section, the typical gate configuration for CNT-FET biosensors is based on a bottom gate configuration which is usually operated under dry conditions. In such device, incubation and specific binding of chemical or biological entities is performed in physiological conditions. Then, the removal of weakly bound species is performed by thorough washing steps and finally, the acquisition of the sensor response is taken in dry conditions. Another configuration is the liquid-gate transistor in which the entire device is immersed and operated in buffer solution with a nearby reference electrode also immersed in the liquid which is held at a desired gate voltage. This kind of configuration allows following up in situ and in real time the (bio)chemical interactions or (bio)recognition processes in a friendly environment for the (bio)molecules in contrast to the dry conditions. The operating voltage regime for liquid-gate needs to be confined away from any electrochemical side reactions and normally the gate potential range is much narrower than in the case of the back-gate FET but the transconductance of FETs in liquids is much higher which make them more sensitive.

Another critical point in the CNT-FET (bio)sensors is the Debye length (λ_D). The Debye length is the typical distance required for screening the surplus charge by the mobile carriers present in a material (is the characteristic thickness of the double layer formed at the conducting CNT channel). The CNT-FET can only be sensitive to the detection of a (bio)molecule interaction or biorecognition event if such processes are taken place inside the Debye length. The thickness of the Debye length varies as the inverse square root of the ionic strength (I). For this reason, it results very important to adjust the ionic strength conditions. Figure 1.36 shows a hybridized DNA strand and the Debye length (as a function of the ionic strength) and how it scales with the length of biomolecule. By decreasing the ionic strength, the Debye length is bigger and the hybridization process can be detected in a major extent [264].

Thus, the issue with the Debye length restricts the detection to the size of the biomolecule or to the distance at which the biorecognition event is taken place. For instance, some authors have found that in some cases, the electronic protein detection based on an antigen/antibody protocol is not so sensitive because the immune-recognition process exceeds the limits of the Debye length. In such cases the lack of sensitivity has been overcome by using aptamers. Figure 1.37 shows an scheme showing such effect.

1.4.2 Surface Characterization: SEM, TEM, AFM

Microscopes have changed the way we approach the micro/nanoscopic world and analyse surface phenomena in physics, chemistry, biology, biochemistry and engineering. First designed as techniques to image surfaces with unprecedented spatial resolution, they have extended their capabilities to follow atomic and (bio)molecular processes in different environments and to probe local chemical and physical

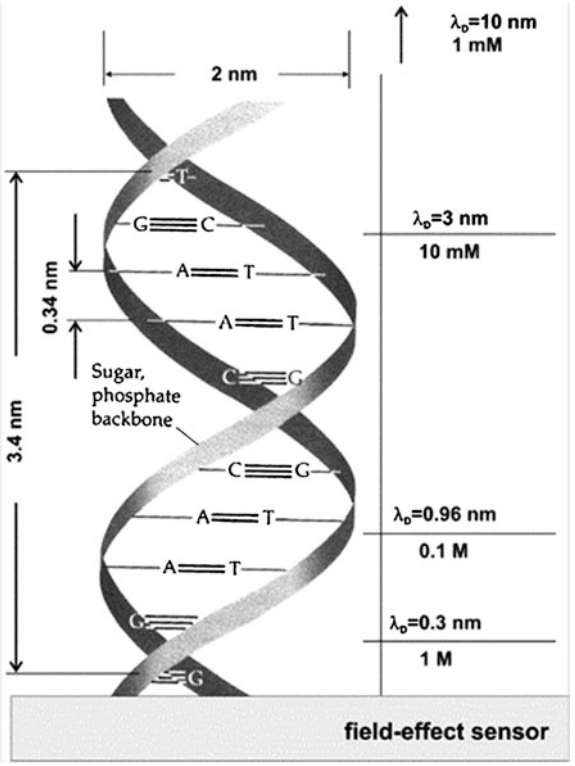

Fig. 1.36 Illustration showing the changes of the Debye length as a function of the ionic strength and in comparison with a double strand DNA

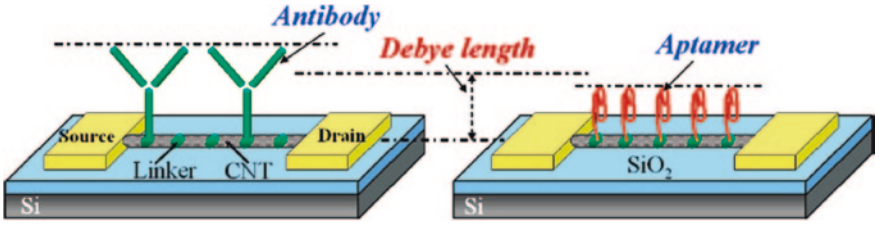

Fig. 1.37 Schematic representation of label-free protein biosensors based on CNT-FETs: **a** antibody-modified CNT-FET, **b** aptamer modified CNT-FET. It can be observed that in case (**a**) the antibody is much larger in size than the Debye length. In such case the charges of the bound protein may be screened by the double layer and their effect on the equilibrium carrier distribution would then vanishingly small. On the other hand, aptamers enable sensitive detection possibilities, partly derived from their small size. Reproduced from Ref. [264]

properties, producing a wealth of related techniques. They have also evolved from a qualitative technique to a more quantitative one [265].

In few lines, the surface characterization techniques used to follow all the studies of this thesis work such as Scanning Electron Microscopy, Transmission Electron Microscopy and Atomic Force Microscopy have been described.

1.4.2.1 Scanning Electron Microscopy

Scanning Electron Microscopy (SEM) is one of the most versatile methods for observation and characterization of heterogeneous organic and inorganic materials on a nanometre (nm) to micrometer (μm) scale. In SEM, an electron beam is moved in a raster pattern across the surface of a sample or is static to obtain an analysis at one position. The beam interacts with the sample surface, producing a number of different signals (secondary electrons, backscattered electrons, characteristic X-rays and other photons of various energies), which after amplification can be analysed to provide useful information about surface topography, composition, crystallography, etc. The imaging signals of greatest interest are the secondary and backscattered electrons (BSE) because these vary primarily as a result of differences in surface topography or provide information about the distribution of different elements in the sample (the intensity of the BSE signal is strongly related to the atomic number of the specimen). The analysis of the characteristic x-radiation emitted from samples can yield both qualitative identification and quantitative elemental information from regions of a specimen nominally 1 μm in diameter and 1 μm in depth under normal operating conditions [Energy-dispersive X-ray spectroscopy (EDS)]. Electromagnetic lenses are used to focus and deflect the electron beam. The primary motivation for using SEM instead of light microscopy is related to the fact that electrons have a much shorter wavelength than light (higher resolution) obtaining topographic images in the magnification ranges 10–10,000X and that SEM uses a larger focal length (greater depth of focus) yielding a characteristic three-dimensional appearance useful for understanding the surface structure of a sample [266, 267].

Scanning electron microscopy and sometimes combined with other techniques which help to gain resolution, is used to determine impurities such as amorphous carbon or catalyst particles that coexist with bundles of SWNTs in the sample.

For instance, Fig. 1.38 shows a SEM image of non-purified MWNTs material in the form of spaghetti grown with the CVD technique. Next to the nanotubes, the bright spots indicate the presence of catalyst particles in the sample.

1.4.2.2 Transmission Electron Microscope

In a conventional transmission electron microscope, a thin specimen is irradiated with an electron beam (acceleration voltage 100–300 keV) of uniform current density. Under high vacuum, electrons interact strongly with the specimen as it passes through by elastic and inelastic scattering. The specimen must therefore be very thin, typically of the order of 5–100 nm for 100 keV electrons, depending on the density and elemental composition of the object and the resolution desired.

Electrons are emitted in the electron gun by thermionic, Schottky, or field emission. A three or four-stage condenser lens system permits variation of the

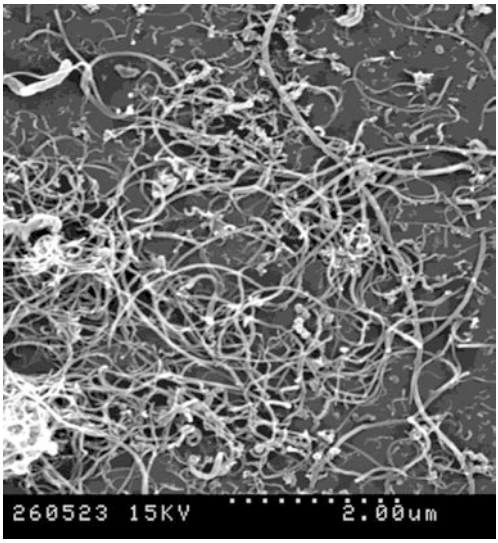

Fig. 1.38 SEM image of non- purified MWNTs (as-prepared)

illumination aperture and the area of the specimen illuminated. Because the TEM is a multiple lens system, the electron intensity distribution behind the specimen is imaged with three to eight lenses, onto a fluorescent screen. The image can be recorded by direct exposure of photographic emulsion or an image plate inside the vacuum, or digitally via fluorescent screen coupled by a fibre-optic plate to a CCD camera [268].

The aberrations of the objective lens are so great that it is necessary to work with very small objective apertures (10–25 mrad) to achieve resolution of the order of 0.1–0.3 nm. This small resolution has proved extremely valuable in the examination of biological ultra-structures such as DNA and viruses, and the structure of materials such as grain boundary properties in metallic specimens, and failures in semiconductor devices.

Crystalline materials diffract electrons due to their short wavelengths. A parallel beam of electrons passing through a regular spaced crystal lattice in the sample holder of a TEM will form a diffraction pattern in the back focal plane of the objective lens. This can be projected onto a viewing screen or recorded on film for measurement. Study of these diffraction patterns is very useful to explain the structure of materials. As well as SEM, TEMs are equipped with elemental analysis capabilities.

Transmission electron microscopy is a useful tool for our work because can determine whether the nanotubes are single-layer or multilayer, characterize lengths and diameters and identify the presence of catalyst particles, amorphous carbon or structural defects in the nanotubes grown.

As an example, in Fig. 1.39a we observe different MWNTs. In addition to nanotubes, catalyst particles can be observed as black dots in the picture. In picture b), we observe a catalyst particle covered by graphitic layers.

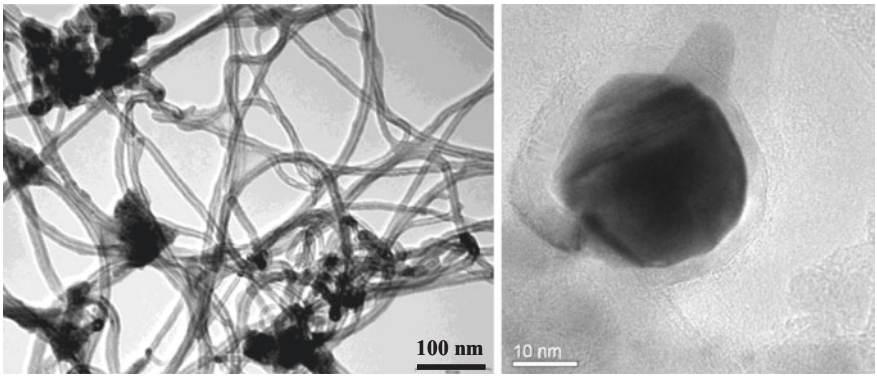

Fig. 1.39 **a** TEM image of as-prepared MWNTs; **b** catalyst particle covered by graphitic layers

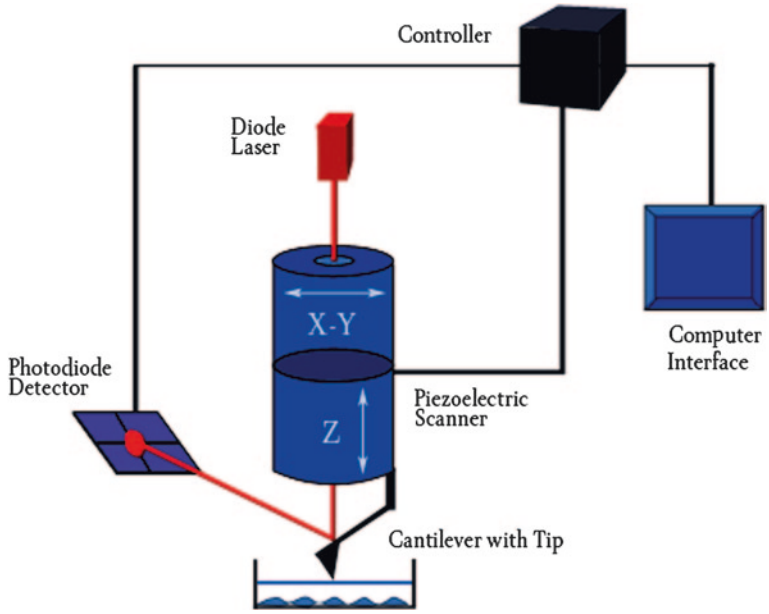

Fig. 1.40 AFM operation. The interactions between atoms in the tip and atoms of the surface can be monitored by controlling the oscillations of the cantilever through the deviation of a laser beam whose reflection impacts on a photodetector

1.4.2.3 Atomic Force Microscopy

The principle of AFM relies on the use of a tip mounted on a cantilever which is brought into close proximity to the surface where intermolecular forces acting between tip and sample cause the cantilever to bend (Fig. 1.40). The system cantilever plus tip, is connected with a xyz piezoelectric element and is moved line

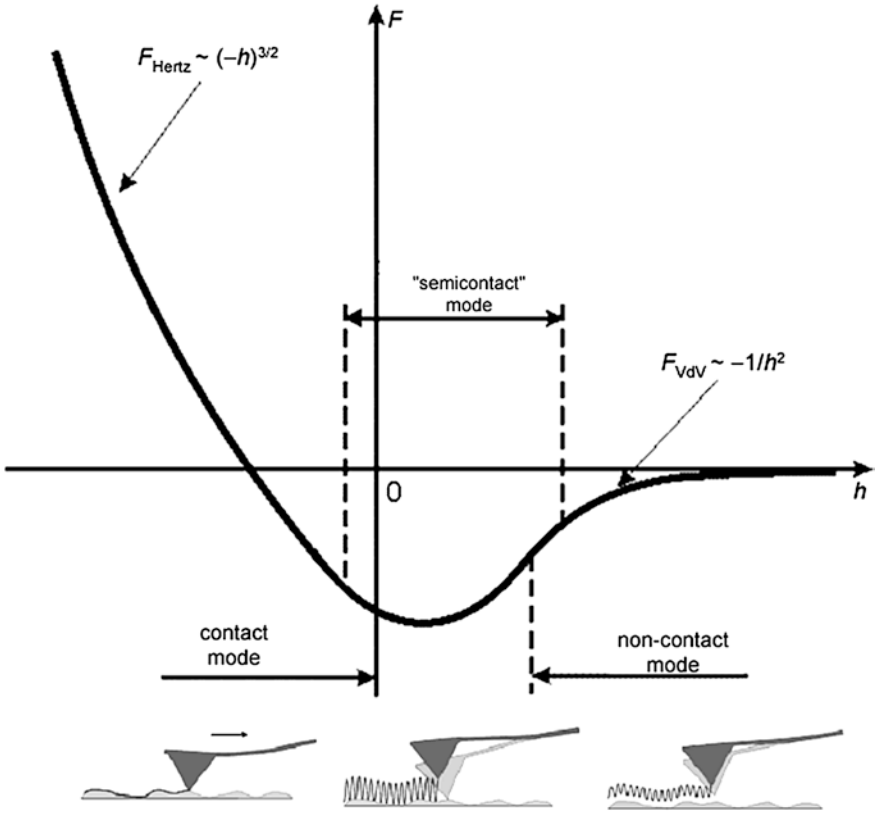

Fig. 1.41 Different modes of operation of an AFM reflected in a curve of force versus distance. Non-contact mode (attractive forces), intermittent mode or "semicontact" mode (forces of attraction/repulsion) and contact mode (repulsive forces)

by line over the sample surface. In order to detect the bending, which is as small as 0.01 nm, a laser beam is focused on the back of the cantilever. From there, the laser beam is reflected towards a position-sensitive photodetector. Depending on the cantilever deflection, the position of the reflected beam changes. The photodetector converts this change in an electrical signal which gives the topographic image of the surface. This technique can also achieve very good spatial resolution (*x*, y: 2–10 nm, z: 0.1 nm) and resolve interaction forces with piconewton sensitivity.

There are several types of forces that can be registered: Van der Waals forces, repulsive forces, magnetic, electrostatic forces, etc. There are also different ways to register these forces, either by non-contact between tip and sample (where mainly attractive forces are measured), by intermittent contact with the sample (where both forces attraction and repulsive are measured) or by full contact between tip and sample (where repulsive forces are measured) (Fig. 1.41).

The first development of the AFM was based on measuring the repulsive forces by contacting the sample with the tip. Since in this standard operating mode the tip is mechanically in contact with the surface, lateral forces are also present and exert a torsional movement of the cantilever as the tip scans the surface. This information can be also collected since the photodetector is a quadrant which measures both normal cantilever bending (due to topographic effects) and torsion. Thus, lateral forces, usually due to differences in friction forces on the sample, can be measured with AFM simultaneously with the topographic images.

The dragging motion of the tip in contact AFM, combined with adhesive and lateral forces, can cause substantial damage to soft samples. To alleviate this problem, dynamic AFM modes, in which the topography is monitored by the changes in the oscillation of a vibrating tip, are preferable [269] (e.g. non-contact or intermittent contact AFM mode). Very quickly, it was realized that the dynamic AFM modes could bring about additional valuable information. The existence of several parameters such as the oscillation amplitude, frequency and phase shift which are sensitive to the tip-sample interactions could be used to extract quantitative and qualitative information about material properties at nanometre scale. This sophistication was even increased by applying bias potential between tip and sample and by using AFM tips of a different nature.

The main advantages of AFM are: the capacity to work in air, vacuum and liquid medium (for biological samples), and analyse both insulating materials and conductors of electricity, in addition to allowing dynamic monitoring of physicochemical and biological processes in situ.

As stated, AFM provides topographical information; as an example, the AFM is very useful to visualize isolated nanotubes grown directly on silicon substrates by CVD method. Although the resolution is not as high as the one found with the TEM, the diameter can be estimated fairly accurately measuring the heights of the CNTs; one can also measure the lengths of the nanotubes, metal particles and to observe the distribution of disordered forms of carbon. Thus, the atomic force microscopy is an important tool in the investigation of nanotubes.

Figure 1.42 shows 2 μm $\times$ 2 μm acquired AFM topographic images where the height of an individual single-walled carbon nanotube is estimated, few nanometres, grown on silicon substrate by the CVD technique. The diameter of the particle catalyst, 3–6 nm, is also observed.

As anticipated and beyond topographic information, the AFM can access local physiochemical properties at the nanometre scale depending on the mode of operation and the nature of the tip. For example one can acquire information about the mechanical properties (adhesion, elasticity, friction), magnetic and electronic of the sample. One can also infer chemical properties. Note that the AFM can not provide chemical microanalysis determining elements or the nature of the composition of a sample as in the case of SEM and TEM but in some cases can infer chemical properties.

By using the AFM in the current sensing mode, conductance mappings of surfaces are also performed. This technique consists in the use of a conductive tip operating in standard contact mode. As a voltage is applied between tip and

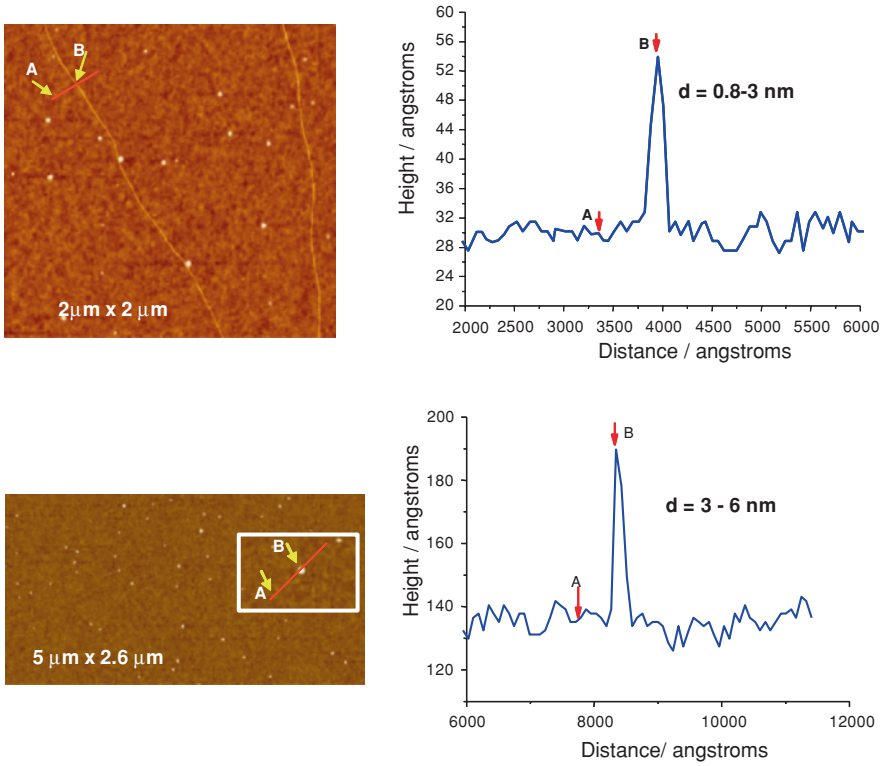

Fig. 1.42 AFM images and topographic profiles where the diameter of a nanotube and a catalyst particle are estimated

sample, a current is generated, the intensity of which will depend on the sample nature. Thus, a map of current distribution along the sample is measured simultaneously with the surface topography (Fig. 1.43).

Current sensor mode is suitable for samples with low conductance or composite materials containing insulating regions. This sensor mode has been an interesting tool for characterizing the different phases and their distributions in the composite fabrication.

1.4.3 Other Characterization Techniques: Raman, XPS

Other characterization techniques have been used in order to have more insights on the structural characteristics of the nanotubes, electrodes, or to verify functionalization strategies on carbon nanotubes. These are Raman spectroscopy and X-ray photoelectron spectroscopy (XPS).

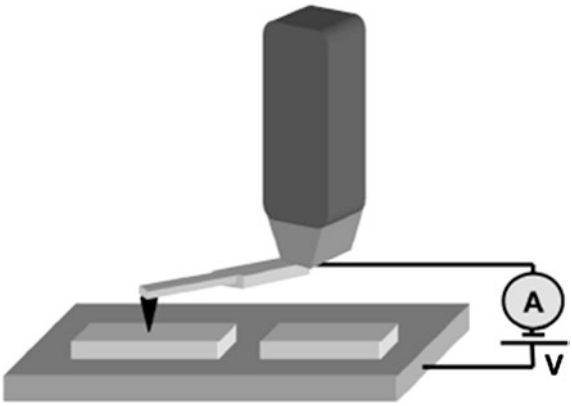

Fig. 1.43 Current sensor mode scheme

1.4.3.1 Raman Spectroscopy

Raman spectroscopy is a spectroscopic technique used to study vibrational, rotational, and other low-frequency modes in a system [270]. It relies on inelastic scattering of monochromatic light, usually from a laser in the visible, near infrared, or near ultraviolet range.

The laser light interacts with molecular vibrations or phonons which make the energy of the laser photons shift up or down. The shift in energy gives information about the vibrational modes in the system and becomes a complementary tool of infrared spectroscopy.

The Raman effect occurs by interaction of radiation with the electron cloud and the bonds of molecules or crystal. It can be explained as follows, when radiation impinges on the sample, the molecule is photoexcited from the ground state to a virtual energy state. When the molecule relaxes it emits a photon and it returns to a different rotational or vibrational state. The difference in energy between the original state and this new state leads to a shift in the emitted photon's frequency away from the excitation wavelength. If the final vibrational state of the molecule is more energetic than the initial state, then the emitted photon will be shifted to a lower frequency so that the total energy of the system remains balanced. This shift in frequency is designated as a Stokes shift. If the final vibrational state is less energetic than the initial state, then the emitted photon will be shifted to a higher frequency, and this is designated as an Anti-Stokes shift. Raman scattering is an example of inelastic scattering because of the energy transfer between the photons and the molecules during their interaction.

To exhibit Raman effect in molecules, a change in the molecular polarization potential—or amount of deformation of the electron cloud—with respect to the vibrational coordinate is required. The amount of the polarizability change will determine the Raman scattering intensity. The pattern of shifted frequencies is determined by the rotational and vibrational states of the sample.

Ramon is a very useful technique to characterize CNTs. For instance, Raman spectra present different features being all sensitive to (n, m), such as the radial

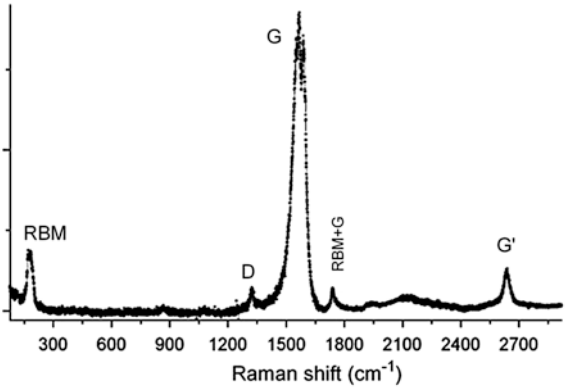

Fig. 1.44 Raman spectrum of well-dispersed single-wall carbon nanotubes (Hipco): *RBM* radial breathing mode, *D* D mode, *G* G mode, *RMB* + *G* combination of RBM and G modes, G' double-phonon scattering of the D mode

breathing mode (RBM), where all the carbon atoms are moving in-phase in the radial direction, the G-band where neighbouring atoms are moving in opposite directions along the surface of the tube as in 2D graphite, the dispersive disorder induced D-band and its second-order related harmonic G'-band. The so-called G-band, around $1{,}580\text{cm}^{-1}$, is a characteristic feature of the graphitic layers. The second characteristic mode is a typical sign for defective graphitic structures (D-band, around 1,350 cm^{-1}). The comparison of the ratios of these two peaks intensities gives a measure of the quality of the bulk samples. If these both bands have similar intensity this indicates a high quantity of structural defects. Therefore, I_D/I_G ratio was extracted as a parameter to determine the structural quality of the carbon materials.

One important feature in the Raman spectrum of SWNT is the Radial Breathing Mode (RBM), which is usually located between 75 and 300 cm^{-1} from the exciting line; an illustration of the spectrum resulting from this mode is displayed in the Fig. 1.44. The frequency of the RBM is very sensitive to the diameter of the nanotubes being directly linked to the reciprocal of the nanotube diameter (d_t) and is expressed as $\varpi_{\text{RBM}} = \text{C}/d_t$ (cm^{-1}) ($\text{C} = 248$ cm^{-1} for isolated SWNTs on a SiO_2 substrate [271]). However, non isolated SWNTs are subject to inter-tube interactions which increase the frequency of the RBM [65, 272–274].

1.4.3.2 Spectroscopy X-ray Photoelectron

Spectroscopy X-ray photoelectron (XPS) is a very sensitive and non-destructive surface technique that provide quantitative information on the chemical status of a system. The sample is irradiated with a monochromatic beam of X-rays (XPS), the photon is absorbed by an atom in a molecule or solid, leading to ionization and the emission of a core (inner shell) electron and the emission energy of the photoelectrons is analysed.

For each and every element, there will be a characteristic binding energy associated with each core atomic orbital i.e. each element will give rise to a characteristic set of peaks in the photoelectron spectrum at kinetic energies determined by the photon energy and the respective binding energies.

The presence of peaks at particular energies therefore indicates the presence of a specific element in the sample under study—furthermore, the intensity of the peaks is related to the concentration of the element within the sampled region. Thus, the technique provides a quantitative analysis of the surface composition and is sometimes known by the alternative acronym, Electron Spectroscopy for Chemical Analysis (ESCA).

With this technique, the empirical formula, chemical state and electronic state of the elements that exist within a material can also be measured.

References

1. Weiss J, Takhistov P, McClements DJ (2006) J Food Sci 71:R107–R116
2. Oberlin A, Endo M, Koyama T (1976) J Cryst Growth 32:335–349
3. Kroto HW, Heath JR, O'Brien SC, Curl RF, Smalley RE (1985) Nature 318:162–163
4. Iijima S (1991) Nature 354:56–58
5. Endo M, Strano M, Ajayan P (2008) In: Jorio A, Dresselhaus G, Dresselhaus MS (eds) Carbon nanotubes, vol 111. Springer, Berlin, pp 13–61
6. Saito R, Dresselhaus G, Dresselhaus MS (eds) (1998) Physical properties of carbon nanotubes. Imperial College Press, London
7. Louie S (2001) In: Dresselhaus M, Dresselhaus G, Avouris P (eds) Carbon nanotubes, vol 80. Springer, Berlin, pp 113–145
8. Ouyang M, Huang J-L, Lieber CM (2002) Acc Chem Res 35:1018–1025
9. Avouris P (2002) Acc Chem Res 35:1026–1034
10. Balasubramanian K, Burghard M (2005) Small 1:180–192
11. Wildöer JWG, Venema LC, Rinzler AG, Smalley RE, Dekker C (1998) Nature 391:59–62
12. Odom TW, Huang JL, Kim P, Lieber CM (1998) Nature 391:62–64
13. Krstić V, Roth S, Burghard M (2000) Phys Rev B 62:R16353
14. Kong J, Yenilmez E, Tombler TW, Kim W, Dai H, Laughlin RB, Liu L, Jayanthi CS, Wu SY (2001) Phys Rev Lett 87:106801
15. Heinze S, Tersoff J, Martel R, Derycke V, Appenzeller J, Avouris P (2002) Phys Rev Lett 89:106801
16. Hamon MA, Itkis ME, Niyogi S, Alvaraez T, Kuper C, Menon M, Haddon RC (2001) J Am Chem Soc 123:11292–11293
17. Han J (2005) In: Meyyappan M (ed) Carbon nanotubes: science and applications. CRC Press, London, p 1
18. Srivastava D (2005) In: Meyyappan M (ed) Carbon nanotubes: science and applications. CRC Press, London, p 25
19. Stone AJ, Wales DJ (1986) Chem Phys Lett 128:501–503
20. Roh S, Lee J, Jang M (2010) J Nanomater 2010:6
21. Liew KM, He XQ, Wong CH (2004) Acta Mater 52:2521–2527
22. Duplock EJ, Scheffler M, Lindan PJD (2004) Phys Rev Lett 92:225502
23. Picozzi S, Santucci S, Lozzi L, Valentini L, Delley B (2004) J Chem Phys 120:7147–7152
24. Dresselhaus MS, Dresselhaus G, Avouris P (eds) (2001) Carbon nanotubes: synthesis, structure, properties, and applications, vol 80. Springer, Berlin
25. Suenaga K, Wakabayashi H, Koshino M, Sato Y, Urita K, Iijima S (2007) Nat Nano 2:358–360
26. Salvetat J-P, Briggs GAD, Bonard J-M, Bacsa RR, Kulik AJ, Stockli T, Burnham NA, Forro LL (1999) Phys Rev Lett 82:944
27. Cornwell CF, Wille LT (1997) Solid State Commun 101:555–558
28. Ruoff RS, Lorents DC (1995) Carbon 33:925–930

29. Yu M-F, Files BS, Arepalli S, Ruoff RS (2000) Phys Rev Lett 84:5552
30. Yu M-F, Lourie O, Dyer MJ, Moloni K, Kelly TF, Ruoff RS (2000) Science 287:637–640
31. Demczyk BG, Wang YM, Cumings J, Hetman M, Han W, Zettl A, Ritchie RO (2002) Mater Sci Eng, A 334:173–178
32. Shen W, Jiang B, Han BS, Xie S–S (2000) Phys Rev Lett 84:3634
33. Mitchell LA, Gao J, Wal RV, Gigliotti A, Burchiel SW, McDonald JD (2007) Toxicol Sci 100:203–214
34. Niyogi S, Hamon MA, Hu H, Zhao B, Bhowmik P, Sen R, Itkis ME, Haddon RC (2002) Acc Chem Res 35:1105–1113
35. Chen Z, Thiel W, Hirsch A (2003) ChemPhysChem 4:93–97
36. Burghard M (2005) Surf Sci Rep 58:1–109
37. McCreery RL (2008) Chem Rev 108:2646–2687
38. McCreery RL (1991) In: Bard AJ (ed) Electroanalytical chemistry, vol 17. Dekker, New York, 1991
39. Merkoçi A (2006) Microchim Acta 152:157–174
40. Wang J (2005) Electroanalysis 17:7–14.
41. Pumera M, Sánchez S, Ichinose I, Tang J (2007) Sens Actuators B Chem 123:1195–1205
42. Agüí L, Yáñez-Sedeño P, Pingarrón JM (2008) Anal Chim Acta 622:11–47
43. Heller I, Kong J, Williams KA, Dekker C, Lemay SG (2006) J Am Chem Soc 128: 7353–7359
44. Gooding JJ, Wibowo R, Liu JQ, Yang W, Losic D, Orbons S, Mearns FJ, Shapter JG, Hibbert DB (2003) J Am Chem Soc 125:9006–9007
45. Nugent JM, Santhanam KSV, Rubio A, Ajayan PM (2001) Nano Lett 1:87–91
46. Moore RR, Banks CE, Compton RG (2004) Anal Chem 76:2677–2682
47. Banks CE, Davies TJ, Wildgoose GG, Compton RG (2005) Chem Commun 7:829–841
48. Banks CE, Compton RG (2006) Analyst 131:15–21
49. Wildgoose GG, Banks CE, Leventis HC, Compton RG (2006) Microchim Acta 152:187–214
50. Banks CE, Crossley A, Salter C, Wilkins SJ, Compton RG (2006) Angew Chem Int Ed 45:2533–2537
51. Gooding JJ (2005) Electrochim Acta 50:3049–3060
52. Gooding JJ, Lai LMH, Goon IY (2009) In: Alkire RC et al (eds) Chemically modified electrodes. Wiley-VCH, Weinheim, pp 1–56
53. Yu X, Chattopadhyay D, Galeska I, Papadimitrakopoulos F, Rusling JF (2003) Electrochem Commun 5:408–411
54. Banks CE, Ji X, Crossley A, Compton RG (2006) Electroanalysis 18:2137–2140
55. Chou A, Böcking T, Singh NK, Gooding JJ (2005) Chem Commun 7:842–844
56. Misewich JA, Martel R, Avouris P, Tsang JC, Heinze S, Tersoff J (2003) Science 300:783–786
57. Chen J, Perebeinos V, Freitag M, Tsang J, Fu Q, Liu J, Avouris P (2005) Science 310:1171–1174
58. Freitag M, Martin Y, Misewich JA, Martel R, Avouris P (2003) Nano Lett 3:1067–1071
59. Itkis ME, Borondics F, Yu A, Haddon RC (2006) Science 312:413–416
60. Star A, Lu Y, Bradley K, Grüner G (2004) Nano Lett 4:1587–1591
61. Miyauchi Y, Oba M, Maruyama S (2006) Phys Rev B 74:205440
62. Iakoubovskii K, Minami N, Kim Y, Miyashita K, Kazaoui S, Nalini B (2006) Appl Phys Lett 89:173108-3
63. Dresselhaus MS, Dresselhaus G, Jorio A (2007) J Phys Chem C 111:17887–17893
64. Heller DA, Barone PW, Swanson JP, Mayrhofer RM, Strano MS (2004) J Phys Chem B 108:6905–6909
65. Oron-Carl M, Hennrich F, Kappes MM, Löhneysen HV, Krupke R (2005) Nano Lett 5: 1761–1767
66. Kim UJ, Furtado CA, Liu X, Chen G, Eklund PC (2005) J Am Chem Soc 127:15437–15445

67. Joselevich E, Dai H, Liu J, Hata K, Windle AH (2008) In: Jorio A, Dresselhaus G, Dresselhaus MS (eds) Carbon nanotubes, vol 111. Springer, Berlin, pp 101–164
68. Shi Z, Lian Y, Liao FH, Zhou X, Gu Z, Zhang Y, Iijima S, Li H, Yue KT, Zhang S-L (2000) J Phys Chem Solids 61:1031–1036
69. Moravsky AP, Wexler EM, Loutfy RO (2005) In: Meyyappan M (ed) Carbon nanotubes: science and applications. CRC Press, London, p 65
70. Meyyappan M (2005) In: Meyyappan M (ed) Carbon nanotubes: science and applications. CRC Press, London, p 99
71. Dai H (2002) Surf Sci 500:218–241
72. Dai H, Rinzler AG, Nikolaev P, Thess A, Colbert DT, Smalley RE (1996) Chem Phys Lett 260:471–475
73. Veronese GP, Rizzoli R, Angelucci R, Cuffiani M, Malferrari L, Montanari A, Odorici F (2007) Phys E Low-Dim Syst Nanostruct 37:21–25
74. Kondo D, Sato S, Awano Y (2006) Chem Phys Lett 422:481–487
75. Song IK, Cho YS, Choi GS, Park JB, Kim DJ (2004) Diamond Relat Mater 13:1210–1213
76. Bower C, Zhou O, Zhu W, Werder DJ, Jin S (2000) Appl Phys Lett 77:2767–2769
77. Meyyappan M et al (2003) Plasma Sources Sci Technol 12:205
78. Ebbesen TW, Ajayan PM, Hiura H, Tanigaki K (1994) Nature 367:519
79. Chattopadhyay D, Galeska I, Papadimitrakopoulos F (2002) Carbon 40:985–988
80. Rinzler AG, Liu J, Dai H, Nikolaev P, Huffman CB, Rodríguez-Macías FJ, Boul PJ, Lu AH, Heymann D, Colbert DT, Lee RS, Fischer JE, Rao AM, Eklund PC, Smalley RE (1998) Appl Phys A Mater Sci Process 67:29–37
81. Zhou O, Shimoda H, Gao B, Oh S, Fleming L, Yue G (2002) Acc Chem Res 35:1045–1053
82. Andrews R, Jacques D, Qian D, Rantell T (2002) Acc Chem Res 35:1008–1017
83. Dillon AC, Gennett T, Jones KM, Alleman JL, Parilla PA, Heben MJ (1999) Adv Mater 11:1354–1358
84. Jurkschat K, Ji X, Crossley A, Compton RG, Banks CE (2007) Analyst 132:21–23
85. Pumera M (2007) Langmuir 23:6453–6458
86. Jones CP, Jurkschat K, Crossley A, Compton RG, Riehl BL, Banks CE (2007) Langmuir 23:9501–9504
87. Swain GM (2006) In: Zoski CG (ed) Handbook of electrochemistry. Elsevier, London, pp 431–469
88. Millan KM, Spurmanis AJ, Mikkelsen SR (1992) Electroanalysis 4:929–932
89. Kang J, Li X, Wu G, Wang Z, Lu X (2007) Anal Biochem 364:165–170
90. Tian Y, Mao L, Okajima T, Ohsaka T (2005) Biosens Bioelectron 21:557–564
91. Wang J, Cai X, Rivas G, Shiraishi H, Farias PAM, Dontha N (1996) Anal Chem 68:2629–2634
92. Millan KM, Saraullo A, Mikkelsen SR (1994) Anal Chem 66:2943–2948
93. Atanasov P, Kaisheva A, Iliev I, Razumas V, Kulys J (1992) Biosens Bioelectron 7:361–365
94. Liu S, Ye J, He P, Fang Y (1996) Anal Chim Acta 335:239–243
95. Karadeniz H, Erdem A, Caliskan A, Pereira CM, Pereira EM, Ribeiro JA (2007) Electrochem Commun 9:2167–2173
96. Pividori MI, Alegret S (2003) Anal Lett 36:1669–1695
97. Santandreu M, Céspedes F, Alegret S, Martínez-Fàbregas E (1997) Anal Chem 69:2080–2085
98. Pereira AC, Aguiar MR, Kisner A, Macedo DV, Kubota LT (2007) Sens Actuators B Chem 124:269–276
99. Wang SG, Zhang Q, Wang R, Yoon SF (2003) Biochem Biophys Res Commun 311:572–576
100. Nuzzo RG, Allara DL (1983) J Am Chem Soc 105:4481–4483
101. Levicky R, Herne TM, Tarlov MJ, Satija SK (1998) J Am Chem Soc 120:9787–9792
102. Paleček E (1996) Electroanalysis 8:7–14
103. Rampi MA, Schueller OJA, Whitesides GM (1998) Appl Phys Lett 72:1781–1783
104. Bryant MA, Pemberton JE (1991) J Am Chem Soc 113:8284–8293

105. Tammeveski K, Kikas T, Tenno T, Niinistö L (1998) Sens Actuators B Chem 47:21–29
106. Burke LD, Lyons MFG (1986) In: White RE, Bockris JOM, Conway BE (eds) Modern aspects of electrochemistry, vol 18. Plenum, New York, pp 169–248
107. O'Sullivan EJM, Calvo EJ (1987) In: Compton RG (ed) Comprehensive chemical kinetics, vol 27. Elsevier, Amsterdam, Chap 3
108. Albery WJ, Bartlett PN (1984) J Chem Soc Chem Commun 4:234–236
109. Brett CMA, Brett AMO (eds) (1993) Electrochemistry: principles, methods, and applications. Oxford Press, Oxford
110. von Sturm F (1988) Angew Chem 100:1260–1261
111. Ruschan GR, Newnham RE, Runt J, Smith E (1989) Sens Actuators 20:269
112. Esplandiu MJ, Baeza M, Olive-Monllau R, Cespedes F, Bartroli J (2011) In: Attaf B (ed) Advances in composite materials for medicine and nanotechnology. InTech, Croatia
113. Godovski DY, Koltypin EA, Volkov AV, Moskvina MA (1993) Analyst 118:997–999
114. Céspedes F, Martinez-Fàbregas E, Alegret S (1996) Trends Anal Chem 15:296–304
115. Céspedes F, Martínez-Fàbregas E, Alegret S (1993) Anal Chim Acta 284:21–26
116. Céspedes F, Martínez-Fàbregas E, Bartrolí J, Alegret S (1993) Anal Chim Acta 273: 409–417
117. Pividori MI, Merkoçi A, Alegret S (2003) Biosens Bioelectron 19:473–484
118. Wang J, Musameh M (2003) Anal Chem 75:2075–2079
119. Zhang M, Smith A, Gorski W (2004) Anal Chem 76:5045–5050
120. Mendoza Gómez E, Orozco J, Jiménez-Jorquera C, González-Guerrero AB, Calle Martín A, Lechuga LM, Fernández Sánchez C (2008) Nanotechnology 19:75102
121. Sánchez S, Pumera M, Fàbregas E (2007) Biosens Bioelectron 23:332–340
122. Pacios M, del Valle M, Bartroli J, Esplandiu MJ (2008) J Electroanal Chem 619–620:117–124
123. Pumera M, Merkoçi A, Alegret S (2006) Sens Actuators B Chem 113:617–622
124. Gong K, Yan Y, Zhang M, Su L, Xiong S, Mao L (2005) Anal Sci 21:1383–1393
125. Gavalas VG, Law SA, Ball JC, Andrews R, Bachas LG (2004) Anal Biochem 329:247–252
126. Zhang B, Xu Y, Zheng Y, Dai L, Zhang M, Yang J, Chen Y, Chen X, Zhou J (2011) Nanoscale Res Lett 6:431
127. Sainz R, Benito AM, Martínez MT, Galindo JF, Sotres J, Baró AM, Corraze B, Chauvet O, Maser WK (2005) Adv Mater 17:278–281
128. Huang J, Li X, Xu J, Li H (2003) Carbon 41:2731–2736
129. Guo M, Chen J, Li J, Tao B, Yao S (2005) Anal Chim Acta 532:71–77
130. Terzic S, Tripkovic D, Jovanovic VM, Tripkovic A, Kowal A (2007) J Serb Chem Soc 72:165–181
131. Jenkins GM, Kawamura K (1971) Nature 231:175–176
132. Milchev A, Zapryanova T (2006) Electrochim Acta 51:4916–4921
133. Merkoçi A, Pumera M, Llopis X, Pérez B, del Valle M, Alegret S (2005) Trends Anal Chem 24:826–838
134. Wang J, Li M, Shi Z, Li N, Gu Z (2002) Anal Chem 74:1993–1997
135. Lawrence NS, Deo RP, Wang J (2005) Electroanalysis 17:65–72
136. Heng LY, Chou A, Yu J, Chen Y, Gooding JJ (2005) Electrochem Commun 7:1457–1462
137. Li J, Cassell A, Delzeit L, Han J, Meyyappan M (2002) J Phys Chem B 106:9299–9305
138. Koehne J, Li J, Cassell AM, Chen H, Ye Q, Ng HT, Han J, Meyyappan M (2004) J Mater Chem 14:676–684
139. Li J, Koehne JE, Cassell AM, Chen H, Ng HT, Ye Q, Fan W, Han J, Meyyappan M (2005) Electroanalysis 17:15–27
140. Lin Y, Lu F, Tu Y, Ren Z (2003) Nano Lett 4:191–195
141. Martin-Fernandez I, Gabriel G, Rius G, Villa R, Perez-Murano F, Lora-Tamayo E, Godignon P (2009) Microelectron Eng 86:806–808
142. Zoski CG (2002) Electroanalysis 14:1041–1051
143. Heinze J (1993) Angew Chem Int Ed Engl 32:1268–1288
144. Arrigan DWM (2004) Analyst 129:1157–1165

145. Fiaccabrino GC, Koudelka-Hep M, Jeanneret S, van den Berg A, de Rooij NF (1994) Sens Actuators B Chem 19:675–677
146. Orozco J, Fernández-Sánchez C, Jiménez-Jorquera C (2010) Sensors 10:475–490
147. Morf WE, de Rooij NF (1997) Sens Actuators B Chem 44:538–541
148. Belmont C, Tercier ML, Buffle J, Fiaccabrino GC, Koudelka-Hep M (1996) Anal Chim Acta 329:203–214
149. Baker WS, Crooks RM (1998) J Phys Chem B 102:10041–10046
150. Ugo P, Moretto LM, Vezzà F (2002) ChemPhysChem 3:917–925
151. Artigas J, Jimenez C, Lemos SG, Nogueira ARA, Torre-Neto A, Alonso J (2003) Sens Actuators B Chem 88:337–344
152. Galán-Vidal CA, Muñoz J, Domínguez C, Alegret S (1997) Sens Actuators B Chem 45:55–62
153. Jessica K et al (2003) Nanotechnology 14:1239
154. Gruner G (2006) Anal Bioanal Chem 384:322–335
155. Tans SJ, Verschueren ARM, Dekker C (1998) Nature 393:49–52
156. Martel R, Schmidt T, Shea HR, Hertel T, Avouris P (1998) Appl Phys Lett 73:2447–2449
157. Derycke V, Martel R, Appenzeller J, Avouris P (2002) Appl Phys Lett 80:2773–2775
158. Cid C (2009) Doctoral thesis. Universitat Rovira i Virgili, Tarragona
159. Baughman RH, Cui C, Zakhidov AA, Iqbal Z, Barisci JN, Spinks GM, Wallace GG, Mazzoldi A, De Rossi D, Rinzler AG, Jaschinski O, Roth S, Kertesz M (1999) Science 284:1340–1344
160. Yun YH, Shanov V, Schulz MJ, Narasimhadevara S, Subramaniam S, Hurd D, Boerio FJ (2005) Smart Mater Struct 14:1526–1532
161. Yun Y, Shanov V, Tu Y, Schulz MJ, Yarmolenko S, Neralla S, Sankar J, Subramaniam S (2006) Nano Lett 6:689–693
162. Hirsch A (2002) Angew Chem Int Ed 41:1853–1859
163. Han W, Fan S, Li Q, Hu Y (1997) Science 277:1287–1289
164. Sloan J, Hammer J, Zwiefka-Sibley M, Green MLH (1998) Chem Commun 3:347–348
165. Dujardin E, Ebbesen TW, Krishnan A, Treacy MMJ (1998) Adv Mater 10:1472–1475
166. Matsui K, Pradhan BK, Kyotani T, Tomita A (2001) J Phys Chem B 105:5682–5688
167. Govindaraj A, Satishkumar BC, Nath M, Rao CNR (1999) Chem Mater 12:202–205
168. Wilson M, Madden PA (2001) J Am Chem Soc 123:2101–2102
169. Smith BW, Monthioux M, Luzzi DE (1999) Chem Phys Lett 315:31–36
170. Tasis D, Tagmatarchis N, Bianco A, Prato M (2006) Chem Rev 106:1105–1136
171. Yang WR, Thordarson P, Gooding JJ, Ringer SP, Braet F (2007) Nanotechnology 18:412001
172. Katz E, Willner I (2004) ChemPhysChem 5:1084–1104
173. Kim SN, Rusling JF, Papadimitrakopoulos F (2007) Adv Mater 19:3214–3228
174. Yin Y, Lü Y, Wu P, Cai C (2005) Sensors 5:220–234
175. Li Y, Lin X, Jiang C (2006) Electroanalysis 18:2085–2091
176. Wang L, Wang J, Zhou F (2004) Electroanalysis 16:627–632
177. Zhao L, Liu H, Hu N (2006) J Colloid Interface Sci 296:204–211
178. Du P, Liu S, Wu P, Cai C (2007) Electrochim Acta 52:6534–6547
179. Zhang L, Zhao G-C, Wei X-W, Yang Z-S (2005) Electroanalysis 17:630–634
180. Zhang L, Zhao G-C, Wei X-W, Yang Z-S (2004) Chem Lett 33:86–87
181. Zhao G-C, Zhang L, Wei X-W, Yang Z-S (2003) Electrochem Commun 5:825–829
182. Zhao G-C, Yin Z–Z, Zhang L, Wei X-W (2005) Electrochem Commun 7:256–260
183. Yin Y, Wu P, Lü Y, Du P, Shi Y, Cai C (2007) J Solid State Electrochem 11:390–397
184. Nelson DL, Lenin MMC (eds) (2000) Principles in biochemistry. Worth Publishers, New York, p 175
185. Roat-Malone RM (ed) (2002) Bioinorganic chemistry. Wiley, New York, pp 158–185
186. Fita I, Rossmann MG (1985) J Mol Biol 185:21–37
187. Murphy L (2006) Curr Opin Chem Biol 10:177–184
188. Armstrong FA, Wilson GS (2000) Electrochim Acta 45:2623–2645

189. Murthy MRN, Reid TJ, Sicignano A, Tanaka N, Rossmann MG (1981) J Mol Biol 152:465–499
190. Jouve H-M, Gouet P, Boudjada N, Buisson G, Kahn R, Duee E (1991) J Mol Biol 221:1075–1077
191. Carot ML, Torresi RM, Garcia CD, Esplandiu MJ, Giacomelli CE (2010) J Phys Chem C 114:4459–4465
192. He P, Xu Y, Fang Y (2006) Microchim Acta 152:175–186
193. Drummond TG, Hill MG, Barton JK (2003) Nat Biotech 21:1192–1199
194. Wang J, Li M, Shi Z, Li N, Gu Z (2004) Electroanalysis 16:140–144
195. Wang J, Kawde A-N, Musameh M (2003) Analyst 128:912–916
196. Fan C, Plaxco KW, Heeger AJ (2003) Proc Nat Acad Sci U S A 100:9134–9137
197. He P, Dai L (2004) Chem Commun 10:348–349
198. Bonanni A, del Valle M (2010) Anal Chim Acta 678:7–17
199. Bonanni A, Esplandiu MJ, del Valle M (2008) Electrochim Acta 53:4022–4029
200. Wohlstadter JN, Wilbur JL, Sigal GB, Biebuyck HA, Billadeau MA, Dong L, Fischer AB, Gudibande SR, Jameison SH, Kenten JH, Leginus J, Leland JK, Massey RJ, Wohlstadter SJ (2003) Adv Mater 15:1184–1187
201. Sassolas A, Blum LJ, Leca-Bouvier BD (2009) Electroanalysis 21:1237–1250
202. Jayasena SD (1999) Clin Chem 45:1628–1650
203. Ellington AD, Szostak JW (1990) Nature 346:818–822
204. Doudna JA, Cech TR, Sullenger BA (1995) Proc Nat Acad Sci U S A 92:2355–2359
205. Lee S-W, Sullenger BA (1997) Nat Biotechnol 15:41–45
206. Rusconi CP, Scardino E, Layzer J, Pitoc GA, Ortel TL, Monroe D, Sullenger BA (2002) Nature 419:90–94
207. Rusconi CP, Yeh A, Lyerly HK, Lawson JH, Sullenger BA (2000) J Thromb Haemost 84:841–848
208. Stoltenburg R, Reinemann C, Strehlitz B (2007) Biomol Eng 24:381–403
209. Hamula CLA, Guthrie JW, Zhang HQ, Li XF, Le XC (2006) Trends Anal Chem 25:681–691
210. Nimjee SM, Rusconi CP, Sullenger BA (2005) Annu Rev Med 56:555–583
211. O'Sullivan C (2002) Anal Bioanal Chem 372:44–48
212. Wang H, Yang R, Yang L, Tan W (2009) ACS Nano 3:2451–2460
213. Wang Z, Lu Y (2009) J Mater Chem 19:1788–1798
214. Di Cera E (2008) Mol Aspects Med 29:203–254
215. Fenton JW, Landis BH, Walz DA, Finlayson JS (1977) In: Lundblad RL, Fenton JW, Mann KG (eds) Chemistry and biology of thrombin. Ann Arbor Science Publishers, Michigan, pp 43–70
216. Lombardi A, De Simone G, Galdiero S, Staiano N, Nastri F, Pavone V (1999) Pept Sci 51:19–39
217. Petrera NS, Stafford AR, Leslie BA, Kretz CA, Fredenburgh JC, Weitz JI (2009) J Biol Chem 284:25620–25629
218. Tegos TJ, Kalodiki E, Daskalopoulou S–S, Nicolaides AN (2000) Angiology 51:793–808
219. Chiu T-C, Huang C–C (2009) Sensors 9:10356–10388
220. Rodríguez MC, Rivas GA (2009) Talanta 78:212–216
221. Huang J, Wu L, Yalda D, Adkins Y, Kelleher SL, Crane M, Lonnerdal B, Rodriguez RL, Huang N (2002) Transgenic Res 11:229–239
222. Wan Y, Lu J, Cui Z (2006) Sep Purif Technol 48:133–142
223. Ireland J, Herzog J, Unanue ER (2006) J Immunol 177:1421–1425
224. Daniels JS, Pourmand N (2007) Electroanalysis 19:1239–1257
225. Lin Y, Allard LF, Sun Y-P (2004) J Phys Chem B 108:3760–3764
226. Shim M, Shi Kam NW, Chen RJ, Li Y, Dai H (2002) Nano Lett 2:285–288
227. Beyer M, Felgenhauer T, Bischoff F, Breitling F, Stadler V (2006) Biomaterials 27:3505–3514
228. Chen ES, Chen ECM (1998) Bioelectrochem Bioenerg 46:15–19
229. Martínez MT, Tseng Y-C, Ormategui N, Loinaz I, Eritja R, Bokor J (2009) Nano Lett 9:530–536

230. Chen RJ, Choi HC, Bangsaruntip S, Yenilmez E, Tang X, Wang Q, Chang Y-L, Dai H (2004) J Am Chem Soc 126:1563–1568
231. Star A, Gabriel J-CP, Bradley K, Grüner G (2003) Nano Lett 3:459–463
232. Lee S-W, Laibinis PE (1998) Biomaterials 19:1669–1675
233. Ruiz-Taylor LA, Martin TL, Zaugg FG, Witte K, Indermuhle P, Nock S, Wagner P (2001) Proc Nat Acad Sci U S A 98:852–857
234. Claesson PM, Blomberg E, Fröberg JC, Nylander T, Arnebrant T (1995) Adv Colloid Interface Sci 57:161–227
235. Wang RLC, Kreuzer HJ, Grunze M (1997) J Phys Chem B 101:9767–9773
236. Kissinger PT, Heineman WR (1983) J Chem Educ 60:702.
237. Steel AB, Herne TM, Tarlov MJ (1998) Anal Chem 70:4670–4677
238. Mansfeld F, Han LT, Lee CC, Chen C, Zhang G, Xiao H (1997) Corros Sci 39:255–279
239. Srisuwan N, Ochoa N, Pébère N, Tribollet B (2008) Corros Sci 50:1245–1250
240. Sagüés AA, Wolan JT, Fex AD, Fawcett TJ (2006) Electrochim Acta 51:1656–1663
241. Sosa E, Cabrera-Sierra R, Oropeza MT, Hernandez F, Casillas N, Tremont R, Cabrera C, Gonzalez I (2003) Electrochim Acta 48:1665–1674
242. Tzvetkov B, Bojinov M, Girginov A, Pébère N (2007) Electrochim Acta 52:7724–7731
243. Nogueira A, Nóvoa XR, Pérez C (2007) Prog Org Coat 59:186–191
244. Wagner N (2005) In: Barsukov E, Macdonald JR (eds) Impedance spectroscopy: theory, experiment and applications. Wiley, New York
245. Manohar AK, Bretschger O, Nealson KH, Mansfeld F (2008) Bioelectrochemistry 72: 149–154
246. Roy SK, Orazem ME (2008) J Power Sour 184:212–219
247. Amstrong RD, Bel MF, Metcalfe AA (1978) Electrochemistry 6:98–127
248. Seland F, Tunold R, Harrington DA (2006) Electrochim Acta 51:3827–3840
249. Kharitonov AB, Alfonta L, Katz E, Willner I (2000) J Electroanal Chem 487:133–141
250. Vladikova D, Raikova G, Stoynov Z, Takenouti H, Kilner J, Skinner S (2005) Solid State Ion 176:2005–2009
251. Kell DB, Davey CL (1990) In: Cass AEG (ed) Biosensors: a practical approach. IRL Press, Oxford
252. Berggren C, Bjarnason B, Johansson G (2001) Electroanalysis 13:173–180
253. Gabrielli C (ed) (1990) Use and application of electrochemical impedance techniques. Solartron analytical, Farnborough
254. Sluyters-Rehbach M, Sluyters JH (eds) (1970) Electroanalytical chemistry. Dekker, New York
255. Katz E, Willner I (2003) Electroanalysis 15:913–947
256. Macdonald JR (ed) (1987) Impedance spectroscopy: emphasizing solid materials and systems. Wiley-Interscience, New York
257. Liu SH (1985) Phys Rev Lett 55:529
258. Heer F, Franks W, Blau A, Taschini S, Ziegler C, Hierlemann A, Baltes H (2004) Biosens Bioelectron 20:358–366
259. Bates JB, Chu YT, Stribling WT (1988) Phys Rev Lett 60:627
260. Kerner Z, Pajkossy T (2000) Electrochim Acta 46:207–211
261. Kong J, Franklin NR, Zhou C, Chapline MG, Peng S, Cho K, Dai H (2000) Science 287:622–625
262. Bradley K, Briman M, Star A, Grüner G (2004) Nano Lett 4:253–256
263. Heller I, Janssens AM, Mannik J, Minot ED, Lemay SG, Dekker C (2007) Nano Lett 8:591–595
264. Maehashi K, Katsura T, Kerman K, Takamura Y, Matsumoto K, Tamiya E (2006) Anal Chem 79:782–787
265. Esplandiu MJ (2005) Contributions Sci 3:33–46
266. Goldstein JI et al. (eds) (1992) Scanning electron microscopy and X-ray microanalysis. Plenum Press, New York
267. Flewitt PEJ, Wild RK (eds) (1994) Physical methods for materials characterization. Institute of Physics Publishing, London

268. Reimer L, Kohl H (eds) (2008) Transmission electron microscopy: physics of image formation. Springer Science, Berlin
269. Zhong Q, Inniss D, Kjoller K, Elings VB (1993) Surf Sci Lett 290:L688–L692
270. Cardiner DJ, Graves PR (eds) (1989) Practical Raman spectroscopy. Springer, Berlin
271. Jorio A, Saito R, Hafner JH, Lieber CM, Hunter M, McClure T, Dresselhaus G, Dresselhaus MS (2001) Phys Rev Lett 86:1118
272. Rafailov PM, Stoll M, Thomsen C (2004) J Phys Chem B 108:19241–19245
273. Anglaret E, Dragin F, Pénicaud A, Martel R (2006) J Phys Chem B 110:3949–3954
274. Mattia D, Rossi MP, Kim BM, Korneva G, Bau HH, Gogotsi Y (2006) J Phys Chem B 110:9850–9855

http://www.springer.com/978-3-642-31420-9

Carbon Nanotubes as Platforms for Biosensors with Electrochemical and Electronic Transduction

Pacios Pujadó, M.

2012, XX, 208 p., Hardcover
ISBN: 978-3-642-31420-9